PHOTODISINTEGRATION INVESTIGATIONS

USING

CLOUD CHAMBER TECHNIQUES

---

by D. Balfour.

Presented as a thesis for the degree of

Ph.D. at Glasgow University.

Department of Natural Philosophy,

Glasgow University.

January, 1959.

ProQuest LLC.
789 East Eisenhower Parkway
P.O. Box 1346
Ann Arbor, MI 48106 – 1346

PREFACE

The investigations reported in this thesis were carried out in the Natural Philosophy Department of the University of Glasgow between September, 1955 and October, 1958.

Chapter I is devoted to a review of photodisintegration with specific reference to the giant resonance energy region. The techniques applied to the study of the photoprocess are critically discussed, and the development of photodisintegration theory is traced up to the present state of knowledge. From this outline it is concluded that there is need for a photodisintegration experiment which would give detailed knowledge of the disintegration process between 20 MeV and 50 MeV. It is indicated how the cloud chamber technique is the most suitable means of performing such an experiment. Most of the thesis is in fact devoted to this particular project.

In Chapter II, however, there is an account of an attempt to study a problem in the photodisintegration of argon, at low energies, using a diffusion

cloud chamber in conjunction with a 23 MeV synchrotron beam. This experiment was performed by the author himself, and is noteworthy for the fact that a diffusion cloud chamber was employed successfully for the first time, in photodisintegration problems, the γ beam being fired through the sensitive volume of the chamber. Much of the experience gained in this experiment was applied in the subsequent nitrogen experiment.

The experimental method adopted in the nitrogen experiment is outlined in Chapter III. Much of the Chapter is devoted to the methods of measuring actual events, revealing how a new microscope method had to be developed to allow accurate measurements of recoils to be made. The full method of analysis was organised jointly by the author and D.C. Menzies. The total number of films was divided between the two and each was responsible for analysing the events quite independently.

The results of the analysis are presented in Chapter IV for the reactions (γ,p), (γ,n), (γ,pn) and (γ,α), and the criteria for the selection of

these is treated in some detail.

The discussion in Chapter V is due entirely to the author. An attempt is made to relate the observed results to theory with a considerable degree of success, and, in conclusion, an assessment is made of the value of the experiment.

In the appendices there is a brief description of technical work carried out by the author himself. This deals entirely with diffusion chamber operation and the experiments carried out in investigating optimum conditions of operation. Finally, a brief description is given of a chamber which the author designed and had constructed for operation inside a D.C. iron cored magnet.

The author is glad to acknowledge the direction and encouragement given by Professor P.I. Dee and Mr. J.R. Atkinson. In addition he wishes to thank: Professor J.C. Gunn, Mr. J.M. Reid, and Mr. B. Lalovic for valuable discussions; Mr. D.C. Menzies, for his excellent collaboration throughout the project; Mr. D. Dixon, for his assistance with the 23 MeV synchrotron; and Dr. W. McFarlane and his

synchrotron team, for their cooperation. The author is grateful to the University of St. Andrews for having provided a Scholarship for the three years of his research.

INDEX

CHAPTER I. THE PHOTODISINTEGRATION PROCESS.

CHAPTER II. ARGON PHOTODISINTEGRATION AT LOW ENERGIES.

CHAPTER I: THE PHOTODISINTEGRATION PROCESS.

Introduction.

In 1934 Goldhaber and Chadwick[1] disintegrated deuterium with natural γ radiation from ThC'', and Szilard and Chalmers[2] detected photoneutrons from Be. A few years later Bothe and Gentner[3] initiated a study of the (γ,n) reaction. These later experimenters employed the $Li^7(p,\gamma)$ reaction to provide a beam of 17.6 MeV γ rays. However, the intensity of this radiation was small and photonuclear cross sections are small, so that more rapid progress had to await the development of betatrons and synchrotrons. With this new source of intense radiation Huber[4] detected the first (γ,p) reaction and Baldwin and Klaiber[5] detected the first (γ,α) and multiparticle events.

The Giant Resonance.

Many subsequent experimenters, using diverse techniques, have succeeded in establishing the existence of the giant resonance in photodisintegration. This was first revealed in 1948 by Baldwin and Klaiber[6], who showed the cross section for emission of a neutron from ~~in~~ C^{12}, Cu^{63}, and Ta^{181} to have a broad resonance, with a half width of ~ 6 MeV, and a maximum at 30, 22 and 16 respectively. Further experiments[7] have shown that the cross

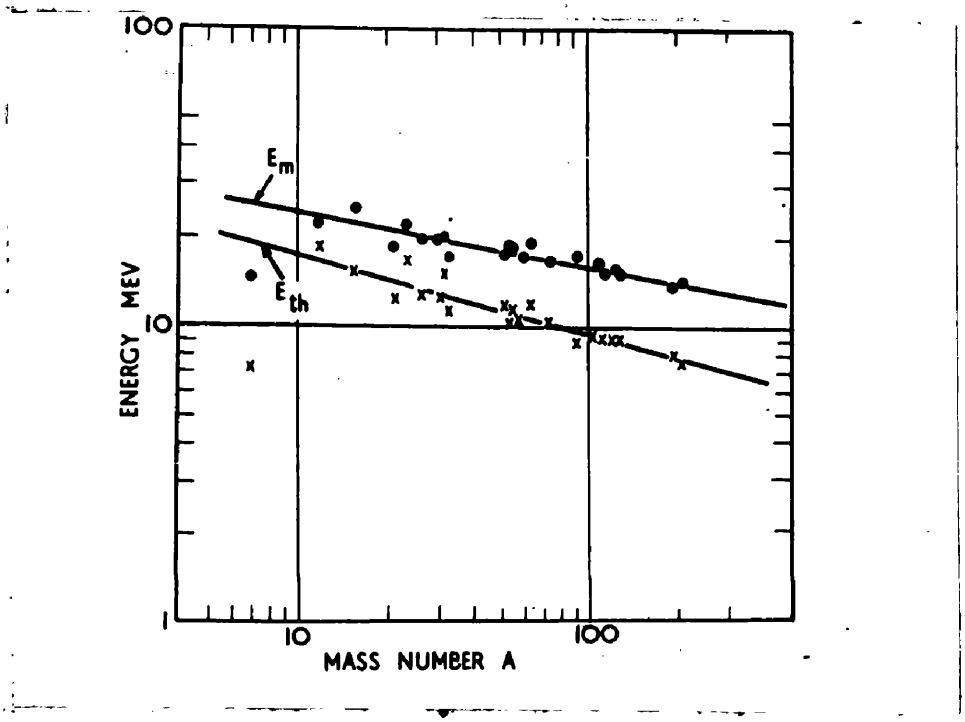

Fig. 1.

Energy at which giant resonance is maximum as a function of atomic mass. (Montalbetti, Katz and Goldemberg).

sections for (γ,p), (γ,pn) etc., all exhibit a giant resonance, provided the thresholds for these reactions occur below the giant resonance region. This behaviour has been shown to be common to all nuclei although the peak in the giant resonance decreases from about 24 MeV, in the lightest elements, to about 15 MeV in the heaviest[8]. There are exceptions in the case of magic nuclei where the behaviour of the excitation function is exceptional, and the half widths of the giant resonance are consistently narrower.

A further property of the giant resonance is that the area under the total cross section is directly proportional to A, the atomic mass[9].

The main properties of the giant resonance may therefore be summarised as follows:-

(i) The peak of the giant resonance occurs at $\sim$ 20 MeV.

(ii) The half width of the resonance is $\sim$ 6 MeV.

(iii) $E_{max} \propto A^{-0.2}$ [10].

(iv) $\int_0^{\infty} \sigma \, dE \propto A$.

(v) Magic nuclei have narrower half widths.

From the generality of this information, it may be concluded that the giant resonance is a manifestation of a property of nuclear matter in absorbing γ-radiation, although it is exposed only in the resulting emission of particles.

The physical process of absorption of γ-rays in this way is essentially a result of the interaction of an electromagnetic field with charged particles. This case is analogous to the absorption or emission of photons by electrons, in which the procedure was to split up the electromagnetic radiation into the various electric and magnetic multipoles. There is now considerable evidence to associate the absorption in the giant resonance with electric dipole absorption.

Unfortunately it is not possible to investigate giant resonance behaviour experimentally from the absorption of γ-rays, since the cross section for absorption to produce a nuclear reaction is small in comparison with the cross section for electronic absorption, Compton scattering, and pair production.

However, the total contribution may be estimated by summing the partial contributions:

$$\sigma_T = \sigma_{\gamma\gamma'} + \sigma_{\gamma,n} + \sigma_{\gamma,p} + \sigma_{\gamma,2n} + \sigma_{\gamma,pn} + \cdots .$$

All experimental work has therefore been related to a particular reaction, or group of reactions with a common product (e.g. (γ,n) and $(\gamma,2n)$ where the neutrons are detected). In most cases the (γ,n) reaction is dominant.

Reactions at Higher Energies.

Above the giant resonance, the cross section curves for nuclear disintegration decrease smoothly, until, at 50 $\sim$ 60 MeV, the value of the cross section for any one reaction is likely to have decreased by a factor of greater than 10. The interest in photonuclear reactions at high energies is on two accounts:-

(i) To account for the high momentum of particles emitted at high energies (γ-rays may carry high energy, but little momentum) it is necessary to assume that the incident photon interacts with a sub-group of the nucleus, which is in a high momentum state. This is equivalent to claiming

that, since the momentum of the γ-ray is small, the momentum of the final state must be present in the initial arrangement of nucleons.

(ii) It is to be expected that above the π meson threshold ($\sim$ 150 MeV), the cross section for any reaction will increase, since there is a probability that any meson created at a nucleon will be absorbed into the nucleus, before being emitted, causing the nucleus to disintegrate.

In the case of (i) considerable work, both theoretical and experimental, has been applied to the case in which a proton and neutron is a high momentum state from the sub-group. This "quasi deuteron" model has been developed by Levinger[11], and there is considerable experimental evidence to support it[12].

In this thesis (ii) is not considered, and (i) is considered only briefly. Most of the results to be discussed can be associated with the giant resonance region.

Remarks on Theory.

Theoretical interest in the photodisintegration

process has developed alongside the progressive accumulation of experimental data. The photodisintegration of the deuteron has received great attention[13], since its position in nuclear physics is analogous to that of the hydrogen atom in atomic physics. The experimental results below 20 MeV are well explained by theory. For heavier nuclei, however, there is no complete theory, and various models have been proposed to explain experimental results. These models will be discussed later in this chapter.

Techniques Applied to Photodisintegration.

The most common method has been that of activation. This may be applied to any reaction in which the resulting nucleus is unstable and decays by β emission. By measuring the decay as a function of time and extrapolating backwards, the yield may be estimated for each energy of irradiation.

However, some (γ,n) and most $(\gamma,2n)$ reactions produce a stable nucleus. For these, Halpern[14] and others have used BF_3 counters to detect the emitted neutrons. To eliminate the difficulty of counting

against the background produced by the γ beam, the neutrons are moderated in a paraffin block and then counted between beam pulses.

Both methods give yield curves as a function of energy. Cross section curves may be produced from these by applying "successive subtraction"[15] or "photon difference"[16] methods. The latter is more accurate, but both inevitably produce curves which smooth out any structure, and which may be inaccurate above E_{max}.

The activation technique effectively studies only one reaction, generally (γ,n), and even when different isotopes are present it is often possible to separate each contribution[17]. In contrast, the neutron "long counter" method detects all reactions in which a neutron is emitted. Hence

$$\sigma\ (\text{detected}) = \sigma\ (\gamma,n) + \sigma\ (\gamma,pn) + 2\sigma(\gamma,2n)$$

By stablising betatron beams to $\pm$ 5 KeV breaks have been detected in yield curves by both methods.[18,19] These correspond to absorption levels in the target nucleus.

Photographic emulsion techniques have also been

used effectively.[20] While individual reactions have been revealed by direct irradiation of plates, most information has been obtained by stacking the plates in set positions round a target to detect the charged particles emitted. Thus angular and energy distributions of the particles may be derived. Unfortunately, the origin of reactions is not detected and hence their nature is not exposed. In addition energy is lost by the particles in reaching and penetrating the plates.

The cloud chamber method[21-24] of observing photodisintegrations has the advantages of recording the origin of events so that they can be quite accurately classified, and in revealing the relative importance of each class. This technique has been used to detect absorption levels and to measure angular distributions. In later chapters it will be revealed how, by measuring nuclear recoil tracks, the scope of the technique may be extended.

Counter methods have been applied mostly for very particular problems. Wilkinson and Carver[25] and Wright and Ophel[26] have reported interesting

experiments in which their target also acted as a detector, the first group using an argon filled proportional counter, and the second using a sodium iodide crystal. In addition, counters are suitable for selecting nucleons of definite energy (e.g. Ferrero's[27] detection of neutrons > 4 MeV, and the application of scintillation counter telescopes to investigate high energy photodisintegration).[28,12]

Theoretical Treatments of Giant Resonance Photodisintegration.

The photodisintegration process may conveniently be considered as consisting of two separate processes:

(a) the absorption of the incident γ quantum, and

(b) the resulting disintegration. Since the giant resonance is known to result from dipole absorption, information about the giant resonance may be deduced by considering only the dipole absorption of electromagnetic radiation without necessarily assuming any model of the nucleus. In the disintegration process, however, a model is

essential as a basis for all calculations. In the following sections, the different theories will be outlined to reveal their limitations and successes.

Calculations Based on Dipole Absorption of Radiation.

Levinger and Bethe[29] have applied ~~new~~ Sum rules to the matrix elements for photon absorption, assuming that the forces between nucleons were all ordinary forces so that they could be replaced by a potential, and they obtained the following expression for the total integrated cross section

$$\int_0^\infty \sigma_T \, dE = \frac{2\pi^2 e^2 \hbar}{Mc} \cdot \frac{NZ}{A} = 0.060 \frac{NZ}{A} \text{ mev barns.}$$

However, since neutron-proton forces are known to be at least partially exchanged in character, this expression has been modified to

$$\int_0^\infty \sigma_T \, dE = 0.060 \frac{NZ}{A} (1+0.8x) \text{ mev barns}$$

where x is the fraction of the force that is of an exchange nature. Unfortunately, on including exchange forces the result is no longer a general one but is dependent on a model. Levinger's result is based upon an independent particle model.

Gell-Mann[30] has obtained a similar expression from a dispersion relation, including the exchange forces by integrating over meson production cross sections:

$$\int_0^{E_{th}} \sigma(E)\,dE = \frac{2\pi^2 e^2 \hbar}{Mc}\frac{NZ}{A} + \int_{E_{th}}^{\infty} [1 - R(E)][Z\sigma_p(E) + N\sigma_n(E)]\,dE .$$

E_{th} is the threshold energy for meson production.

σ_p is cross section for meson production at a proton,

σ_n is cross section for meson production at a neutron,

while the factor in the integral gives the difference between meson production between free nucleons, and nucleons in a nucleus.

These calculations give the dependence of the

integrated total cross section on $\frac{NZ}{A}$ * as has been demonstrated experimentally by Halpern and Mann[9]. The two values, from the separate derivations differ by some 20%, however, and so they can only be regarded as crude estimates.

Levinger and Bethe have also evaluated the mean energy $\bar{k} = \frac{\int k\,\sigma(k)\,dk}{\int \sigma(k)\,dk}$ and the harmonic mean energy $k_h = \frac{\int \sigma(k)\,dk}{\int \sigma(k)\,\frac{dk}{k}}$.

k = photon energy.

Bishop and Wilson have pointed out how these are dependent on the correlation between the position of nucleons. The fact that Levinger and Bethe found gross disagreement with the experiment in evaluating these, when they assumed no correlations, is interpreted as implying that correlation effects are important.

The models suggested by Goldhaber and Teller[32], Steinwedel and Jensen[33], and Danos[34] all include strong correlations between nucleons. In the process of dipole absorption, it is necessary that the centre of electrical charge be displaced from the centre of mass. Goldhaber and Teller consider a

* $N = Z = \frac{A}{2}$ approx. $\therefore \int \sigma\,dE \propto A$ as on p2. (iv).

collective motion in which the neutrons and protons move in opposite directions. By assuming a restoring force proportional to displacement a constant resonant energy E_{max} is obtained. If the neutrons and protons are considered as interpenetrating, incompressible fluids,

$$E_{max} = \hbar\omega_0 = 40 A^{-\frac{1}{6}} \text{ mev.}$$

ω_0 = resonance frequency

If the fluids are considered as being compressible but are constrained within the nucleus, then

$$E_{max} \propto A^{-\frac{1}{3}}$$

In addition they calculate $\int_0^\infty \sigma_T \, dE = \frac{\pi^2 e^2 \hbar}{2Mc} A = 0.015 A$ Since it was assumed that $N = Z = \frac{A}{2}$ this result is the same as that given by Levinger and Bethe when exchange forces are excluded. This is to be expected since the model includes all dipole vibrations and neglects exchange forces.

In a similar argument, Steinwedel and Jensen calculated $\hbar\omega_0 = 60 A^{-\frac{1}{3}}$ MeV & $\sigma_{int.} = 0.0065 A$ MeV barns, assuming the nuclear density to remain constant during the oscillation.

None of the results fit closely to theory and it is not clear whether E_{max} varies according to $A^{-\frac{1}{3}}$ or $A^{-\frac{1}{6}}$.

The Compound Nucleus.

The very nature of the collective motion discussed implies that a compound nucleus is formed in which the energy of the incident γ-ray is shared among all the nucleons in the nucleus. The energy continues to be redistributed randomly among the nucleons until, by chance, one nucleon has energy sufficient to allow it to escape from the nucleus. Then the cross section for the emission of a particle b is given by

$$\sigma(\gamma,b) = \sigma_a(E_\gamma)\, G_b.$$

where $\sigma_a(E_\gamma)$ is the cross section for absorption of quanta of energy E_γ, and G_b is the probability that the nucleus will decay by emission of particle b.

$G_b = \dfrac{\Gamma_b}{\sum_i \Gamma_i}$ where Γ_i is the particle width for emission of particle i.

Titterton[20] points out that the form of the cross

section curve is therefore governed by (a) the absorption probability (b) competition from other particles in the "scramble" for emission (c) selection rules leading to emission of particle b .

Starting from a compound nucleus it is possible to calculate energy distributions and angular distributions of emitted particles and these may readily be compared with experimental results.

Even although the emission of a nucleon from a compound nucleus may be interpreted as an evaporation process, it is not true that all directions of emission of a nucleon are equally probable. Wolfenstein[35] has pointed out that the polarisation of the incident radiation leads to a polarisation of the compound nucleus which reveals itself both in the polarisation of the emitted nucleons, and in the form of the angular distribution. It will be shown later in the thesis, how angular distributions for photodisintegration may be calculated if the spin and parity of the initial and final states be known and if the nature and multipole order of the absorption be known. In all cases the distributions

are symmetrical about 90°. However, interference between quadrupole and dipole absorption, for instance, may yield a distribution which is anisotropic and is not symmetrical about 90°.

Energy distributions of emitted nucleons may be calculated from the statistical theory developed by Weisskopf. The calculation is based on the equation of Weisskopf and Ewing[36] which gives the energy distribution of protons of energy ϵ emitted from a nucleus b which has absorbed a photon of energy E:-

$$I(\epsilon) = \text{const.}\ \epsilon.\ S_b(\epsilon)\ f_b\ \omega_r(E - B_p - \epsilon).$$

where ω_r is the level density of the compound nucleus,

$S_b(\epsilon)$ is the coulomb barrier penetration factor, and

f_b is a sticking factor. B_p is the binding energy of the proton.

This equation has been applied to the case where the irradiation is due to a spectrum with $N(E, E_{max})$ photons/cm^2/MeV interval at energy E

and peak energy E_{max}. The form of the distribution then becomes:-

$$F(\epsilon_p) = \epsilon_p \sigma_p \int_{B_p+\epsilon_p}^{E_m} \frac{\sigma_{\gamma,n}(E)\, N(E, E_{max})\, \omega_r(E-B_p-\epsilon)\, dE}{\Gamma_n}$$

where σ_p is the cross section for formation of a compound nucleus when bombarded by a proton of energy ϵ_p . $\Gamma_n = \int_0^{E-B_n} \epsilon' \sigma_c(\epsilon')\, \omega(E-B_n-\epsilon_n)\, d\epsilon'$ and represents the probability of emission of a neutron. $\sigma_{\gamma,n}(E)$ is the cross section for the (γ,n) reaction.

Normally a Schiff spectrum is assumed and σ_p is taken from the theoretical calculation of Weisskopf which reproduces the continuum of σ_p without resonances. σ (γ,n) is taken from experimental determinations.

The most doubtful factor is the form of the energy level distribution. Weisskopf and Ewing suggest $\omega_r(E) = C e^{\sqrt{aE}}$ where $a = 1.6\ (A - 40)^{\frac{1}{2}}$. Where the excitation does not exceed 10 MeV, Livesey[37] has suggested

$$\omega(E) = C e^{\frac{E}{T}}$$

where T is a constant nuclear temperature in MeV.

Normally curves for different energy level distributions are plotted and compared with theory.

Much of the experimental data obtained is in accord with a compound nucleus interaction. This is true of the heavier elements where the conditions for compound nucleus formation are satisfied.

Typical experiments have been performed by Diven and Almy[38]; Toms and Stephens[39]; Curtis, Hornbostel, Lee and Salant[40]; Byerly and Stephens[41]; Dawson[42] and Livesey[43], in which the angular and energy distributions of nucleons from heavier elements, like copper, rhodium, silver, gold, and even aluminium, have been measured by the photoplate method, using bremsstrahlung from betatrons and synchrotrons. These results show that for the lower energies of emitted particles, the results are in agreement with a compound nucleus formation: the angular distributions are isotropic, and the energy distributions are well fitted by the statistical formula using reasonable level densities. However, at higher energies, there is a disagreement:

the number of high energy nucleons is greater than could be expected from a statistical process, and, furthermore, the angular distribution of protons from these events has been shown to be anisotropic with a peak anywhere between 60° and 90°.

In addition, the classic experiments of Hirzel and Waffler[44] on the ratio of the yields of (γ,p) to (γ,n) events, as investigated by the 17.6 MeV $Li^7(p,\gamma)$ γ-rays, using activation techniques, showed conclusively that this ratio was much higher than could be explained by a statistical decay. Many elements were examined and, for heavier ones, the value obtained was as much as a thousand times the value deduced from a "statistical" calculation.

The Courant Model.

In an attempt to explain these deviations a process was suggested in which the nucleons could be ejected directly. While Jensen and Marquez both suggested this process, Courant treated the problem in detail. He considered the incident quantum to be absorbed by one proton which is then

emitted without sharing energy with the rest of the nucleus. The model consists of a square well, which is assumed to represent entirely the interaction of the nucleons, and in which the Z protons fill the Z lowest states. The photoelectric absorption matrix is computed for transitions of the proton from a bound state into the continuum. The entire absorption process is described by such interactions, but, since the excited nucleon may radiate or collide with other nucleons to form a compound nucleus, which then decays statistically, the cross section for direct emission is only a small part of this. Assuming a Fermi distribution, and taking $R = 1.5 \times A^{\frac{1}{3}} \times 10^{-13}$ cm. the cross section at 17.6 MeV was given as

$$\sigma(\gamma,p) = 0.044 \left(\frac{Z}{A^{\frac{1}{3}}}\right)^2 \int_0^{x_1} P\,dx .$$

P = penetration probability, x = energy of outgoing protons in units of barrier height, and x_1 is the maximum energy of protons.

The proton emission thus obtained, although being closer to experimental results, is still

consistently lower. Courant suggests the difference to be due to the crudity of the square well approximation, pointing out that a "wine bottle" potential would increase the value of $\sigma(\gamma,p)$ by about 4. The neglect of exchange factors would also account for a further factor.

The angular distributions given by this process are certainly closer to the experiments of Diven and Almy etc. giving peaks in the anisotropy at 90°. The angular distributions are given by

$$l \to l+1 \qquad I(\theta) = l(l+1) + \tfrac{1}{2}(l+1)(l+2)\sin^2\theta.$$

$$l \to l-1 \qquad I(\theta) = l(l+1) + \tfrac{1}{2}l(l-1)\sin^2\theta.$$

where l is angular momentum of nucleon.

Experimental results which show a similar behaviour for neutrons have been published by Poss[48] and Byerly and Stephens[41].

Eichler and Weidenmuller[49] have shown that in cases where the above transitions occur with comparable probability it is necessary in computing angular

distributions to include also the interference term which is introduced when the two transitions are superimposed. They imply that this term increases the anisotropy, and gives a better account of experimentally determined distributions.

The Wilkinson Model.

Wilkinson[50] has developed a treatment of the photodisintegration process based on the shell model of the nucleus, which has proved valuable in other fields, and shows how this gives a much better account of the high yields of protons from heavier elements.

He considers a single nucleon in a definite shell state to absorb the incident γ quantum so that it is raised into a higher energy state. There are then two possibilities: the nucleon may be emitted directly, without interacting with the rest of the nucleus, or it may collide with other nucleons, sharing its energy to form a compound nucleus which will then decay as a statistical process.

Wilkinson assesses the relative values of the

direct emission to compound nucleus formation by $C = \frac{2kP \cdot \frac{m\hbar^2}{R}}{2W}$ where P is the penetrability of the coulomb and centrifugal barriers, k is the incident nucleon wave number, and W is the imaginary part of the cloudy crystal ball potential. This ratio is just the ratio of the width for direct emission of a particle to the width for re-absorption of that particle.

Since the giant resonance absorption has been shown to exhaust the dipole sum of Levinger, it may be concluded that the mechanism involved is essentially dipole absorption of the γ quanta. The selection rule for a dipole excitation requires a change in the orbital angular momentum of 0 or 1. Wilkinson therefore considers transitions of $\ell \rightarrow \ell-1$ and $\ell \rightarrow \ell+1$ as constituting the giant resonance. Since all nucleons are included in the dipole sums, they must all contribute to the giant resonance, and since most nucleons are contained in the core of the nucleus, Wilkinson claims that the transitions from the closed shells should be sufficient

to account for the resonance behaviour. An additional reason for neglecting the valence nucleons is that they have many possible transitions which are spread over many MeV, and are not restricted to a small energy group as in the case of the giant resonance.

Since for any nucleon in the ℓ^{th} level the level $\ell - 1$ will normally be filled, the Pauli Principle implies that transitions of the type $\ell \rightarrow \ell+1$ will be most important.

The radiative width for any transition is in most cases considerably enhanced over the single particle width as computed by Weisskopf. The enhancement factors have been calculated by Radicatti and Lane[51]. The transition strength is determined largely by D the square of the overlap integral where D is measured in units of the nuclear radius, since $D^{\frac{1}{2}}R = \int_0^\infty \psi_i \, r^3 \psi_f \, dr$. where ψ_i and ψ_f are the normalised radial wave functions of the initial and final states. In the case of heavy elements the sum of the strengths of the transitions is almost equal to the dipole sum

calculated by Levinger and Bethe so that the mechanism seems to be a valid one.

Wilkinson has calculated the integrated cross section to be

$$\int \sigma \, dE = 4\pi^2 \varepsilon^2 \frac{E_m}{\hbar c} \cdot R^2 \sum \frac{\ell+1}{2\ell+3} F_{j\ell} D_\ell .$$

where the summation is over all closed shells.

$F_{j\ell}$ is the enhancement factor for the j^{th} shell of the ℓ^{th} orbit.

While this gives a good value for light nuclei, it is too small by a factor of 2 for heavy nuclei. The treatment, however, does not include transitions associated with radial modes in the wave function e.g. $1\ell \rightarrow 2\ell+1$ In addition Wilkinson suggests that the experimental measurements may be over-estimated.

For the case of lead, Wilkinson has shown that the main transitions cluster in energy in a way characteristic of the giant resonance. The actual width of the resonance is determined by a number

of factors:(i) each single particle transition is separated in energy, (ii) the effect of W, is to smear out the width of any resonance, (iii) the valence nucleons have transitions spread over many MeV, and (iv) any coupling between shells would lead to a widening of each level. These factors are sufficient to give the total width of the resonance the right order of magnitude. The energy of the maximum, however, is much too low being $\sim$ 9 MeV instead of $\sim$ 14 MeV for heavy elements. Wilkinson gives a plausible argument to show that this value can be brought closer to reality by, (a) using a velocity dependent potential instead of a static potential, (b) using a larger value of R. (This is particularly true for lower atomic weights) (c) including the pairing energy required to separate any nucleon, in view of the fact that there is a pairing of nucleons in a nucleus.

The angular distribution of nucleons resulting from the Wilkinson type of model is given by

$$W(\theta) = 1 + \frac{1}{2}\left(1 + \frac{2}{l}\right) \sin^2\theta .$$

where the nucleon is initially in the l shell. This distribution with a peak at 90°, like Courant's theory, is close to the experimentally measured distributions for heavier elements.

Thus the Wilkinson model has been shown to give a semi quantitative explanation of the giant resonance.

The energy distribution and angular distributions of protons emitted from the disintegration of Pb^{208} by Toms and Stephens[52] is excellently accounted for on the basis of this model. Other evidence in support of this theory is that for closed shell nuclei the resonance width is quite small ($\sim$ 3 MeV). Since there are no valence nucleons, the only factors causing the width are W and the energy spacing between the possible transitions, and so the width should be considerably smaller in these cases. Also, a break in E_m as a function of A might be expected at a shell filling. This is in fact observed for the $1d_{\frac{5}{2}}$ shell (A = 28).

Recent Experimental Work.

Recent work on the rare earth elements by Petree et al[53] has shown that the giant resonance width is much larger than 6 MeV (~ 10 MeV), and there have been claims of two separate peaks. Such nuclei are known to be elliptical in shape, and thus exhibit a measurable quadrupole moment. Okamoto[54] and Danos[55,56,58] using a collective model, have shown that, corresponding to the two different axes of an ellipsoid, there should be two modes of oscillation of the proton-neutron systems. This is completely successful in explaining the increased width of the giant resonance, and also, the occurrence of two peaks. This seemed a major success for the hydrodynamical model; but now, Wilkinson[56] has shown that, when a nucleus is deformed, the independent particle levels are split, and many more transitions are made possible. Wilkinson has calculated the form of the giant resonance for various degrees of deformity, and has shown that, as the deformity increases, so also does the resonance width, until two peaks are observable, in accord with experiment.

The success of such contrasting models as the collective model, and the Wilkinson single particle model, in explaining the main properties of the giant resonance, seems quite surprising. However, Brink[57] has shown that, for a pure harmonic oscillator, the operation of the dipole operator on the total wave function changes only the part concerning the collective motion of protons. He argues that, in reality, this effect will still hold to some extent, and that it is therefore understandable that both models give similar results.

At present, considerable effort is being applied to reveal fine structure in the giant resonance. Several experimenters[58] claim to have revealed such structure. On the other hand Titterton's group at Canberra have performed the reverse (p,γ) interaction accelerating protons over the full range of the absorption resonance, and have been unable to detect any fine structure.

Using threshold counters, Ferrero[59] et al have studied the fast neutron component from (γ,n) reactions and have shown the resonance direct

neutrons to exhibit a resonance peak at the same energy as that of the giant resonance, in accord with Wilkinson's work. The Courant model does not imply that the directly emitted nucleons should exhibit a resonance.

Conclusions.

It has been indicated how most of the information on photodisintegration has been built up from experiments involving activation methods and photographic emulsions. Activation techniques inevitably reveal only one mode of disintegration, and the conversion of activation curves into cross section curves may involve large errors, so that, above $\sim$ 25 MeV, the form of the cross section curves is very uncertain. In the case of both neutron counting, and photographic emulsion experiments in which a target is irradiated, the precise nature of the reactions is not known, and several modes of disintegration are usually detected.

Thus there is value in an experiment which could reveal the relative importance of the various modes of disintegration, and which might give a

true indication of the form of the cross section curves above the giant resonance. Detailed measurement of the higher energy events would then provide a test for the Wilkinson shell model and for other direct interaction models.

The precise classification of each event requires that the origin must be seen, and, for this, it is best to use a cloud chamber containing the target gas. A light gas would have the advantage of yielding, according to Wilkinson's calculations, a higher proportion of directly emitted nucleons. In addition, the resulting recoils would have a longer range and could be more accurately measured.

In order to obtain events resulting from absorption of γ quanta of $\sim$ 50 MeV, a bremsstrahlung of peak energy $\sim$ 150 MeV would be required, since the absorption cross section, and the number of quanta/MeV interval in the beam are both known to decrease with increasing energy.

For these reasons it was decided to disintegrate nitrogen gas in a conventional cloud chamber using bremsstrahlung from the 330 MeV synchrotron. The

major part of this thesis is devoted to this work. In the next chapter, however, a definite problem, demanding the use of a cloud chamber with low energy γ-beam, is described.

CHAPTER II. ARGON PHOTODISINTEGRATION AT LOW ENERGIES.

Introduction.

In this chapter some surprising results from the photodisintegration of A^{40} are discussed and an experiment is described which might give a greater understanding of the problem. As a result of the complete breakdown of the 23 MeV synchrotron, it has not been possible to derive conclusive results from this experiment, but it is described here since much of the technical experience gained was employed in the later nitrogen photodisintegration, and since this is the first time that a diffusion cloud chamber has been applied successfully to photodisintegration.

Discussion of A^{40} Photodisintegration Experiments

Wilkinson & Carver's experiment[25], in which A^{40} was disintegrated in a proportional counter by 17.6 MeV γ-rays, did not give the large proton contribution at higher energies that was expected from a Courant type of interaction.

McPherson et al[60] determined the (γ,p) and (γ,n)

f 34.

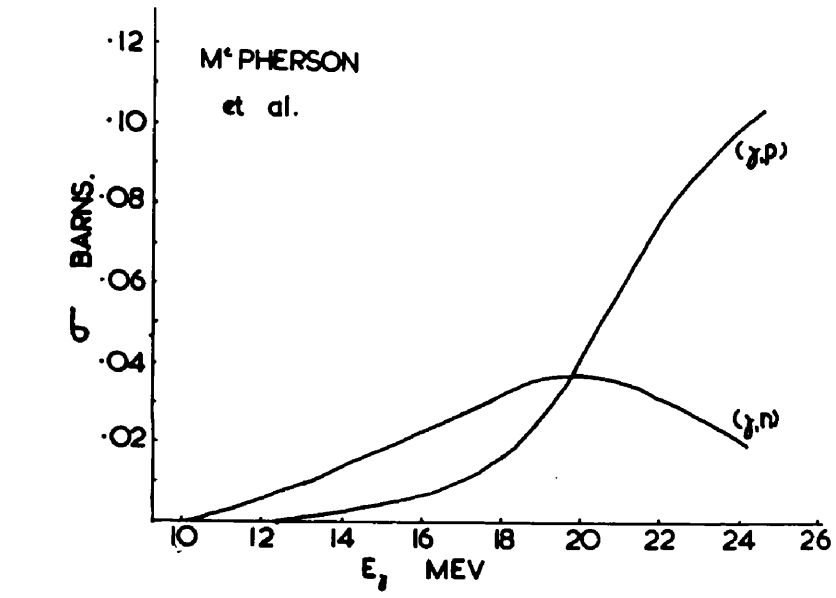

Fig. 2.

(γ,n) and (γ,p) cross section curves for A^{40}.

cross sections up to 25 MeV using an activation technique, and obtained a high $\frac{\gamma,p}{\gamma,n}$ ratio. They showed the (γ,p) cross section curve to equal the (γ,n) curve at 19 MeV, and to be still on the increase at 25 MeV where the (γ,n) curve has fallen off to a small value. This is surprising if the disintegration is to be considered as a statistical process involving competition for emission between neutrons and protons, for the (γ,n) reaction, with a lower threshold, might be expected to be favoured. The ratio $\frac{\gamma,p}{\gamma,n}$ is $\sim$ 1 whereas statistical theory predicts $\sim$ 0.01.

Spicer[61] has observed A^{40} photodisintegration in photographic emulsions, and has obtained a proton energy spectrum in agreement with that of Wilkinson and Carver, and a yield of protons in agreement with McPherson et al. The angular distributions of protons of all energy groups, as measured by Spicer, have the form $(a + b \sin^2\theta)(1 + c \cos\theta)$. He explains the $(1 + c \cos\theta)$ term as being due to interference between electric dipole and electric quadrupole components.

A compound nucleus model is incapable of giving an $a + b \sin^2\theta$ distribution with a $\frac{b}{a}$ ratio as high as was measured. With a direct interaction model it is possible to have such a large $\sin^2\theta$ component if the proton emitted has $\ell = 0$. This can be achieved by emission from the $2s_{\frac{1}{2}}$ level since the argon proton configuration is

$$(1s_{\frac{1}{2}})^2(1p_{\frac{3}{2}})^4(1p_{\frac{1}{2}})^2(1d_{\frac{5}{2}})^6(2s_{\frac{1}{2}})^2(1d_{\frac{3}{2}})^2$$

In such a case, however, the residual nucleus is left in a $\frac{1}{2}+$ state. The spin of the Cl^{39} ground state as measured by β decay is $\frac{3}{2}+$.[62.] Thus the protons observed by Spicer must all have resulted from transitions to excited states if this interaction is accepted.

To explain the results of McPherson et al, Spicer suggests that the increase in (γ, p) emission above 16 MeV may be due to the newly started emission from the $2S_{\frac{1}{2}}$ shell. Hence below 16 MeV this argument implies that only $1d_{\frac{3}{2}}$ protons can be emitted and these would give an angular distribution of $1 + \sin^2\theta$.

Hence it was proposed to disintegrate argon in

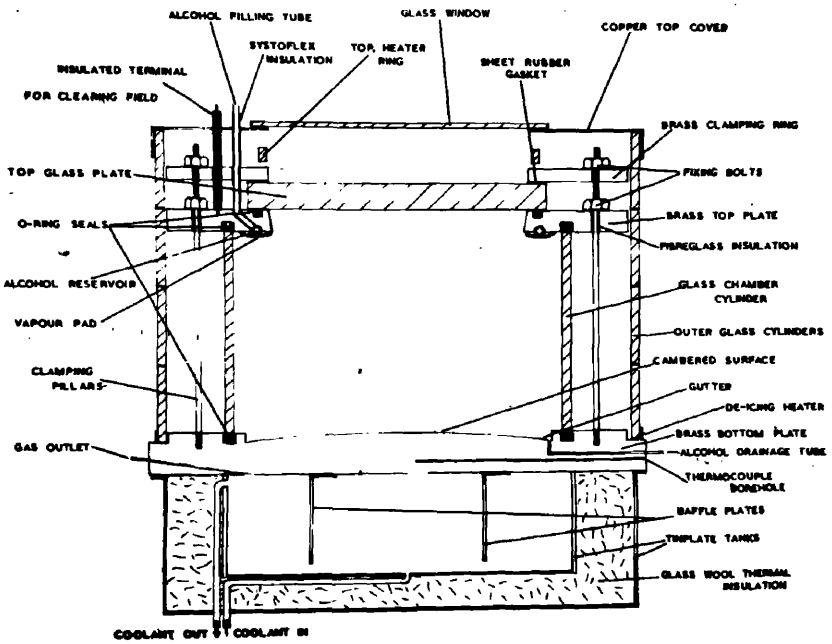

Fig. 3.

Diagram of diffusion chamber.

a diffusion chamber using the 23 MeV synchrotron to provide beams of 16, 18, 20, 23 MeV, so that McPherson's yield might be checked, and the proton angular distributions at each energy might be obtained.

A diffusion chamber was used since it is possible to obtain a faster cycling time than with a conventional expansion chamber. (See appendix).

Diffusion Chamber.

The chamber used consisted of a 10" diameter cylinder with a depth of 5". The entrance window was of 5 "thou." copper foil 2" x $\frac{1}{2}$" soldered to a brass base. The centre of the window was about 2 cms. from the base at a height corresponding to the middle of the sensitive depth. The top of the chamber was heated by an annular electrical heater to a temperature of about $+45^{\circ}C$., while the base was cooled, by pumping methyl alcohol underneath it and through a heat exchanger containing a methyl alcohol dry ice mixture at $-70^{\circ}C$. A base temperature of -45° to $-50^{\circ}C$ was attainable. The vapour source was a felt pad clamped to the underside of the top

plate and it was soaked with methyl alcohol injected from the top through a copper pipe. The windows around the discharge lamps were prevented from frosting by winding a few turns of constantan wire round them and connecting this to a 24v. supply. Two xenon filled discharge tubes were used for illumination, the discharge coming from a bank of six 50 μF condensers charged to 1.5 k.v. Two Shackman cameras clamped to a rigid stand were used to photograph each beam pulse.

An ionisation chamber placed in the γ-ray beam was used as a measure of the beam strength, lead blocks being interposed in front of the ionisation chamber to create pairs.

Alignment of Cloud Chamber in Synchrotron Beam.

The point on the donut of the synchrotron from which the γ-rays emerged was determined by clamping, a few ~~mms.~~ cms. apart, and in the region of the point, a series of copper rods of the same copper sample and of the same dimensions. These were irradiated for several minutes and the induced activity (resulting from $Cu^{63}(\gamma,n)Cu^{62}$ giving Cu^{62}, which has a half

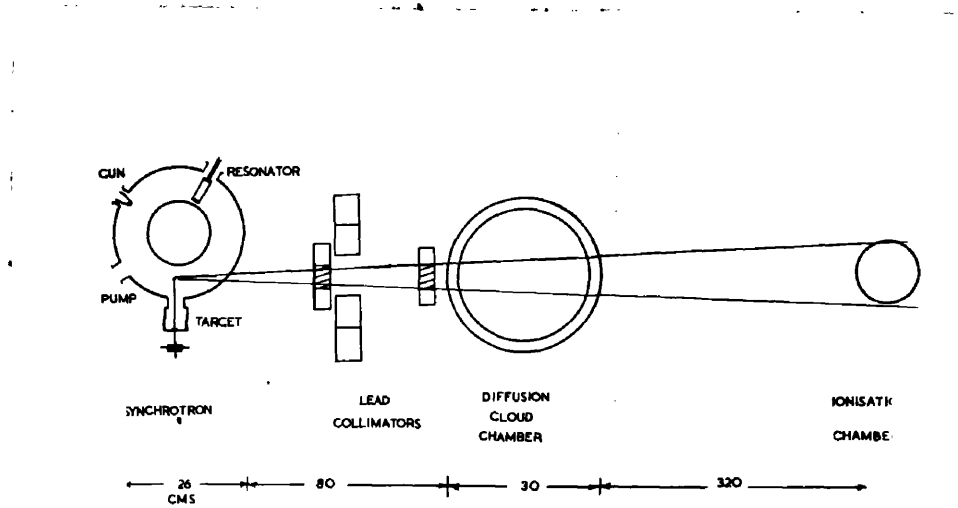

Fig. 4.

Position of diffusion chamber in 23 MeV synchrotron beam.

life of 10.5 mins.) of each rod was then measured with a Geiger tube, using standard counting geometry. A plate, underneath the Geiger, containing a grooved surface ensured that all of the rods would be similarly situated when being counted. The method of counting was to place each rod, in turn, under the counter for one minute and record the counts on a conventional scaler. The rods were counted in succession in numbers 1 to 6, and then again 6 to 1, the sum of the two counts being taken to correct for the difference in time delay in counting each rod. The rod with maximum activity therefore gave the point on the donut at which the beam was strongest.

The same procedure was repeated but with slightly bigger rods, some 12 ins. from the donut, to determine the position of the first lead collimator that would allow the largest γ flux to pass through.

To align the diffusion chamber in the beam, a telescope was set up in a clamp, at the far side of the room, with cross wires set on the point of emergence of the beam from the donut, and on the centre point of the gap in the first collimator.

The chamber was then put into position so that the cross wires fixed the centre point of the thin copper window. (See fig. 4).

The beam was further collimated so that it might pass through the thin window, and not create electron-positron pairs in the surrounding material. X-ray plates placed over the window and irradiated for several minutes were used to show that the beam was, in fact, passing cleanly through the chamber.

Method.

The experimental procedure was similar to that used by Wright[21] et al. The synchrotron was operated under "single shot" conditions, and the cloud chamber was photographed immediately after each beam pulse, so that any disintegration produced in the gas might be recorded. By choosing the correct time delay between the beam pulse and the flashing of the discharge lamps, a relatively high degree of discrimination was obtained between the tracks due to heavy particles and to the electron background.

Timing Sequence.

In the course of taking one picture the following sequence was necessary:-

(i) opening of the camera shutters.

(ii) firing of the γ-ray beam.

(iii) flashing of the discharge tubes.

(iv) closing of shutters.

(v) winding on of film.

With the Shackmann cameras the sequence was quite easy, since, on connecting the cameras to a 24 volt supply, the shutters opened, and, on breaking the circuit, they closed; the film then wound on automatically, powered by a clockwork spring. For simplicity of operation, the beam room was left in darkness and the cameras were operated by remote control from the control room.

In order that the tracks formed in the chamber may grow to visible size before being photographed, it is necessary to introduce a delay between the gun pulse and the flashing of the discharge tubes. This was done by passing the gun pulse through a delay unit (see diagram) which consisted of two

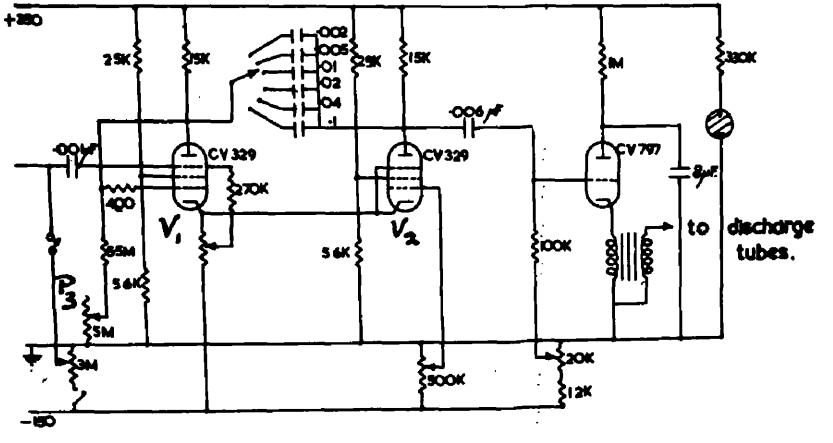

Fig. 5.

Circuit of delay unit.

cathode coupled CV329 with a variable condenser between the anode of the second and the grid of the first.

Normally the first valve was conducting; the second cut off. The 50 volt negative gun pulse supplied to the suppressor of the first valve cut it off. The cathode voltage therefore dropped until the second valve started to conduct. The anode voltage of V_2 consequently dropped suddenly forcing the grid of V_1 still further below cut off. V_1 would start to conduct again only when the condenser between its grid and the anode of V_2 charged up, a time determined by P_3, 5.5 M, the particular condenser, and the 15 K resistor. Thus the time delay could be varied by choosing different condenser values, and potentiometer P_3 gave a fine control.

The voltage pulse from the anode of V_2 was fed on to the grid of the thyratron CV797 through a differentiating circuit so that the thyratron was triggered on the back edge of the pulse. A condenser of 8 μF discharged through the thyratron and the primary winding of an induction coil to give the

voltage spark to discharge the flash lamps.

The time delays of the various condensers as measured on a C.R.O were

1.	20	to	40	msecs.
2.	50	"	100	"
3.	85	"	170	"
4.	250	"	480	"
5.	430	"	850	"
6.	900	"	1800	"

In the argon experiment a time delay of 120 msecs. was used.

Measurement of Output.

In order to be able to estimate the yield of photoprotons emitted in the experiment some method of summing the individual pulses was required. This was achieved by photographing the amplified output pulses from the ionisation chamber as displayed on an oscilloscope. The amplifier settings were kept constant throughout.

An absolute calibration could then be made by irradiating copper foil for 15 mins. maintaining a constant beam, and photographing pulses every few

seconds. By making an absolute count of the induced activity in the copper, and assuming Katz[63] yield curves for copper to be accurate, the output in r/min, and hence in r/unit pulse height could be calculated.

Analysis.

The thresholds for the most important reactions were calculated from mass data and these are shown below.

Reaction	Threshold MeV.	
(γ,p)	11.2	(12.44 exptlly.)
(γ,α)	5.9	
(γ,d)	18.6	
(γ,pn)	21.4	

The maximum possible energy of a Cl^{39} nucleus recoiling from an $A^{40}(\gamma,p)$ reaction was $\sim$ 0.3 MeV in this experiment. Such a recoil would have a range of less than 1 m.m. and consequently could not be measured accurately. Thus the recoil nucleons from (γ,n) reaction were not detected for a similar reason, and it was not possible to separate (γ,p) from (γ,pn) and (γ,d) reactions. However, since the

cross sections for these reactions are generally much lower than that for (γ, p), the numbers of these reactions was considered to be small. Other uncertainties are due to impurities like oxygen and carbon in the diffusing vapour. For reactions in either of these the recoils are likely to be $\sim \cdot 1$ cm. Thus no events were accepted in which a measurable recoil was visible. One definite example of the disintegration of an impurity is ~~the~~ a three pronged star which might well be $C^{12}(\gamma, 3\alpha)$.

To measure the angle between directions of emission and the direction of the incident γ beam the method of reprojection was used, the films being replaced in the cameras and being illuminated from behind so that an image of the photograph was projected onto a moveable plane. By moving this plane until coincidence of the two projected images of any one track from the two cameras was obtained, it was possible to fix the position in space of the original track.

In order to measure the direction of protons with respect to the direction of the incident beam,

a wire was fixed to the reprojection stand in the direction, with respect to the reprojected photographs, of the γ-ray beam. A fine needle, six inches long was suspended over this and counterbalanced so that it could be lowered into a horizontal position above the reprojection table. The shadow cast by this needle on the reprojection table was then used as an aid to measuring the angle of emission of the protons, since, in most cases, it was possible to tilt the table into a plane that contained both the track and the horizontal shadow representing the beam direction. The required angle could then be read off directly using a protractor. By this means the proton angle could be measured to an accuracy of about 3^{o}.

Conclusions of Argon Experiment.

An angular distribution was constructed from the 118 proton tracks that were confidently interpreted. These were plotted in both 20^{o} and 30^{o} intervals. A correction was made for the solid angle subtended by each angular interval. This correction is largest for small angles, and so the

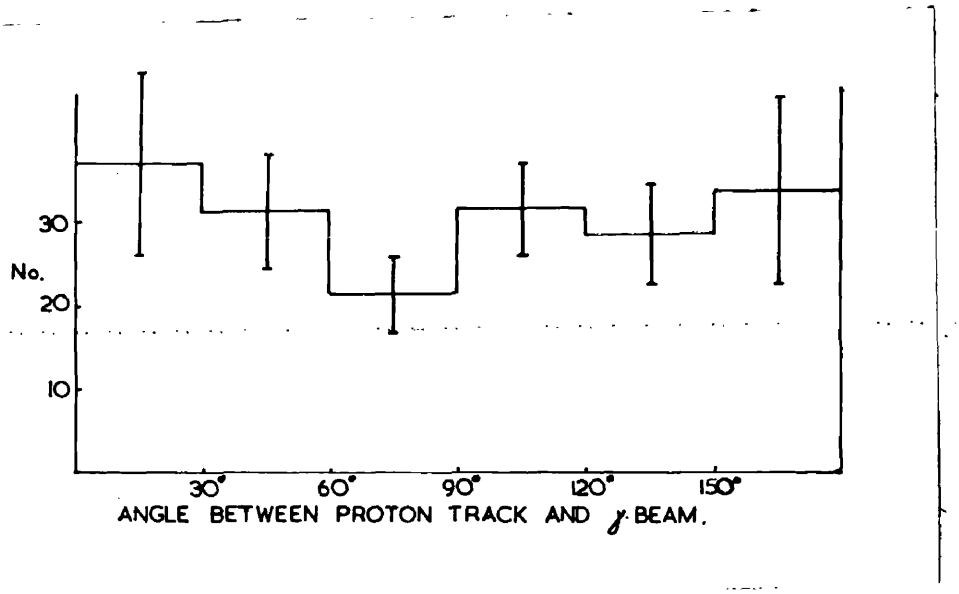

Fig. 6.

Angular distribution with respect to γ beam direction of protons from $A^{40}(\gamma,p)Cl^{39}$.

error in the 0° to 20° and 160° to 180° groups may be large.

The distribution resulting from this correction might well be taken as an isotropic distribution. Such a distribution could not be related to emission from a shell model since emission from the $(2S_{\frac{1}{2}})$ shell would give a pure $\sin^2\theta$ distribution, and the $(1d_{\frac{3}{2}})$ level would give $1 + \sin^2\theta$. In general, the distribution resulting from a shell model would be $a + b \sin^2\theta$.

The isotropic distribution obtained could be related only to a compound nucleus model. A calculation of the angular distribution resulting from a compound nucleus can be made if it is assumed that the compound nucleus has a well defined spin. Assuming electric dipole absorption into the ground state $(0+)$ of A^{40}, a 1^- state is obtained for the compound nucleus state. If this should decay by emission of a proton with $\ell = 0$ to leave a residual nucleus with $I = \frac{3}{2}^-$ or $\frac{1}{2}^-$, then the resulting angular distribution would be isotropic.

If we argue from the angular distribution to

claim that the Cl^{39} is left in either a $\frac{3}{2}-$ or $\frac{1}{2}-$ state, then since Penning[62] et al. have shown the ground state of Cl^{39} to be $\frac{3}{2}+$ (by β decay expts.) we must conclude that the transitions observed were all to an excited state.

In an attempt to explain the discrepancy in angular distribution between that obtained by Spicer and this one, it might be claimed that the majority of protons emitted have energy less than 2 MeV and would be missed by Spicer's photographic plate method, so that he saw only the more energetic protons resulting mainly from a direct interaction.

Komar and Iavor[24] have reported a proton angular distribution from A^{40}, measured by means of a cloud chamber, and have claimed to find agreement with Spicer. They make no mention, however, of having applied the solid angle correction to their results.

This preliminary experiment has given too few events to be conclusive. Many more events would be required at each of several peak energies to verify the curve obtained by McPherson et al. and to obtain angular distributions which might give a clue to the mechanism involved in the proton emission.

Photograph showing disintegrations produced in a diffusion cloud chamber by 23 MeV γ beam.

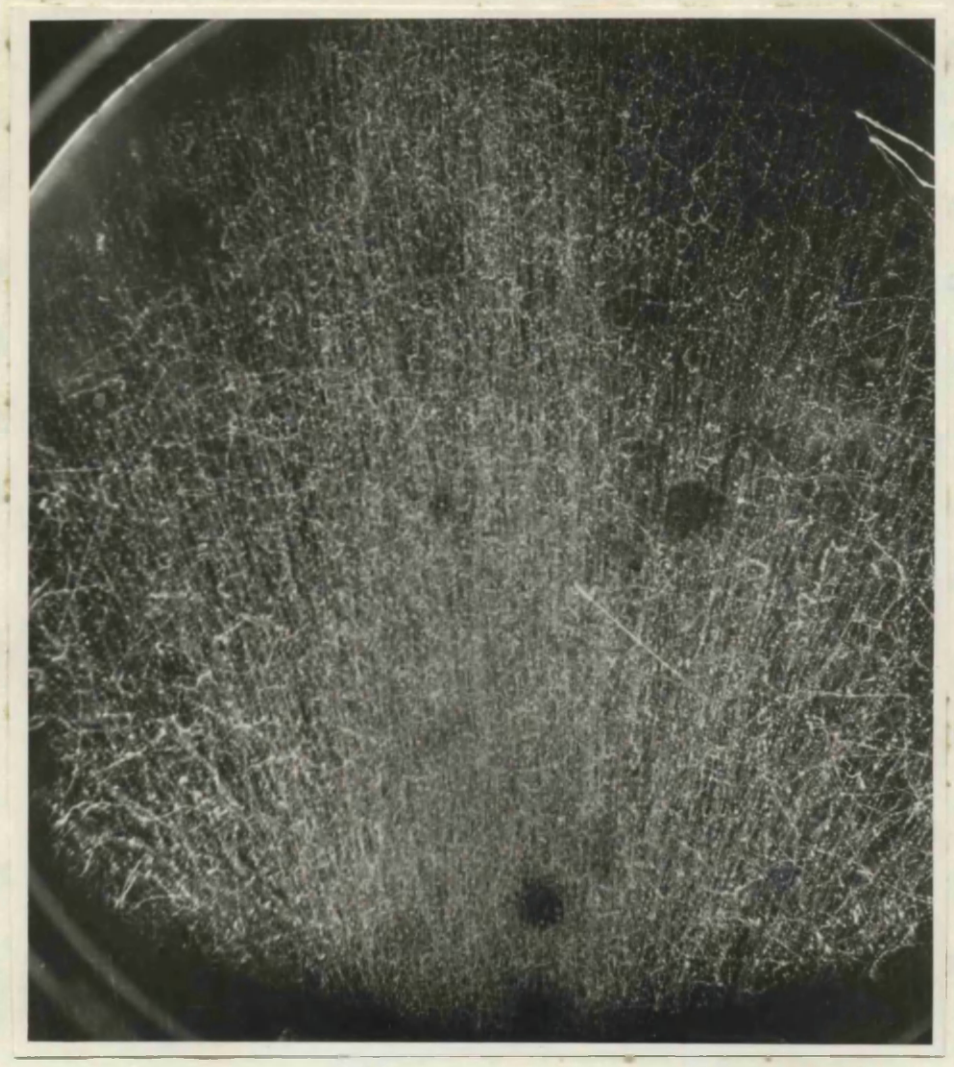

f 48(b).

Photograph showing disintegrations produced in a diffusion cloud chamber by 23 MeV γ beam.

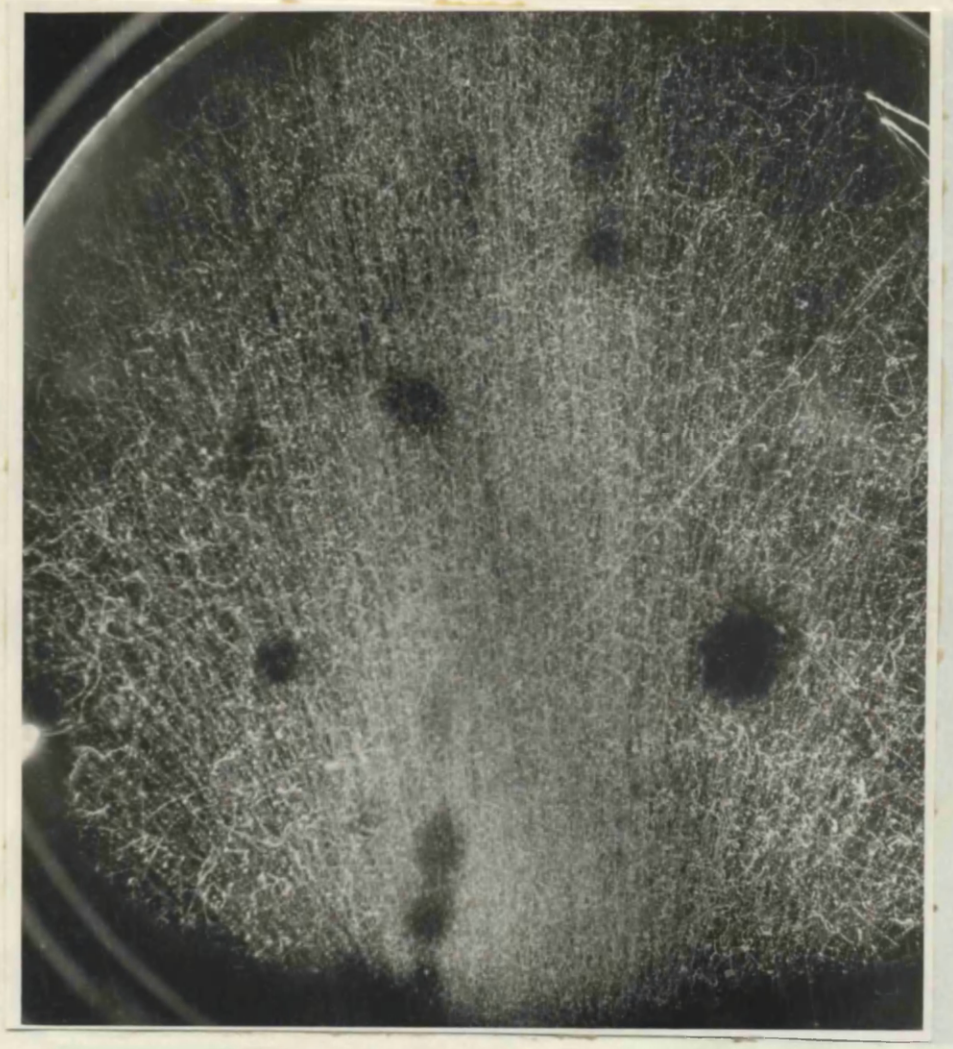

$A^{40}(\gamma, p)Cl^{39}$

f 48(c).

Photograph showing disintegrations produced in a diffusion cloud chamber by 23 MeV γ beam.

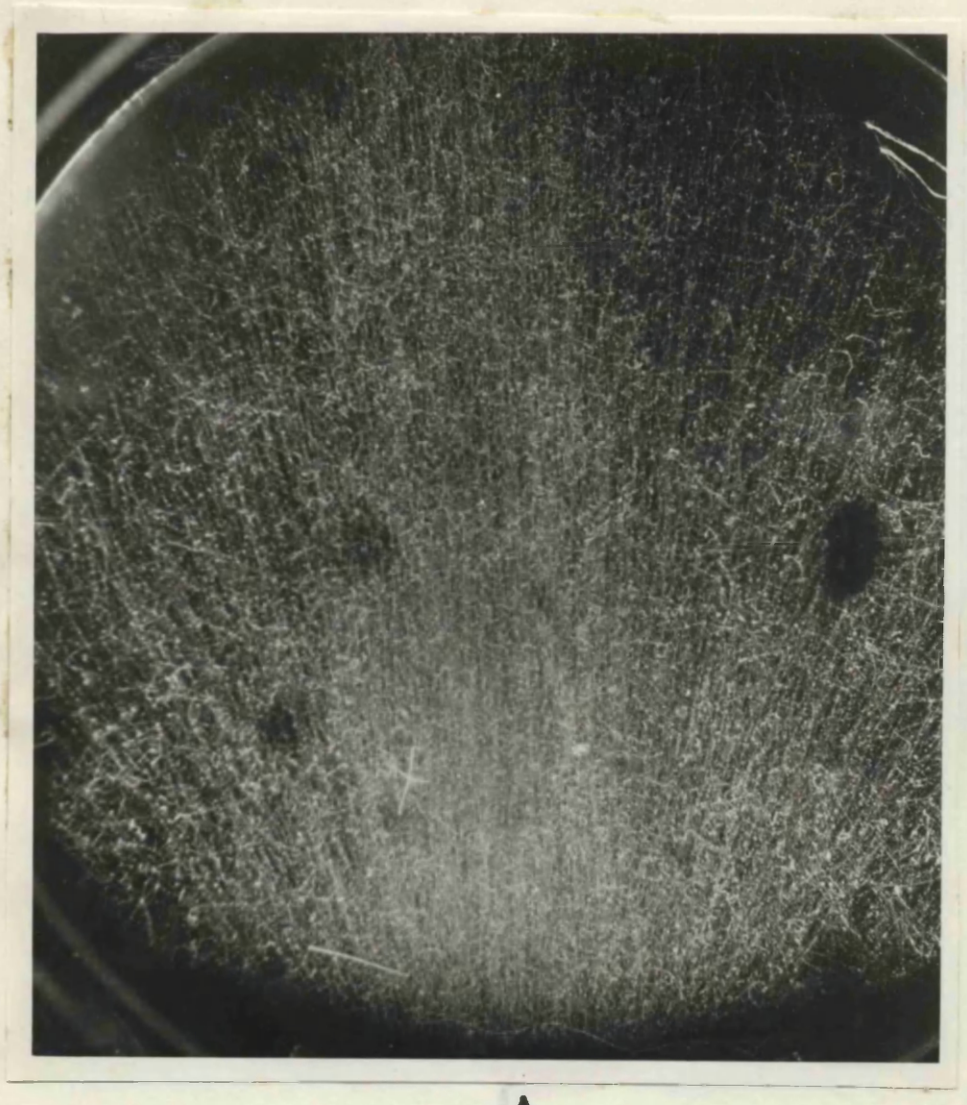

Star : $O^{16}(\gamma, 4\alpha)$.

It was unfortunate that the synchrotron broke down before more results could be obtained, and, up to date, it has not operated satisfactorily again. It was not even possible to perform the calibration experiments to assess the yield properly. Fortunately, however, Eichler and Gudden[65] took up the same experiment in Heidelberg with 15 MeV bremsstrahlung and have since published results which invalidate Spicer's hypothesis.

The experiment, however, proved valuable in showing the applicability of the diffusion chamber to this kind of study. Photographs of excellent track quality and contrast with the electron background were obtained. These compare well with the photographs of Wright et al. and justify the importance of the diffusion cloud chamber as another technique for exploring photodisintegration in gases.

CHAPTER III. NITROGEN PHOTODISINTEGRATION: EXPERIMENTAL PROCEDURE AND ANALYSIS.

In the experiment about to be described nitrogen gas was disintegrated in an expansion chamber by a 200 MeV bremsstrahlung from a synchrotron, the timing of the chamber expansion being adjusted to reveal the tracks of the charged particles resulting from photodisintegration.

In this laboratory nitrogen photodisintegration has been studied by Wright et al[21] at low energies (23 MeV) and by Lalovic and Reid,[83] using a triggered chamber, at high energies (≯80 MeV). The experiment described here bridges the energy gap between these two, and reveals for the first time how information about the nuclear photoprocess may be obtained from a study of the recoil nuclei.

Recoil Measurements.

The measurements which can be made on recoils are:

(a) the angle with respect to the γ beam.

(b) the angles between the recoil and other fragments.

(c) range.

The conventional expansion chamber is by far the best means of recording this information. To obtain recoil ranges long enough to be measured accurately, the chamber was operated at 36 cms. Hg pressure. This reduced pressure had the additional advantage of reducing the electron background in the beam, thereby allowing the charged particle tracks to stand out more clearly.

An examination of the angles which the recoil track makes with the direction of the γ beam and with the direction of the fragment track makes possible a classification of events according to criteria which will be described in the next chapter. Thus events in which the directions of the γ beam, the track of the recoiling nucleus, and the track of the fragment are all coplanar, and in which the fragment and recoil tracks are inclined slightly forward on account of the γ-ray momentum, are classified as single particle events, and include (γ,p), (γ,d), (γ,α) etc. Where these tracks are not coplanar, or where the angle between the recoil and the fragment track differs from 180° by more than 20°, it may be concluded that

a neutron must also have been emitted to account for the lack of balance of momentum. Such events include (γ,pn), $(\gamma,p2n)$, $(\gamma,\alpha n)$, etc.

An examination of the range of the recoiling nucleus makes possible an assessment of the recoil energy, since range energy relations for the residual nuclei are now available. It is rarely possible using cloud chamber means to measure, with any degree of accuracy, how much residual energy a nucleus may have. However, for reactions in which energetic particles are emitted, it is often permissible to assume that the residual energy is negligible in comparison with the initial γ-ray energy. N^{14} is a fortunate choice of element because, in the case of neutron emission, the recoil nucleus must be left in its ground state (see later). Thus, from the range of the recoil it is possible to deduce a fairly close estimate, at least, of the incident γ-ray energy.

By observing only recoils and the direction of emission of fragments with respect to the γ-beam, it is thus possible to deduce the relative importance of competing reactions, $\frac{\gamma.p}{\gamma.n}$ for example. With

results in the form of a ratio, like this, the uncertainty of the range-energy relations, and of the shape of the γ spectrum, are both largely eliminated.

Events like (γ,p), (γ,d), etc., involving a fragment and recoil, are two body problems. Two body problems are by far the most important in nuclear photodisintegration. In the case of the three body problem, the most important reaction below the meson threshold is the (γ,pn) reaction. The reaction mechanism by which a proton and neutron are ejected from a nucleus has been described by different processes which may assume different ~~relation~~ relative importance at different energies. All of these mechanisms will be discussed in Chapter V, and it will be shown how measurements of the recoil parameters assist in assessing the relative importance of these interactions.

Experimental Arrangement.

The expansion chamber used in this investigation consisted essentially of a glass walled cylinder of diameter 12 inches and depth 3 ins. operated by a rubber diaphragm. This membrane was free to move

between the brass block, which represented the base of the chamber, and another plate, the position of which could be altered by a screw to give control of the expansion ratio. The illumination was produced by discharging a 300 μF condenser bank charged to 1.5 KeV through two Mullard discharge tubes, the light beam being collimated by cylindrical lenses to illuminate only that region of the chamber through which the γ beam passed.

The entrance window of the chamber was made of terylene, 1½" in diameter and 1 "thou" thick. The thin window was connected directly to the synchrotron port with the coupling being evacuated to cut down the electron background in the beam. Three cameras were used to photograph each beam pulse, and each was clamped, in unique position, on a stand, in order to minimise reprojection troubles. Two valves connected to the volume below the diaphragm effected the control of the chamber. The slow valve, magnetically operated, could be either open to the atmosphere, or connected to a vacuum tank, so that the chamber might be either compressed or expanded, the pressure of the

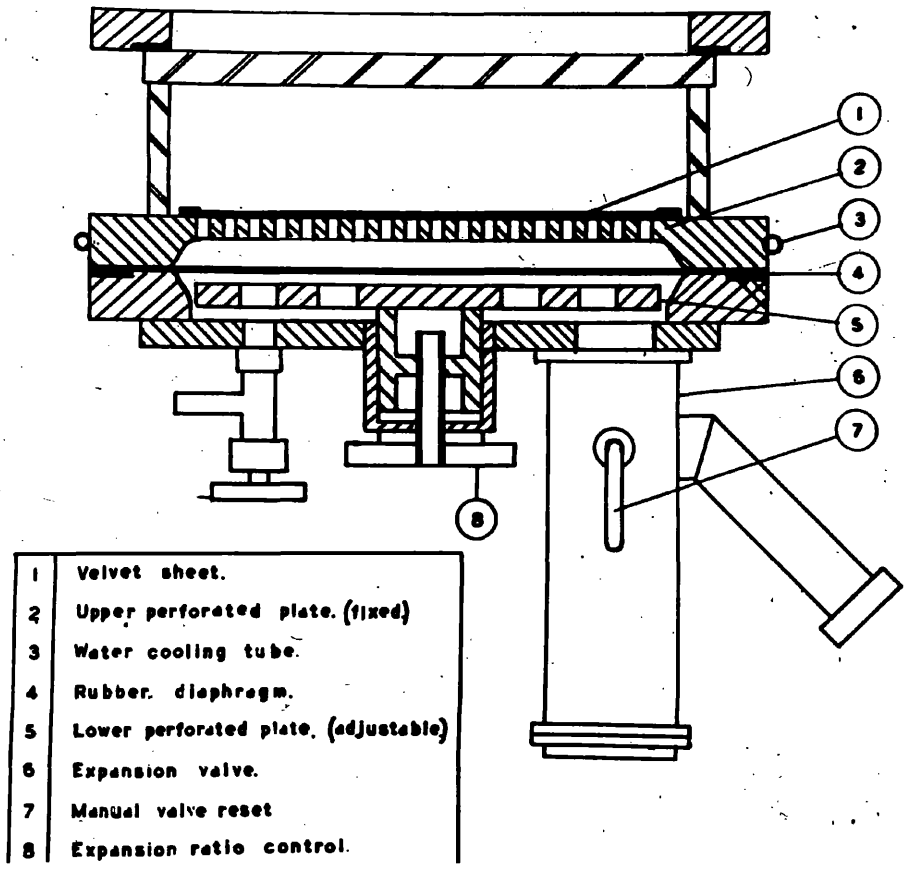

1	Velvet sheet.
2	Upper perforated plate. (fixed)
3	Water cooling tube.
4	Rubber. diaphragm.
5	Lower perforated plate. (adjustable)
6	Expansion valve.
7	Manual valve reset
8	Expansion ratio control.

Fig. 7.

Diagram of expansion chamber used in nitrogen experiment.

gas within the chamber being $\sim \frac{1}{2}$ atmosphere. The fast valve was normally sealed, but on breaking the current holding the valve closed, it could be opened by an inch diameter tube to a vacuum tank to effect a fast expansion of the chamber. Under normal operation, these valves were operated at the appropriate part of the chamber cycle by electronic control.

The choice of gas pressure within the chamber was decided by two factors. For the success of the experiment in measuring recoils it was required that the recoils should be several mms. long, necessitating a low gas pressure. On the other hand, the expansion of the chamber was dependent on the gas pressure to force the diaphragm down. Thus it was necessary to compromise, and it was found that the chamber could be operated at half an atmosphere pressure, when the C^{13} recoils, resulting from a 25 MeV γ-ray, would have a range of more than 6 mms.

To obtain the very best photographs of nuclear disintegrations certain factors must be satisfied:-

(i) It is necessary that the supersaturation should be just sufficient to give condensation on ions, a condition governed by the expansion ratio.

(ii) The γ-ray beam should be introduced when maximum supersaturation is reached, and this can be arranged by adjusting the timing of the expansion with respect to the beam pulse.

(iii) The lamp flash should occur when tracks have grown to visual size and when there is maximum contrast between the tracks and the electron background. The timing between the beam pulse and the lamp flash may be adjusted to suit this condition.

(iv) For optimum operation of the chamber itself there must be a sufficient number of slow expansions to clean the chamber while, at the same time, to minimise the time cycle, the number of "slows" must be kept to a minimum. The process of finding these optimum conditions requires several test runs. Thus to obtain the most economic use of the synchrotron, these preliminary experiments were all carried out using radioactive sources and an X-ray set.

A polonium α source was placed in the chamber

on a brass rod, and the expansion ratio was varied until α tracks were observed. Thus the optimum expansion ratio to give sharp α particle tracks was obtained by slowly varying the expansion ratio and observing the track quality. A similar experiment was repeated using a Co^{60} γ source fixed to the outside wall of the chamber, the expansion ratio being adjusted so that optimum track quality was obtained on the electron tracks. (~~See print~~). However, while a radioactive source is sufficient to reveal the correct expansion ratio and the number of slow expansions required to clear the chamber, it is totally useless, because of its continuous emission, in attempting to find out optimum timing. Thus it is necessary to have a pulsed source with a beam length of the order of a millisec. For this purpose, a medical X-ray set was modified, to give a pulsed beam, by discharging a condenser through a thyratron and through the primary winding of the main transformer.

For a timing source a dekatron unit was used, and, from this, pulses could be obtained with a time

difference in multiples of twenty millisecs. Pulses from this unit were used to operate the chamber expansion, the triggering of the thyratron to operate the X-ray set, and the flashing of the discharge tubes. Thus it was possible to simulate completely the cycle later to be used with the synchrotron, and to determine, in advance, the correct expansion ratio, and the time intervals between chamber expansion and beam, and between beam and lamp flash, so that optimum track quality could be obtained. The X-ray pulses were photographed using Ilford 5G91, 60 mm. film, by all three cameras, so that all defects in the experimental cycle were corrected before the main experiment was started.

In practice the optimum conditions were :-

expansion ratio ~ 1.30

time period between expansion and X-ray pulse ~180 msecs.

" " " X-ray pulse " lamp flash ~ 120 "

Synchrotron Output.

In order to record the dose of radiation used to disintegrate the gas, the pulse from an ionisation chamber in the beam was displayed on an oscilloscope

and also on a ballistic ~~metre~~ meter. Since the C.R.O. was found to "saturate", it was found more reliable to note the ballistic deflections obtained for each pulse and to relate these to constant deflection conditions over a fixed time during which the total dose was recorded on an integrating monitor.

Reprojection of Photographs.

The conventional method of analysing cloud chamber photographs is that of reprojection. The films, having been developed, are replaced in the cameras and a powerful light source, fitted to the back of ~~the~~ each camera, projects the film through the camera lens on to a moveable plane situated, with respect to the cameras, in the position originally occupied by the chamber. In the experimental work described here, this moveable plane consisted of a table free to tilt about a horizontal axis through its centre. In the course of the reprojection, the axis was set in the direction of the incident γ-rays so that events in which the incident quantum, the fragment and recoil directions were all coplanar were easily separated from non-coplanar events. In addition to this

f 59.

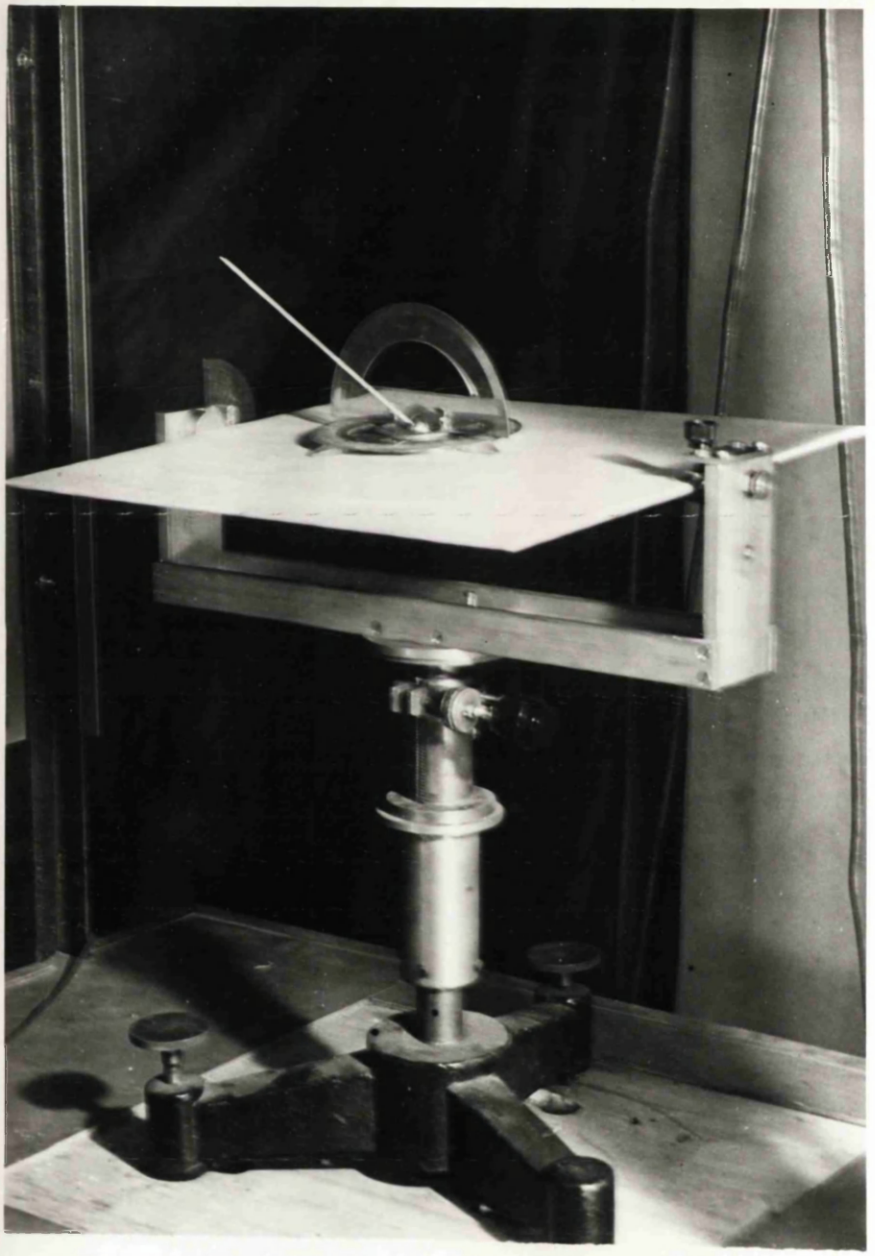

tilting movement, the reprojection table was adjustable, by a racking device, to any required height. Thus, to measure any track, the images cast by two of the cameras could be made parallel by tilting the table and could be brought coincident by adjusting the vertical height of the table. This required that the films be properly located in all three cameras just as they were when the photographs were recorded. Grid wires on the base of the chamber were used in lining up the films. Three films were used rather than two, and the two cameras with which the track made the largest angle were used in the reprojection of that track. This was done because a track, parallel to the line between two cameras, gives parallel images irrespective of the tilt of the reprojection table.

Having obtained coincidence of the reprojected images, the ~~direction~~ range and ~~range~~ direction of the initial track may be determined by straightforward measurement of the image length, and of the angle which it makes with the incident γ beam.

For tracks of a few cms. length, the angle γ

between the track and the γ beam may be determined by this means to an accuracy of greater than 2^{o}.

For tracks of only a few millimetres the accuracy is more likely to be $\sim 5^{o}$. However, since most angular distributions are plotted in histograms in groups of 10^{o} or 20^{o} this error is not serious. The measurement of the range of short recoils, on the other hand, cannot be carried out with a high degree of accuracy and since, in this experiment, much of the information is derived from measurements of the recoil, it was necessary to find a more sensitive method. Thus a method based on examining the recoils by microscope was developed.

Microscope Method.

This is a modification by the author and Menzies of ~~the~~ a method developed by Wright and Morrison.

The films were clamped between glass plates on a binocular microscope stage, which could be racked in the direction of, and at right angles to, the length of the film. A pair of x10 eyepieces and a x 2.5 objective were used in the microscope to

Track Simulator.

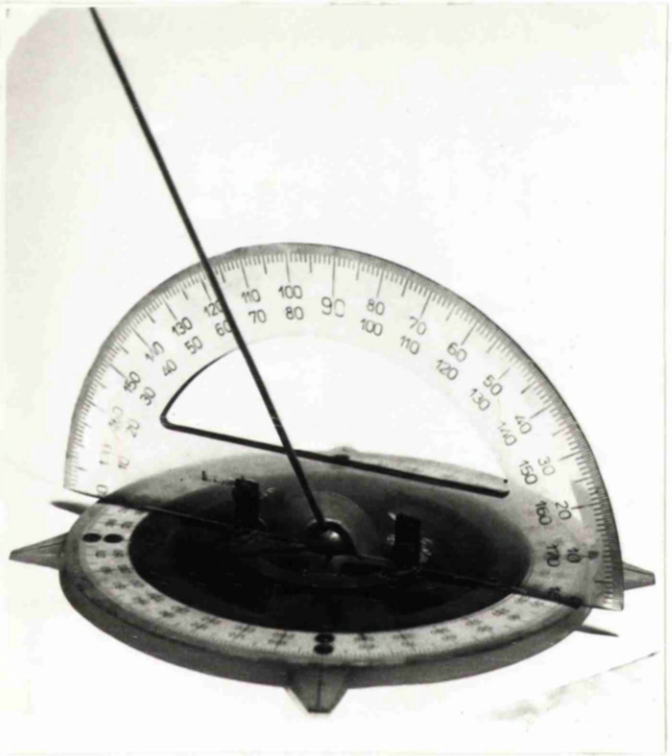

examine the film. The microscope was fitted with a cross wire and scale in one of the eyepieces, together with a goniometer head to measure angles. The grid wires in the photographs were taken as reference directions since, in the experiment, these were fixed parallel, and at right angles, to the γ beam direction. Thus the microscope measurements on any track consisted of measuring the angle ψ_i which it made with the beam in all three films (i = 1, 2, 3). Likewise the three values for the length of the track as measured on the eyepiece scale were recorded.

The determination of the actual angle and range of the track from the microscope measurements was simplified by the use of a track simulator. This consisted of a needle of about 16 cms. length fixed into a ball joint in a metal base, so that the needle could be moved to any position above the plane of the base. An angular scale, 0^{o} to 360^{o}, was fixed to the base, while a 0^{o} to 180^{o} protractor was attached to a stand, so that it was held in a vertical plane, and was free to rotate about a vertical axis through

the centre of the horizontal scale. Thus the angle which was made by the projection of the needle on the horizontal plane with respect to the γ beam direction, and also the inclination of the needle, could both be measured directly.

The determination of the actual angle of the track is based on the fact that the projection of the track on the horizontal plane, and the image obtained on the film, are both inclined to the γ beam by the same angle. The table was adjusted in a horizontal position until coincidence was obtained on the origin of the event. The track simulator was placed over this point, and the zero on the horizontal scale was set along the direction of the beam. The position of the needle was set so that the angles formed on the horizontal scale by the shadow from each of the three cameras, were equal to the corresponding angles measured by the microscope. This position of the needle gave the direction of the actual track. In the case of the track sloping down, the angles to which the simulator had to be set were $180^{\circ}+\psi_i \ (i=1,2,3)$. in each case. Thus the angle made by the projection of the track on the horizontal plane with the γ beam

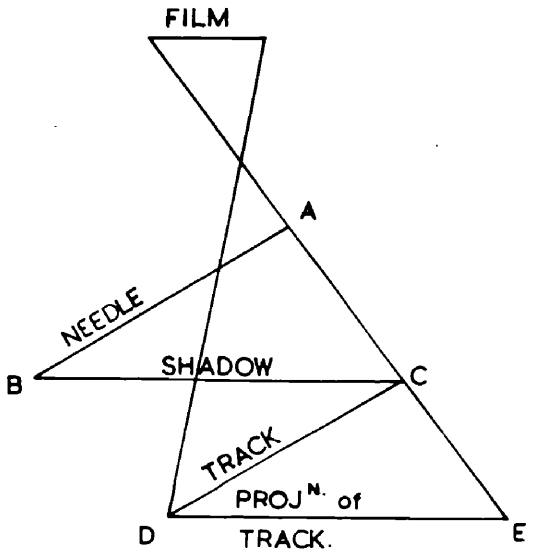

Fig. 8.

Diagram to illustrate the calculation of ranges of tracks.

direction, θ, and the angle of inclination of the track α, could be measured from the scales on the simulator. θ was considered + ve or -ve depending on whether the angle was to the right or left of the beam. α was + ve or -ve depending on whether the track was tilted up or down with respect to the horizontal. To determine the length of the track, the horizontal table was raised to the highest point of the track. The track simulator, still in the direction just described, was then moved until the tip of the shadow of the needle, projected by one camera, corresponded with this point of the track. This was repeated using shadows projected by the other two cameras. By measuring the length of the shadow of the needle in each case it was then possible to calculate a mean value for the real length of the track. The calculation can best be seen from the diagram.

ABC and CDE are similar

$$\therefore \quad \frac{CD}{AB} = \frac{DE}{CB}.$$

DE = (projection of DC on base of chamber) $(1 - \frac{Z}{R})$

$= ML \ (1 - \frac{Z}{R})$

where L = length on film, M = magnification, Z = height of the highest point of the track above the chamber base. h is the height of the lenses ..

$$\ell = L \frac{\ell(\text{needle})}{\ell(\text{shadow})} M \left(1 - \frac{Z}{R}\right)$$

Thus for each film ℓ was calculated and an average value was assessed.

For tracks not steeper than 60°, ℓ(needle), ℓ(shadow) and M can be measured to within 1% accuracy. The largest error is in the microscope measurement where, for a recoil of length $\sim$ 3 mm, the error is about $\pm$ 10%.

In the analysis of the nitrogen results the films were scanned under the microscope and each event was given a provisional classification. The recoils were all measured for range and angle as outlined above. The films were then placed in the cameras and reprojected. The longer tracks were reprojected directly, while the track simulator was employed to calculate the angles, and range, required

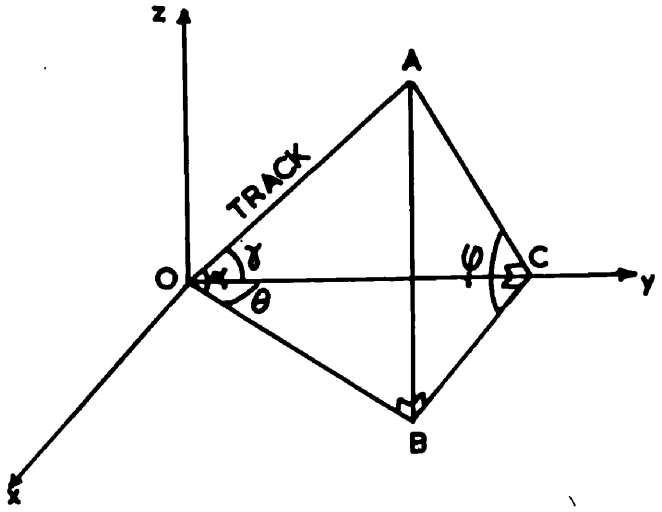

Fig. 9.

$$\cos\alpha = \frac{OB}{OA} \qquad \sin\alpha = \frac{AB}{OA}$$

$$\cos\theta = \frac{OC}{OB} \qquad \sin\gamma = \frac{AC}{OA}$$

$$\therefore \cos\gamma = \frac{OC}{OA} = \cos\alpha\cos\theta \qquad \therefore \sin\varphi = \frac{AB}{AC} = \frac{\sin\alpha}{\sin\gamma}.$$

to describe each recoil. Tracks which were long enough to be measured by reprojection could be checked against their ranges, calculated by the microscope method, and excellent agreement was obtained in all cases. Thus for each recoil track the following data was recorded:- range; θ, the angle between the horizontal projection of the track and the γ beam; α, the inclination of the track. From the angles θ and α, the actual angle between γ beam and the track was calculated from

$$\cos \gamma = \cos \alpha \cdot \cos \theta. \quad \text{(Fig 9)}.$$

Also if φ be the angle between the horizontal and the plane containing the track and the direction of the γ beam, then it can be calculated from

$$\sin \varphi = \frac{\sin \alpha}{\sin \gamma}$$

For cases where there was doubt about the coplanarity of recoil and fragment, the criterion for coplanarity was taken to be $| \varphi(\text{recoil}) + \varphi(\text{fragment}) | \leq 5^\circ$ where φ is +ve or -ve depending on whether the plane containing the particular track is tilted upwards or downwards with respect to the origin.

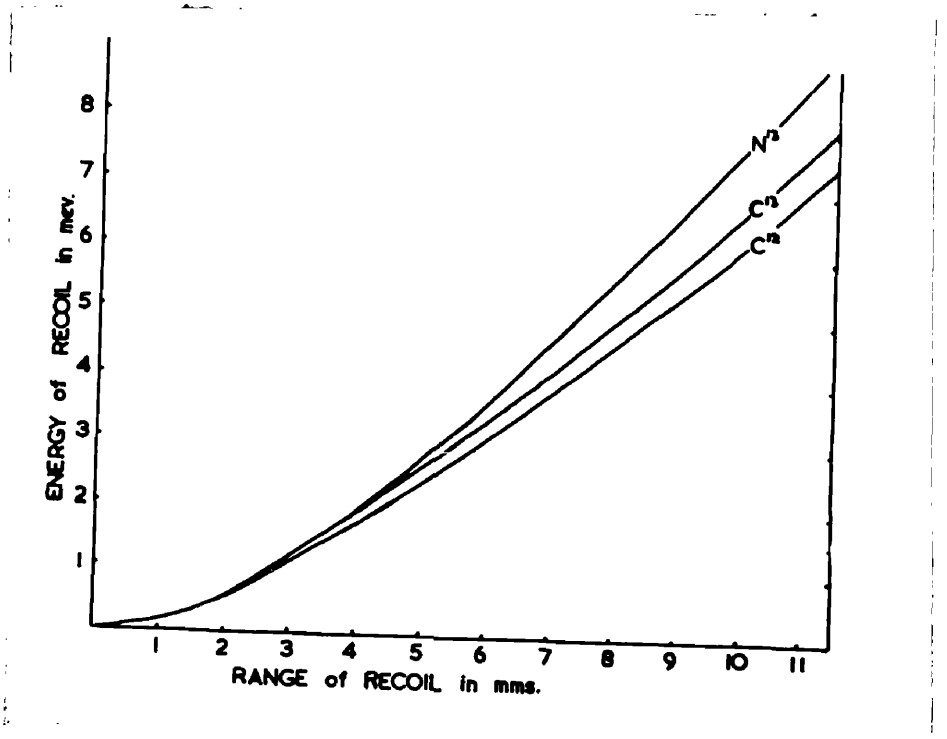

Fig. 10.

Range-energy curves for C^{13}, N^{13} and C^{12} (due to Lillie).

A few cases were recorded in which both fragment and recoil stopped within the chamber, the directions being almost directly opposite. By momentum balance these were mostly shown to be (γ,α) events. The heavy intensity of the fragment track supported this interpretation.

Range Energy Relations.

Since the rate at which a nucleus loses energy in passing through a gas is dependent on the charge of the recoil, and on the number of collisions it makes with the atoms of the gas, the factors determining the actual range are of a statistical nature.[66] For the nuclei involved in this investigation the resultant straggling is significant. According to Morrison, the straggling for C^{13}, C^{12} and N^{13} nuclei of $<$ 2 MeV is $\sim$ 10% of the total range.

The range energy curve used as a basis for our results is deduced from the experimental results of Lillie[67] who studied recoil ranges of C^{13} resulting from $O^{16}(n,\alpha)C^{13}$ induced by 14.1 MeV neutrons. Bethe's[68] range energy relationship for α particles was assumed. (See Additional Note, page 127).

CHAPTER IV. NITROGEN PHOTODISINTEGRATION: RESULTS.

Selection Criteria.

In the analysis of events, the following criteria have been observed in classifying the results.

(i) Stars.

These involve more than one charged particle together with a recoiling nucleus. In general, there is no check on the number of neutrons emitted. Only in the case of all particles stopping within the chamber, and when there are no neutrons emitted, is it possible to solve the reaction by a momentum balance.

(ii) Single Charged Particle and Recoil.

This class may be further subdivided:

(a) Events in which the directions of the charged particle, recoil and γ-ray are all coplanar, and where the sum of the angles made by the recoil and fragment with the direction of the incident beam lies between 165° and 180°. (See next section). This class includes all events in which only one particle is emitted, the recoil making an angle

slightly less than 180° on account of the momentum of the incoming γ-ray. The most important reactions involved here are (γ,p), (γ,d) and (γ,α).

α particles being doubly charged, produce greater ionisation, and this property in itself is usually sufficient to enable these to be ~~detected~~ recognised. In addition, the recoils are longer than from similar energy protons. If the α particle stops within the chamber then a momentum balance on the reaction is sufficient to determine it with certainty.

e.g. Consider a recoil of known range.

If the event be interpreted as (γ,α), and the range of recoil corresponds to 2 MeV, then the energy of the α particle will be about 5 MeV. There is a very large probability of such an α particle stopping within the chamber. If the event be interpreted as (γ,p) then the recoil will have energy greater than 2 MeV. The proton ~~which~~ will certainly leave the chamber.* It is comparatively easy to distinguish between a 5 MeV α particle and a 30 MeV proton on the grounds of ionisation density.

* Proton energy ~ 26 mev.

There is, however, no effective means of discriminating between (γ,p) and (γ,d) events, since protons and deuterons have both unit charge. Only if the particle stops within the chamber is it possible to distinguish between the two.

(b) Events in which the directions of the beam, fragment and recoil are not coplanar. In this case the conservation of momentum implies that a neutron must also have been emitted. All angles between neutron and proton are possible.

The most important reaction in this class is the (γ,pn). Others like (γ,dn), (γ, n), (γ,tn), (γ,p2n), etc. are all possible, but the (γ,pn) reaction is by far the most important.

(iii) Recoils Only.

Short recoils may be detected resulting from reactions which do not involve the emission of a charged particle. This group includes (γ,n), (γ,2n), (γ,3n) etc. The (γ,n) is considered to be the most important of these.

Non-collinearity of γ,p Events.

By applying energy and momentum conservation to

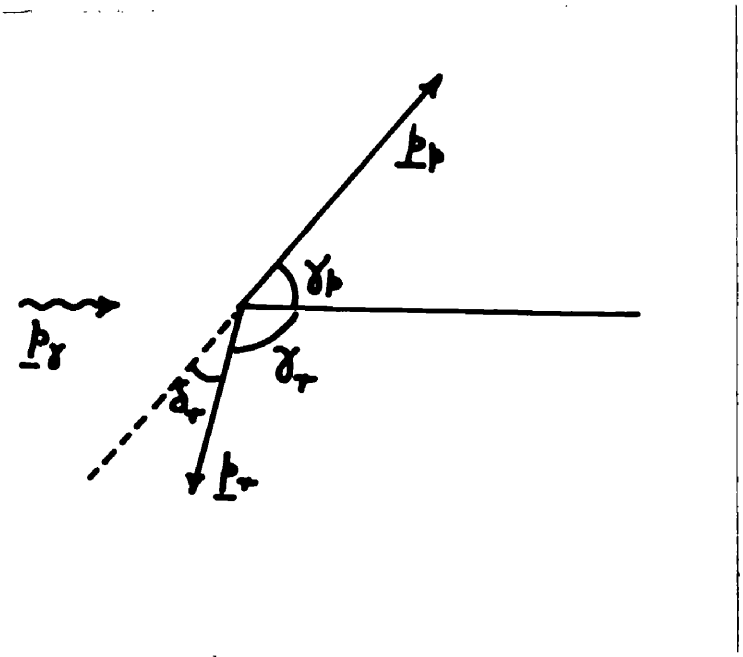

Fig. 11.

Diagram to illustrate the derivation of δ_r in terms of E_γ and γ_p.

p_p = momentum of proton = $\sqrt{2M_p E_p}$ $\frac{\text{MeV}}{c}$ where M_p is the mass of the proton in $\frac{\text{MeV}}{c^2}$

p_r = momentum of recoil = $\sqrt{2M_r E_r}$ $\frac{\text{MeV}}{c}$ where M_r is the mass of the recoil in $\frac{\text{MeV}}{c^2}$

p_γ = momentum of γ ray in $\frac{\text{MeV}}{c}$

Q = threshold energy of the reaction.

f 70 b.

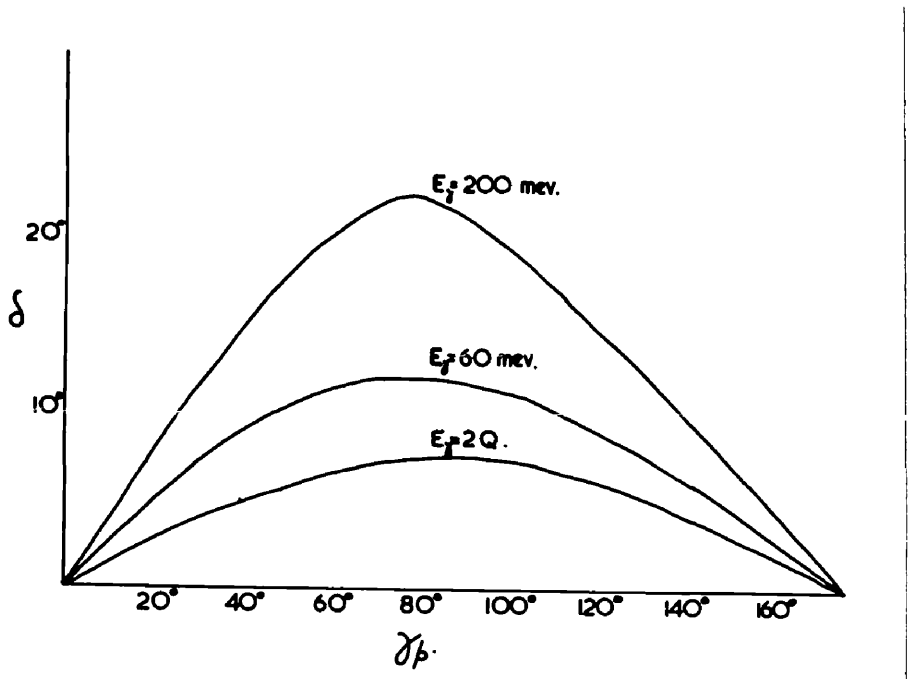

Fig. 12.

Plot of δ against γ_p for E_γ = 20, 60 MeV and 200 MeV.

the (γ,p) disintegration the following equations are obtained:

$$p_\gamma \cos\gamma_p = p_p - p_\nu \cos\delta_\nu. \quad (\text{mom}^m \text{ along } \not\perp p_p)$$

$$p_\gamma \sin\gamma_p = p_\nu \sin\delta_\nu. \quad (\text{mom}^m \perp \not\perp p_p)$$

$$E_\gamma = E_p + E_\nu + Q. \quad (\text{energy eqn.}).$$

$Q = 7.54$ mev for $N^{14}(\gamma,p)C^{13}$.

where the various terms are as defined in fig. 11.

The excitation of the residual nucleus is considered to be small compared with E_γ.

E_p and E_ν may be eliminated to obtain δ_ν in terms of E_γ and γ_p. Curves of δ_ν against γ_p were calculated for different E_γ and are shown in fig. 12.

The curve which gives the minimum values of δ_ν occurs at $E_\gamma = 2Q$. Since all recorded events had recoil ranges corresponding to energies of <60 MeV, only those coplanar events which lay between the minimum curve and that for $E_\gamma = 60$ MeV were accepted as (γ,p) events. A certain laxity in this criterion was allowed at small and large angles.

f 71.

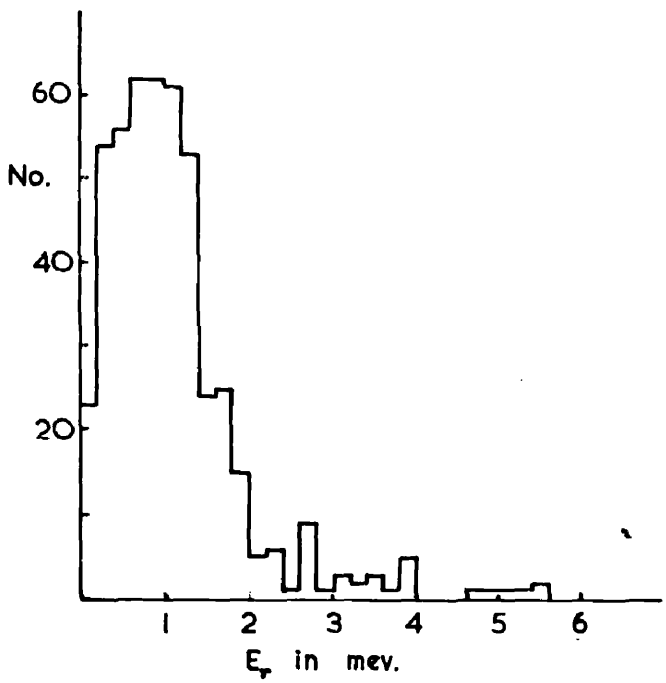

Fig. 13.

Energy distribution of recoils from $N^{14}(\gamma,p)C^{13}$

B.

Ratio of Events.

Following the criteria outlined in the earlier section, the events on the photographs were separated into the classes: (γ,p), (γ,n), (γ,pn) and (γ,α). 1969 events were recorded in which the angles of the fragments were less than 60^{o} to the horizontal. 528 were identified as (γ,p) events, 627 as (γ,n), 786 as (γ,pn) and 28 as (γ,α).

Hence the ratio of the number of events is

$(\gamma,p) : (\gamma,n) : (\gamma,pn) : (\gamma,\alpha)$ 1 : 1.18 : 1.49 : 0.05.

This ratio is in effect that of the integrated cross sections for these reactions.

C.

The Reaction $N^{14}(\gamma,p)C^{13}$

The energy of each recoil was obtained from the range energy curve due to Lillie for C^{13} nuclei, as described in Chapter III.

Energy Distribution of Recoils.

A plot of the number of recoils with energy E_r as a function of E_r is shown in fig. 13 . This has the form of a broad peak centred on 0.8 MeV with a high energy tail falling off to a low value at 4 to 5 MeV.

The error resulting from the measurement of the length of the track is of the order of 0.1 MeV. However, errors due to straggling of the recoils are important in this energy range, and these errors might be $\sim$ 0.2 MeV. Thus the histogram was plotted in 0.2 MeV steps.

To obtain an energy distribution of the protons it is necessary to calculate E_p , the energy of each proton, for each event, from the recorded measurements.

Calculation of E_p

If in the (γ,p) reaction the momentum of the incident quantum be very small, the proton and recoil directions would be opposite. Then, by applying momentum conservation

$$E_p = \frac{M_n}{M_p} E_n$$

However, in the (γ,p) events recorded, the direction of the proton and recoil tracks differed from 180° by as much as 15° and, consequently, it was considered necessary to apply some correction for the

γ momentum.

The equations governing the (γ,p) reaction may be written

$$p_p \sin\gamma_p = p_r \sin\gamma_r \qquad (\text{mom}^{n} \perp \gamma \text{ direction})$$

$$p_\gamma = p_p \cos\gamma_p + p_r \cos\gamma_r \quad (\text{mom}^{n} \parallel \gamma \text{ direction})$$

$$E_\gamma = E_p + E_r + Q + E^* \quad (\text{energy eqn}).$$

The terms are as defined in section A fig.11. except that E^* represents the excitation energy of the residual nucleus.

The unknown terms are E_p, E_γ and E^*, and so the three equations can be solved for each of these

$$E_p = \frac{M_r}{M_p} E_r \left(\frac{\sin\gamma_r}{\sin\gamma_p}\right)^2, \qquad E_\gamma = \sqrt{2M_r E_r}\,\frac{\sin(\gamma_r+\gamma_p)}{\sin\gamma_p}$$

$$E^* = E_\gamma - (E_p + E_r + Q)$$

However these solutions for E_p and E_γ are

unsatisfactory in that large errors result from the ratio of sin terms, and consequently E^* is very inaccurate.

e.g. (i) E_γ = 0.4 MeV $\gamma_\gamma = 99°$ $\gamma_p = 68°$.

This gives E_p = 5.9 MeV and E_γ = 24 MeV.

Consequently E^* = 24 - (5.9 + 0.4 + 7.5) = 10.2 MeV. The errors in E_γ however are large as a result of the factor

$\frac{\sin(\gamma_\gamma + \gamma_p)}{\sin \gamma_p}$ or $\frac{\sin \delta}{\sin \gamma_p}$ where $\delta = 180° - (\gamma_\gamma + \gamma_p)$

δ is small and subject to errors of measurement of a few degrees. Sin δ varies rapidly in this region and consequently, E_γ changes by a factor of 2 as δ increases from 7° to 14°. With a short recoil, γ_γ cannot be determined to an accuracy of greater than a few degrees.

(ii) $E_\gamma = 1.2$ mev $\gamma_\gamma = 115°$. $\gamma_p = 154°$.

$\therefore E_p = 5.4$ mev.

Again with small γ_p , sin γ_p varies rapidly and any inaccuracy is doubled by the square. Hence, values of E_p computed in this way are liable to large inaccuracies.

A more suitable determination of E_p can be obtained by assuming that $E^*_{residual} << E_\gamma$ so that E^* may be neglected. Since the excitation energy can never be more than a few MeV (fig. 26), and typical γ- energies are $\sim$ 25 MeV, this assumption is a reasonable one.

Thus three equations are available for each reaction and there are only two unknowns, E_γ and E_p . Thus E_p may be obtained in terms of γ_r and γ_p , E_r and γ_r , E_r and γ_p and the inaccuracy of one experimental determination may be removed. E_p in terms of γ_p and γ_r is inaccurate, and so E_p was calculated from E_r and γ_r, a form that can also be applied to (γ,n) events where the neutron direction is not known.

The full solution of E_p is complicated and not suited to the rapid calculation of a few hundred events. Approximations were therefore introduced

f 76a.

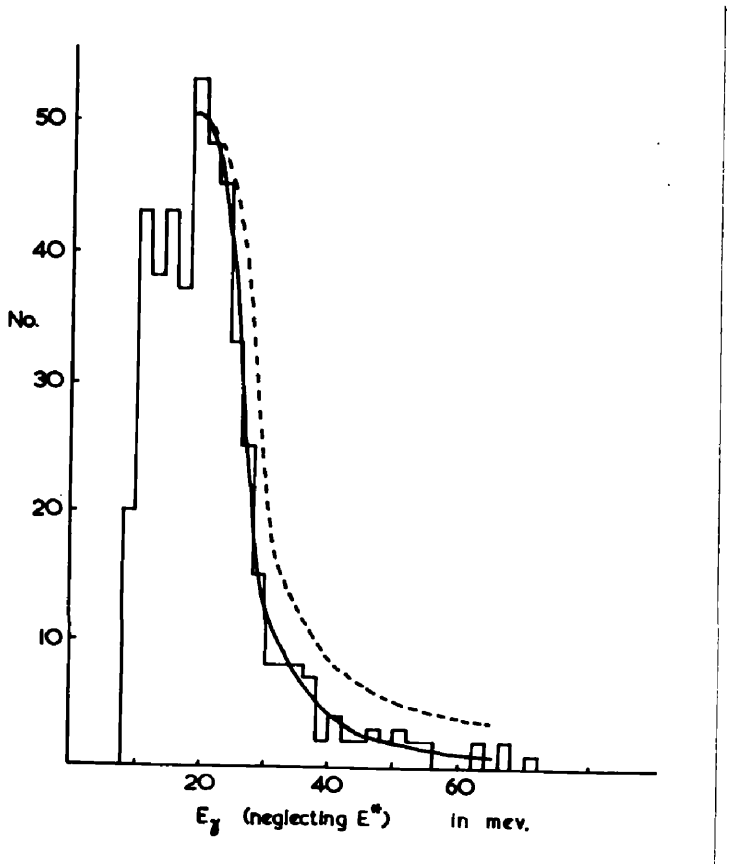

Fig. 14(a)

Number of $N^{14}(\gamma,p)C^{13}$ events as a function of E_γ.

The residual excitation energy is neglected.

f76b.

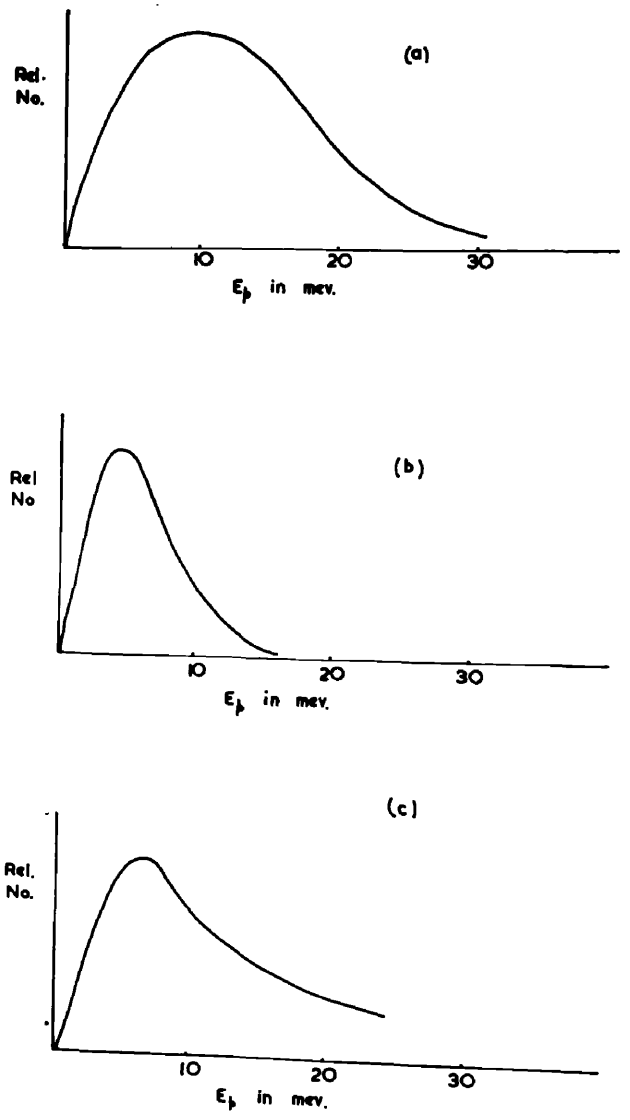

Fig. 14(b)

Energy distribution of protons from $N^{14}(\gamma,p)C^{13}$.

(a) obtained from smooth curve through the measured histogram.

(b) calculated from evaporation theory.

(c) calculated from a "direct" theory.

to give the form:

$$E_p = \frac{M_n}{M_p} E_\gamma \frac{1}{1 + \frac{\sqrt{M_n E_\gamma}}{M_p} \cos\gamma_\gamma}.$$

The inaccuracy in the correction due to these approximations is appreciable at small angles and decreases as $\gamma_\gamma \to 90^\circ$. However the maximum inaccuracy is $\sim$ 10% where $\gamma_\gamma = 0^\circ$. This error is not so serious since few events were recorded in the relatively small solid angle formed by small γ_γ. For larger angles the error is $\sim$ 2%.

Thus this formula was applied to give E_p for each event. Fig. 14a shows a histogram of events as a function of E_γ

The uncertainty in the energy of any proton of energy greater than 10 MeV is less than 2 MeV on the basis of Lillie's range-energy curves being accurate.

Angular Distributions of Protons from $N^{14}(\gamma,p)C^{13}$.

The directions of protons, emitted in the reaction $N^{14}(\gamma,p)C^{13}$ were measured with respect to the direction of the γ-ray beam. Protons making

f 77.

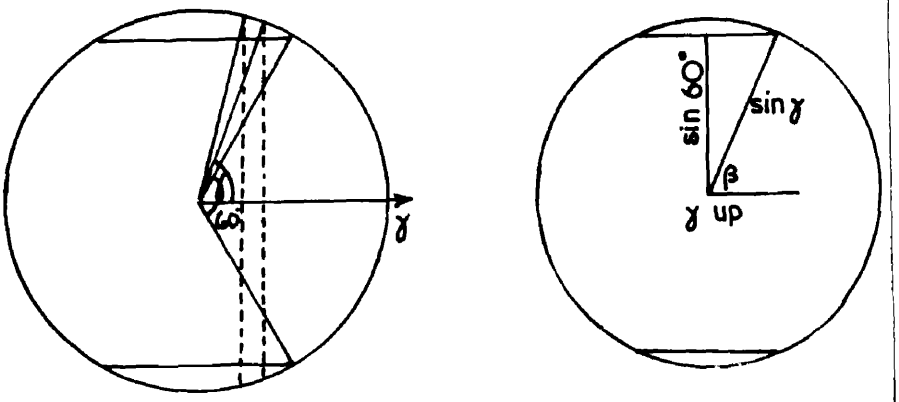

Fig. 15.

Diagram to illustrate the solid angle correction.

an angle γ_p (angle between direction of emission and beam) between 0^o and 10^o are emitted into a much smaller solid angle than those for which γ_p lies between 80^o and 90^o. Thus the distributions were corrected to the number/unit solid angle for each energy group of the distribution.

However, in order to avoid inaccuracies in track measurement due to a track being very steep, it was decided to use only those tracks whose slope was less than 60^o to the horizontal. This introduces a further correction. For $\gamma > 60^o$ the solid angle subtended by γ and $\gamma + d\gamma$ is sliced by planes which cut the unit sphere where $\gamma = 60^o$. The solid angle within the 60^o limit can be obtained by considering only the belt within the planes.

The circumference of the circle of radius $\sin\gamma$ and lying within the planes is given by

$$4 \sin^{-1}\left(\frac{\sin 60^o}{\sin\gamma}\right) \cdot \sin\gamma .$$

The solid angle between γ_0 & $\gamma_0 + d\gamma_0$ is given ven

by

$$d\Omega = 4 \sin^{-1}\left(\frac{\sin 60^\circ}{\sin \gamma}\right) \cdot \sin\gamma \, d\gamma.$$

$$\therefore [\Omega]_{\gamma_1}^{\gamma_2} = \int_{\gamma_1}^{\gamma_2} 4 \sin^{-1}\left(\frac{\sin 60^\circ}{\sin \gamma}\right) \cdot \sin\gamma \, d\gamma.$$

By integrating by parts, this expression may be reduced to

$$\Omega = 4\left\{\left[\cos\gamma \cdot \sin^{-1}\left(\frac{\sin 60^\circ}{\sin\gamma}\right)\right]_{\gamma_2}^{\gamma_1} - \left[\sin^{-1}\left(\frac{\cot\gamma}{\cot 60^\circ}\right)\right]_{\gamma_2}^{\gamma_1} + \sin 60^\circ \left[\sin^{-1}\left(\frac{\cos\gamma}{\cos 60^\circ}\right)\right]_{\gamma_2}^{\gamma_1}\right\}.$$

The solid angles subtended by the 10° intervals to contain no regions steeper than 60° to the horizontal are given in the following table:-

(See ~~opposite~~)

Angular Interval.	0°-10° 170°-180°	10°-20° 160°-170°	20°-30° 150°-160°	30°-40° 140°-150°	40°-50° 130°-140°	50°-60° 120°-130°	60°-70° 110°-120°	70°-80° 100°-110°	80°-90° 90°-100°
Solid Angle.	·095	·283	·463	·628	·774	·898	·816	·750	·733.

f79a.

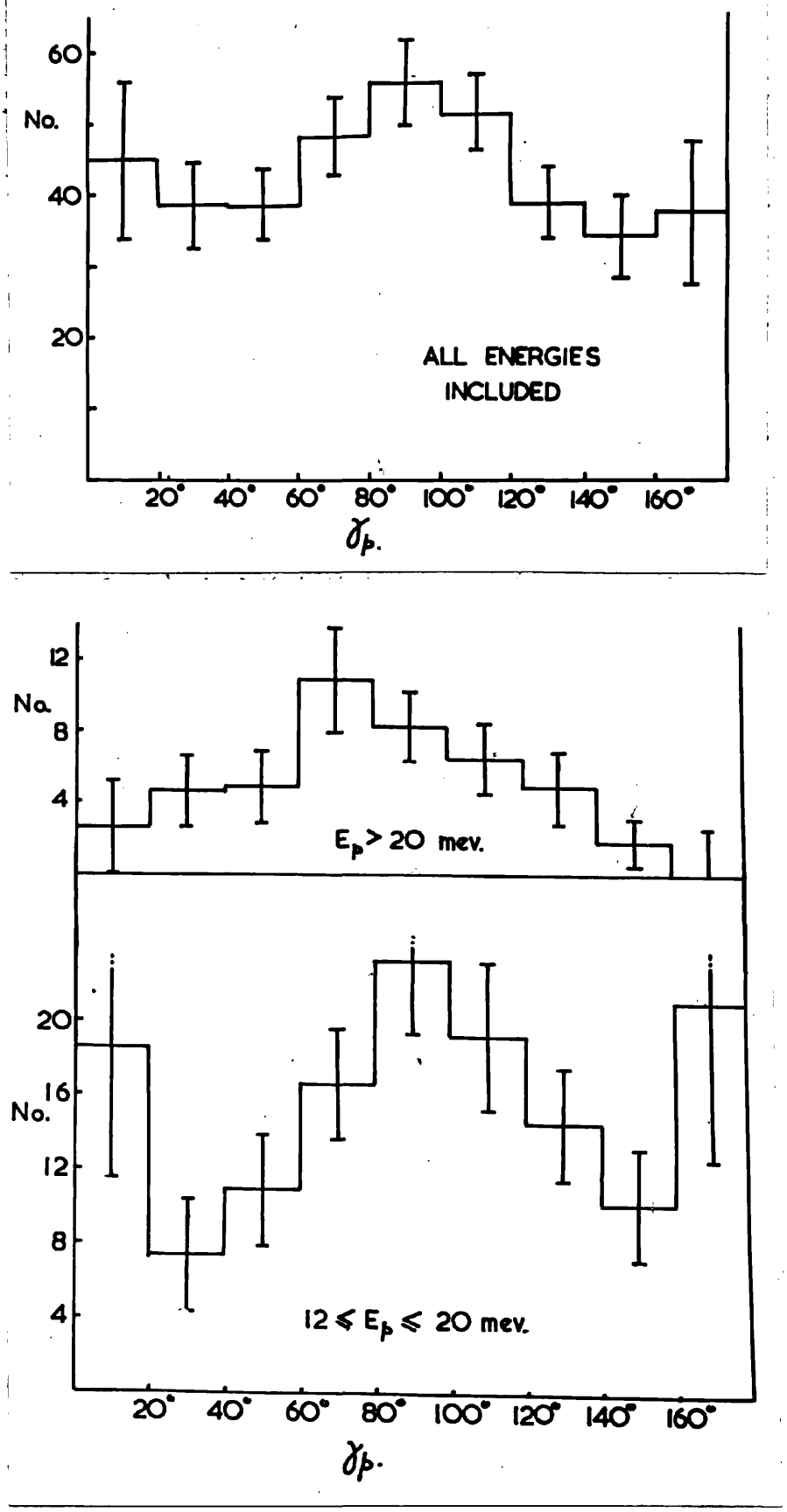

Fig. 16a.

Angular distributions of proton with respect to the γ beam direction for $N^{14}(\gamma,p)C^{13}$.

f 79 b.

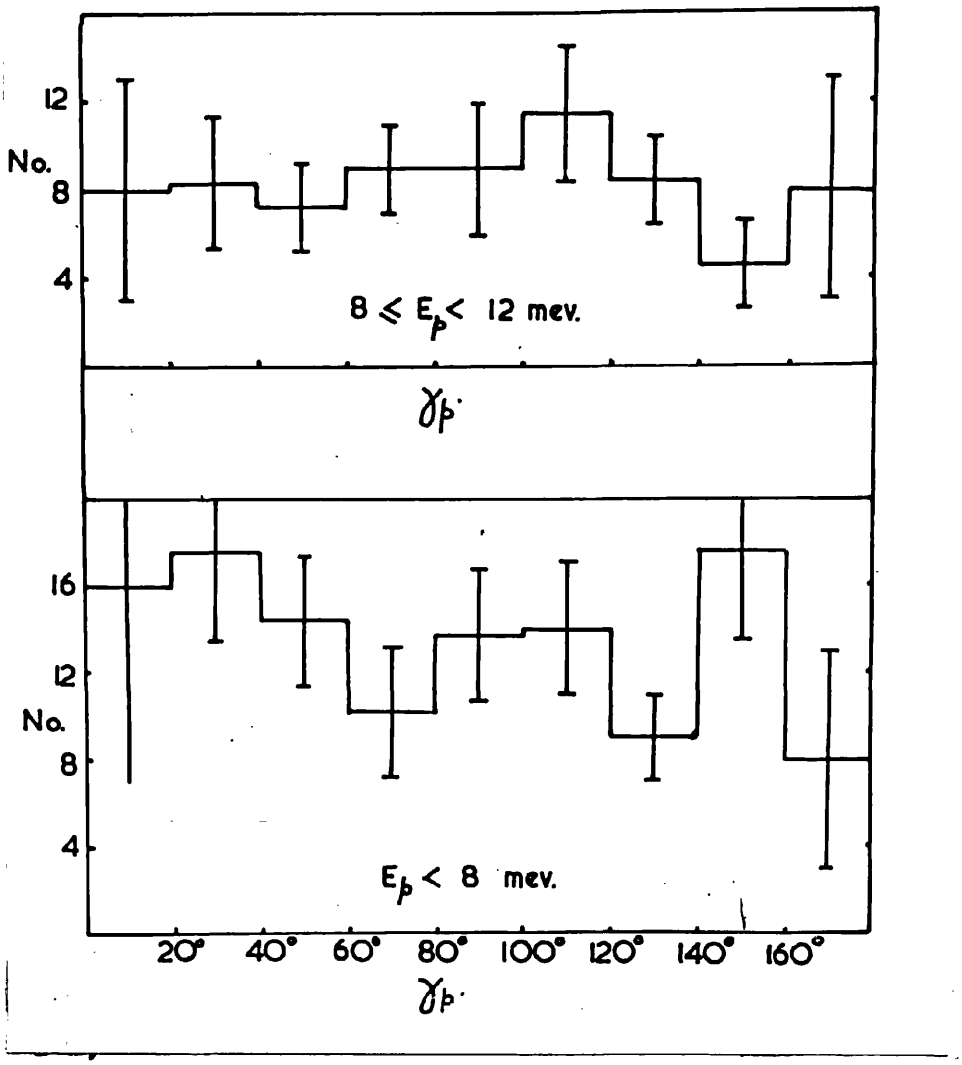
12
No.
8
4
8 ≤ Ep < 12 mev.
γp.
16
12
No.
8
4
Ep < 8 mev.
20°
40°
60°
80°
100°
120°
140°
160°
γp.

Fig 16b.

Angular Distributions.

A histogram to show the number of events per unit solid angle with 20° angular intervals is shown in fig. 16a . It contains all protons measured, and so all energies are included.

The angular distributions for particular energy groups are shown in fig. 16a,b.

These distributions show that the anisotropy revealed by the distribution including all energies is to be attributed largely to the protons corresponding to total energies greater than $E_\gamma >$ 20 MeV (i.e. protons > 12 MeV). The lower energy protons exhibit an angular distribution which is much closer to being isotropic.

D.

The Reaction $N^{14}(\gamma,n)N^{13}$.

An energy distribution of recoils from the $N^{14}(\gamma,n)N^{13}$ reaction is shown in fig. 17 . This was obtained from the measurements of the range of recoils and converted to an energy by means of the range-energy relation deduced from Lillie's curve.

Again, the error in measuring the length of the

f80a.

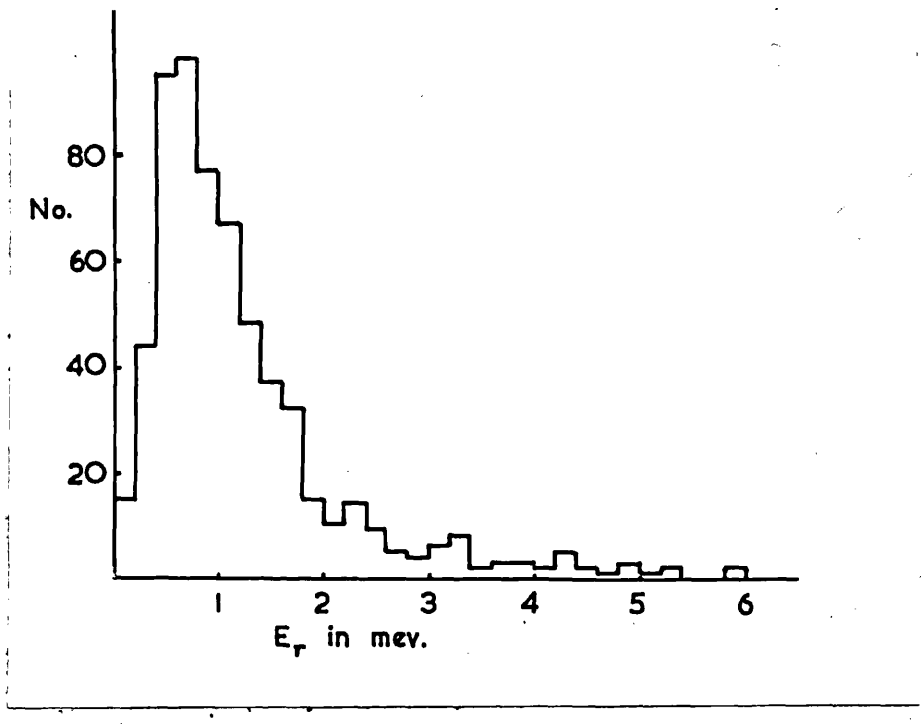

Fig. 17.

Energy distribution of recoils from $N^{14}(\gamma,n)N^{13}$.

f 80b.

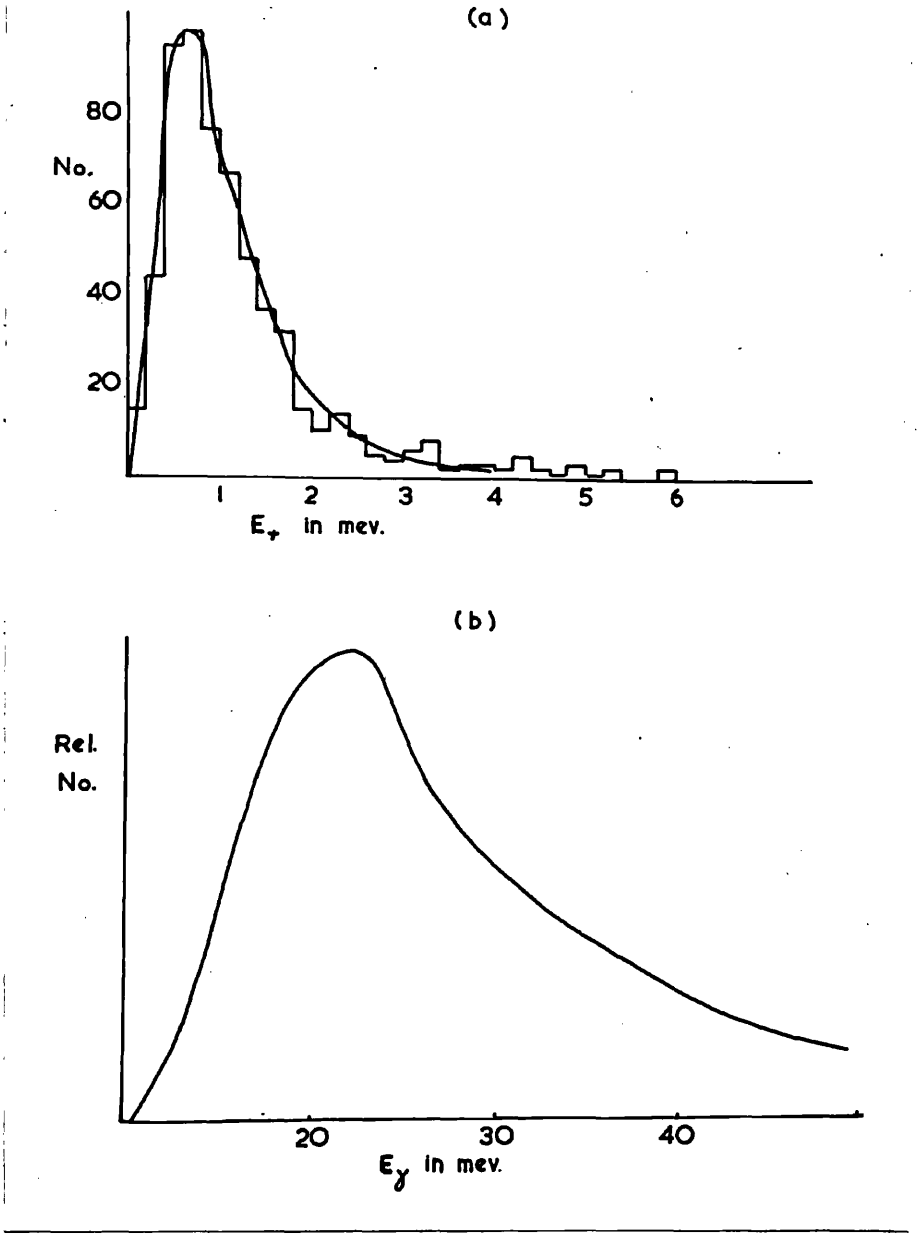

Fig. 18.

Number of $N^{14}(\gamma,n)C^{13}$ events as a function of (a) E_+ (b) E_γ

recoil, and correcting for pressure, would be less than 0.1 MeV for recoils of energy greater than 0.5 MeV.

Unfortunately, since in many photographs recording recoil nuclei from (γ,n) events it is not possible to establish from which end of the recoil track the neutron was ejected, it is not possible to obtain a value for the neutron energy, E_n, which includes a correction for the momentum of the incident quantum (c.f. proton case). On the assumption that the correction is generally small, an energy distribution of neutrons was calculated from $E_n = \frac{M_r}{M_n} . E_r$. and is shown in fig. 18b.. The error involved in this assumption is largest when $\gamma_r = 180^\circ$ or 0° in which cases the error is $\sim$ 15%; but the magnitude of the error decreases as γ_r increases. Because of the small solid angle formed by small angles, few events have $\gamma_r < 20^\circ$, and consequently the mean error in the derivation of E_n is less than 10%.

This same uncertainty about the origin of events prevents full angular distributions from

f81.

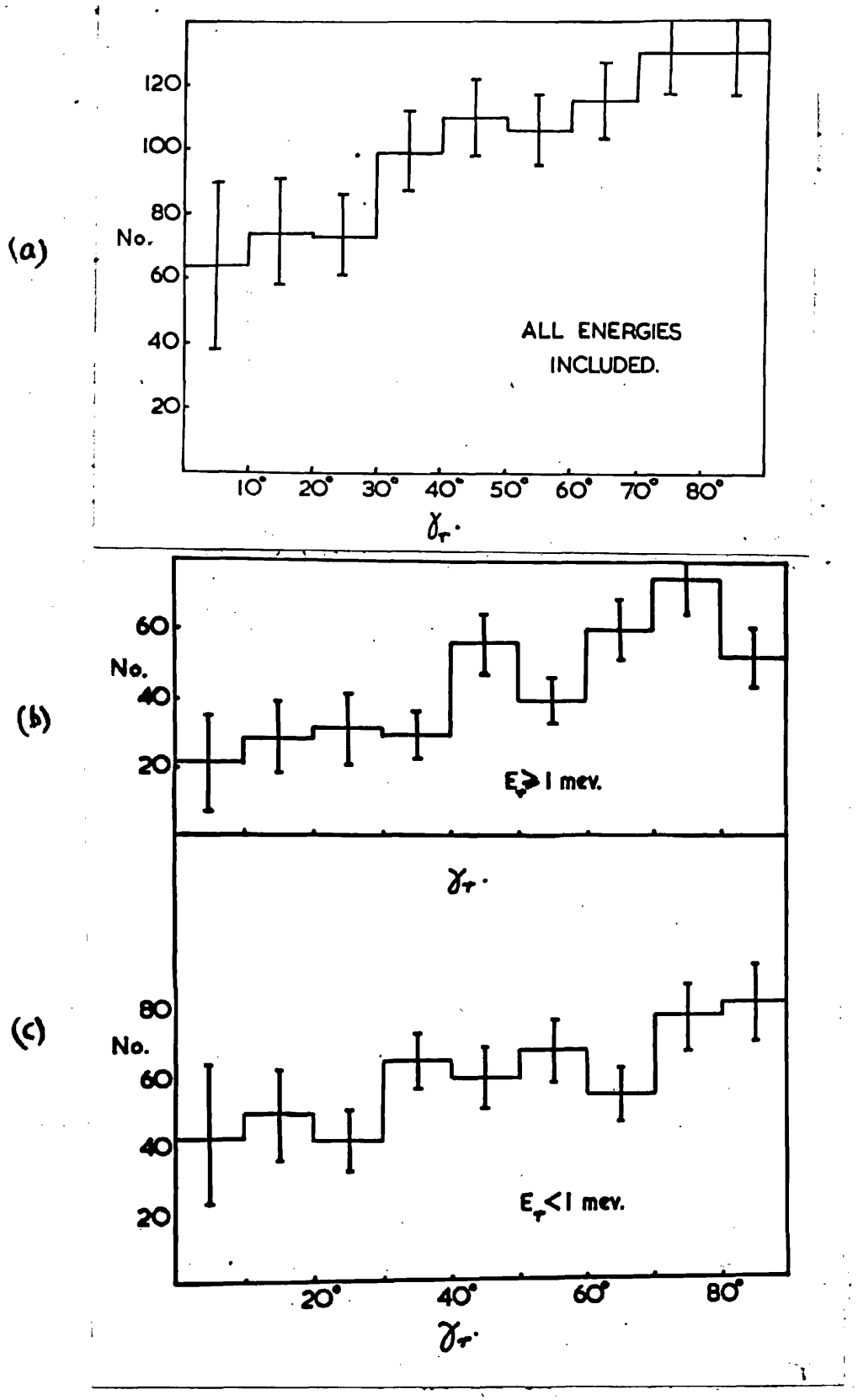

Fig. 19.

Angular distributions of recoils with respect to the γ beam direction for $N^{14}(\gamma,n)N^{13}$.

being determined: an angle γ_n could also be $180^\circ - \gamma_n$. Angular distributions were drawn however for angles 0° to 90°, assuming a symmetry about 90°. The form of the distribution so obtained suggests, in fact, that there is a tendency towards a peak at 90°. These distributions were again corrected by the solid angle factor.

The sub-group distributions show that, as the energy of the recoil decreases, so also does the degree of anisotropy. This will be discussed later.

Figs. 19b and 19c give the angular distributions for $E_\gamma \geqslant 1$ MeV and $E_\gamma < 1$ MeV.

E.

The Reaction $N^{14}(\gamma,pn)C^{12}$

Kinematics of Reaction.

Consider a typical (γ,pn) reaction in which the angles γ_i, θ_i, and α_i (i = r, p, n) are as in fig. 20 for recoil, proton and neutron respectively. The momenta of these products is $\sqrt{2M_iE_i}$ in $\frac{mev}{c}$ where M_i is in $\frac{mev}{c^2}$ and E_i is in MeV. (i = r, p, n).

By considering a momentum balance along three

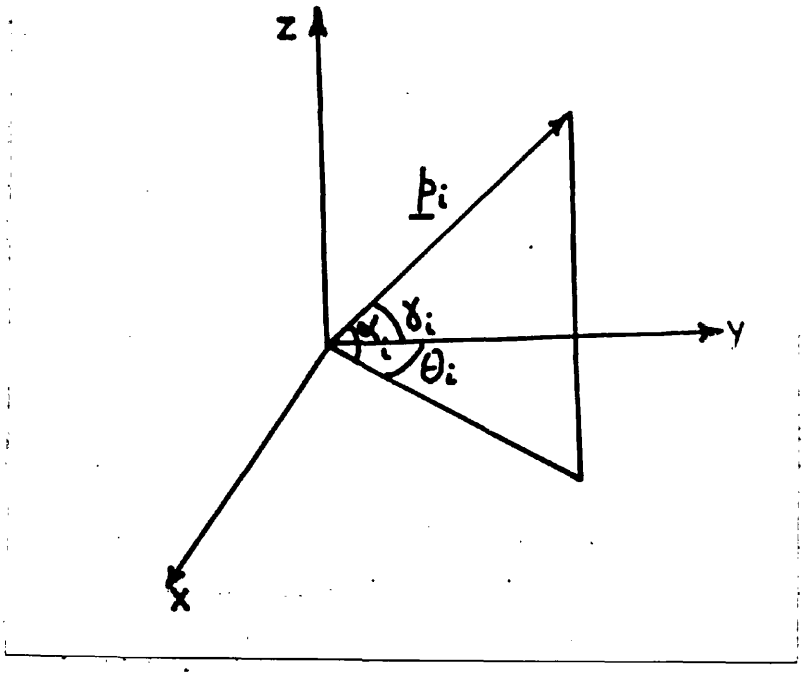

Fig. 20.

Kinematics of the (γ, pn) reaction.

p_i = momentum of particle $i = \sqrt{2 M_i E_i}$ in $\frac{\text{MeV}}{C}$,

where E_i is the energy of the i^{th} particle and M_i is its mass in $\frac{\text{MeV}}{C^2}$

Component of p_i along y = $p_i \cos \gamma_i$

" " " " x = $p_i \cos \alpha_i \sin \theta_i$

" " " " z = $p_i \sin \alpha_i$

i = r, p, n for recoil, proton and neutron respectively.

perpendicular axes and also by using energy conservation four equations are obtained:

$$p_\gamma E_\gamma = \sum_{i=n,p,\alpha} \sqrt{2M_i E_i}\, \cos\gamma_i \qquad (1)$$

$$\sum_i \sqrt{2M_i E_i}\, \cos\alpha_i \sin\theta_i = 0 . \qquad (2)$$

$$\sum_i \sqrt{2M_i E_i}\, \sin\alpha_i = 0 \qquad (3)$$

$$E_\gamma = \sum_i E_i + Q \qquad (4)$$ where

Q is the threshold of the reaction in MeV.

In the energy equation it has again been assumed that the excitation of the residual nucleus is small in comparison with the incident γ energy.

In the case of most (γ, pn) reactions observed, the proton did not stop within the chamber, and hence E_p, the proton energy, was not measurable. In addition there are four other unknowns - α_n, θ_n, E_n and E_γ, so that it is not possible to solve the above equations in terms of the measured quantities to obtain E_n.

f 83.

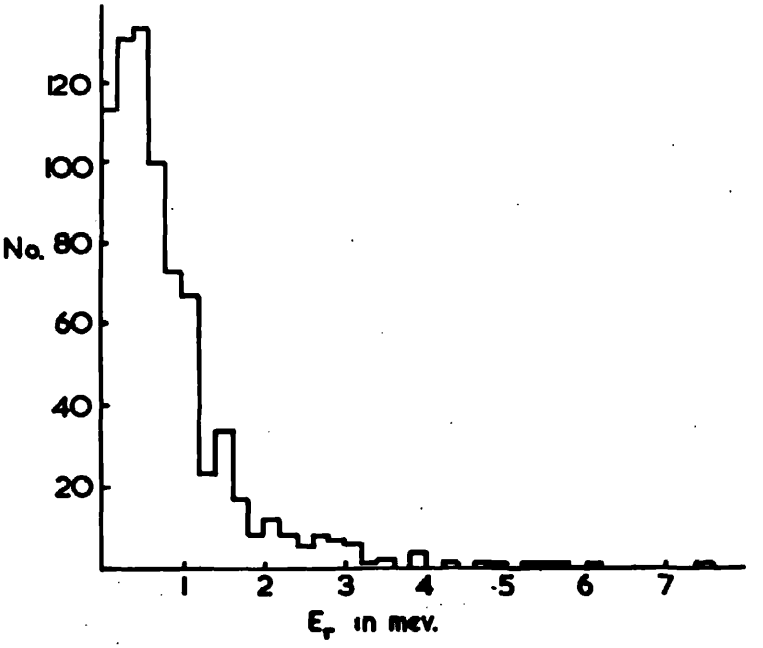

Fig. 21.

Energy distribution of recoils from $N^{14}(\gamma,pn)C^{12}$.

Where the proton is stopped in the chamber so that E_p may be measured, there are then only four unknowns, and the equations may be solved to give E_n in terms of the measured energy of recoil, and angles. The full solution of E_n is

$$E_n = M_p - \frac{A}{2M_p} - \sqrt{M_p^2 - (A+B^2+C^2)}$$

where $A = 2M_p\{(E_r+E_p+Q) - (\sqrt{2M_pE_p}\cos\gamma_p + \sqrt{2M_rE_r}\cos\gamma_r)\}$

$$B = -(\sqrt{2M_pE_p}\cos\alpha_p \sin\theta_p + \sqrt{2M_rE_r}\cos\alpha_r \sin\theta_r)$$

$$C = -(\sqrt{2M_pE_p}\sin\alpha_p + \sqrt{2M_rE_r}\sin\alpha_r).$$

Case of Proton Not Stopping

As before the energy distribution of the recoils was calculated and is presented in fig. 21 . The form is quite different from that of either the (γ,p) or (γ,n) distributions in that the peak occurs at only 0.5 MeV. This is discussed in the next Chapter.

It will also be outlined how angular distributions derived from (γ,pn) interactions might give an indication of the actual mechanism of disintegration. The

f84a.

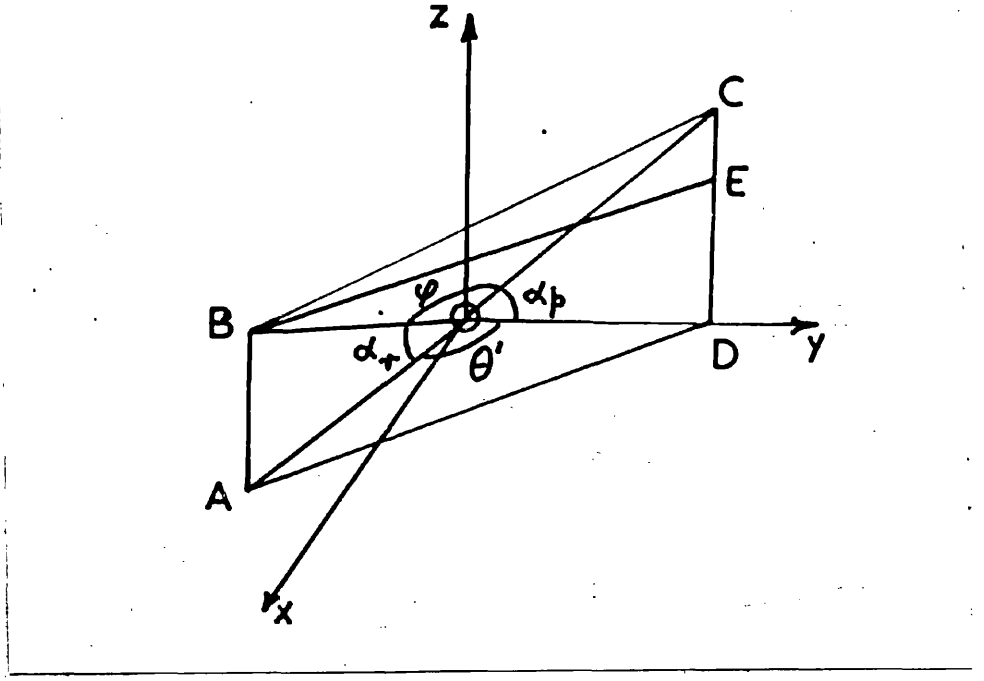

$$\zeta \equiv \varphi$$

Fig. 22.

Diagram to illustrate the derivation of ζ

f84b.

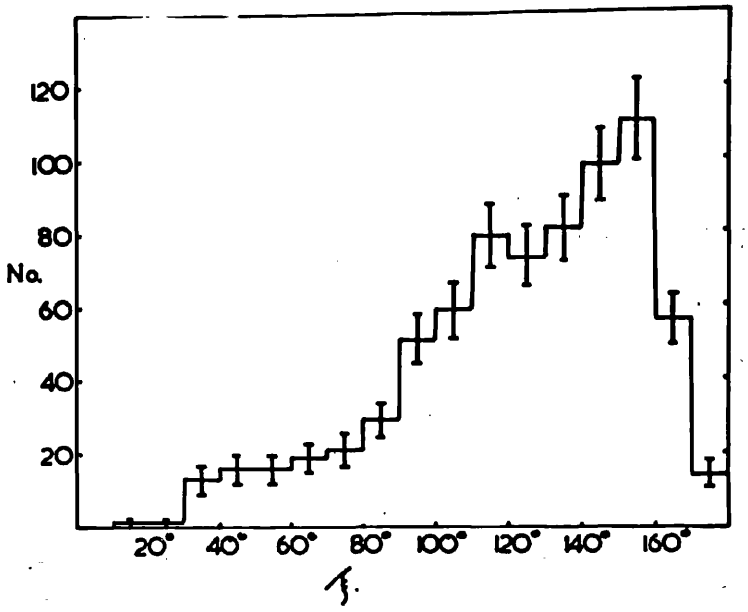

Fig. 23.

Distribution of the angle ϑ between proton and recoil in $N^{14}(\gamma,pn)C^{12}$.

f 84 c.

(a)

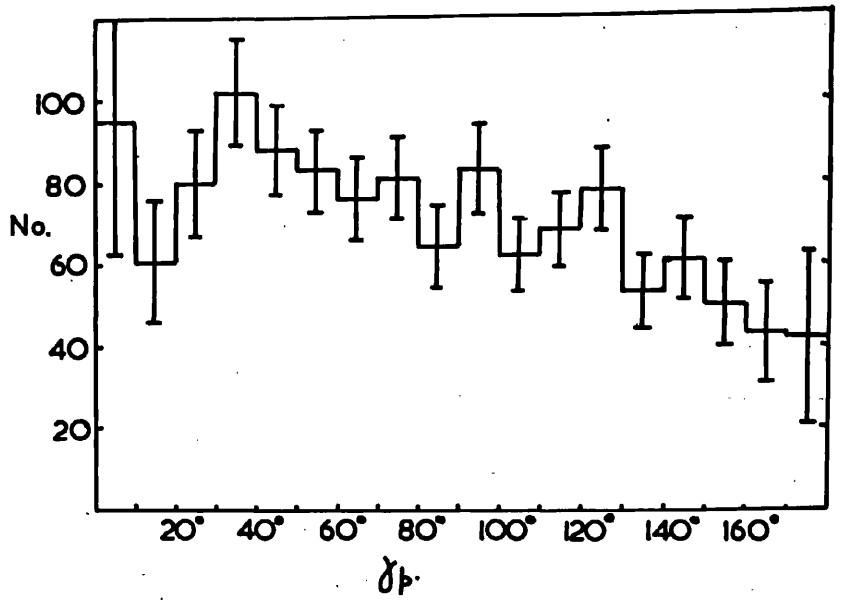

(b)

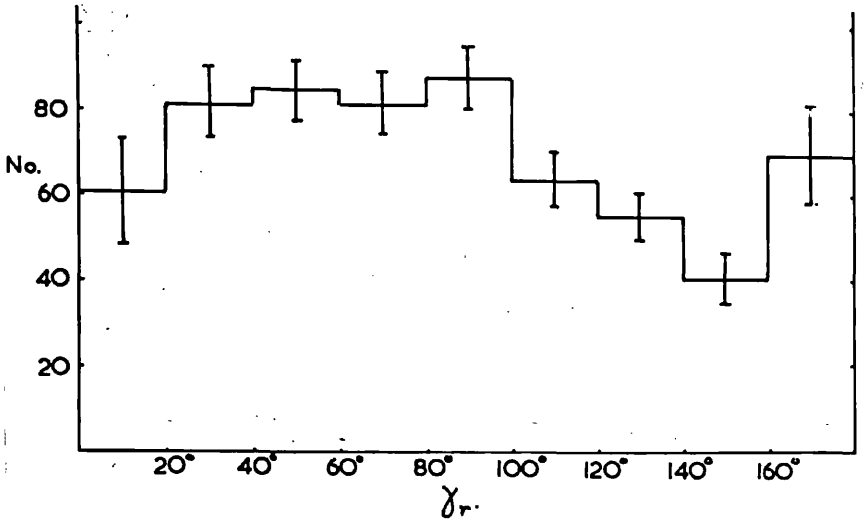

Fig. 24.

Angular distribution of (a) protons (b) recoils with respect to the γ beam direction.

most useful distribution for this argument is that of the angle between the proton and recoil. This angle, ξ, may be calculated from the measured proton and recoil angles by

$$\xi = \cos^{-1}\{\cos\alpha_r \cos\alpha_p \cos\theta' + \sin\alpha_r \sin\alpha_p\}$$

where $\theta^1 = |\theta_p - \theta_r|$, and θ_p and θ_r, α_p and α_r are as defined in the last section. The signs of α_r and α_p must be observed.

A distribution of ξ is shown in fig.23 plotted in 10° intervals. This distribution increases from low values below 90° to show a peak at about 155° falling off again to 180°. This distribution has not been corrected by the solid angle factor.

Other angular distributions are given in figs.24a,b.

Case of Proton Stopping.

In this case the neutron energies have been calculated from the equation developed on page 83. γ_p, γ_r, E_p and E_r having been measured.

Fig.25a shows the energy distribution of the (γ,pn) events as a function of E_γ for cases in

f 85

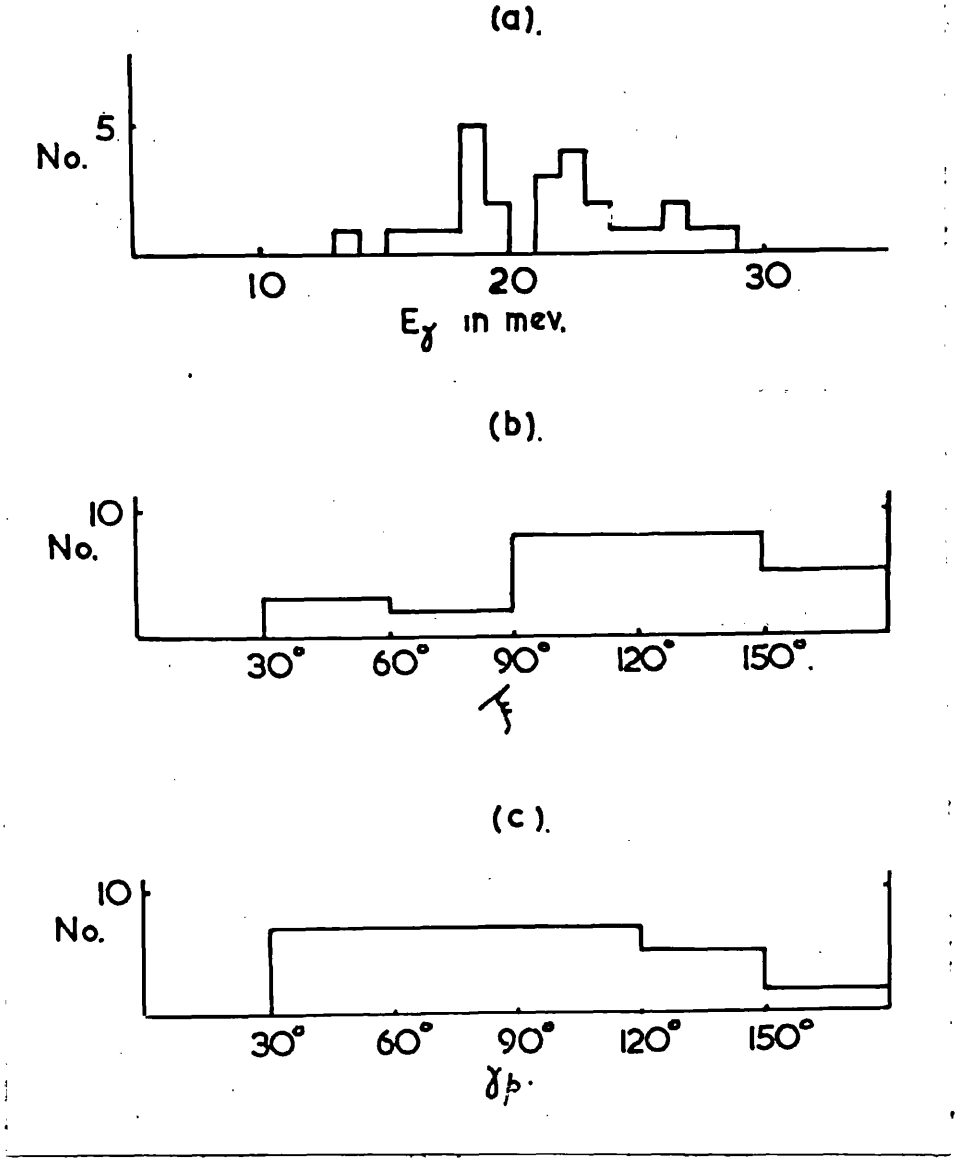

Fig. 25.

$N^{14}(\gamma,pn)C^{12}$ events in which the proton stopped in the chamber.

(a) number of events as a function of E_γ

(b) distribution of angle between proton and recoil.

(c) angular distribution of protons with respect to beam direction.

which the proton stopped within the chamber. The events are too few for any strong claims to be deduced, but the distribution is in keeping with a giant resonance at 22 MeV.

Figs. 25 b, c show the angular distributions deduced from these reactions. These reproduce the characteristics obtained for the same reaction in cases where the proton was too energetic to be stopped within the chamber.

f86.a.

Typical expansion chamber photograph to show disintegrations produced by the 200 MeV γ beam.

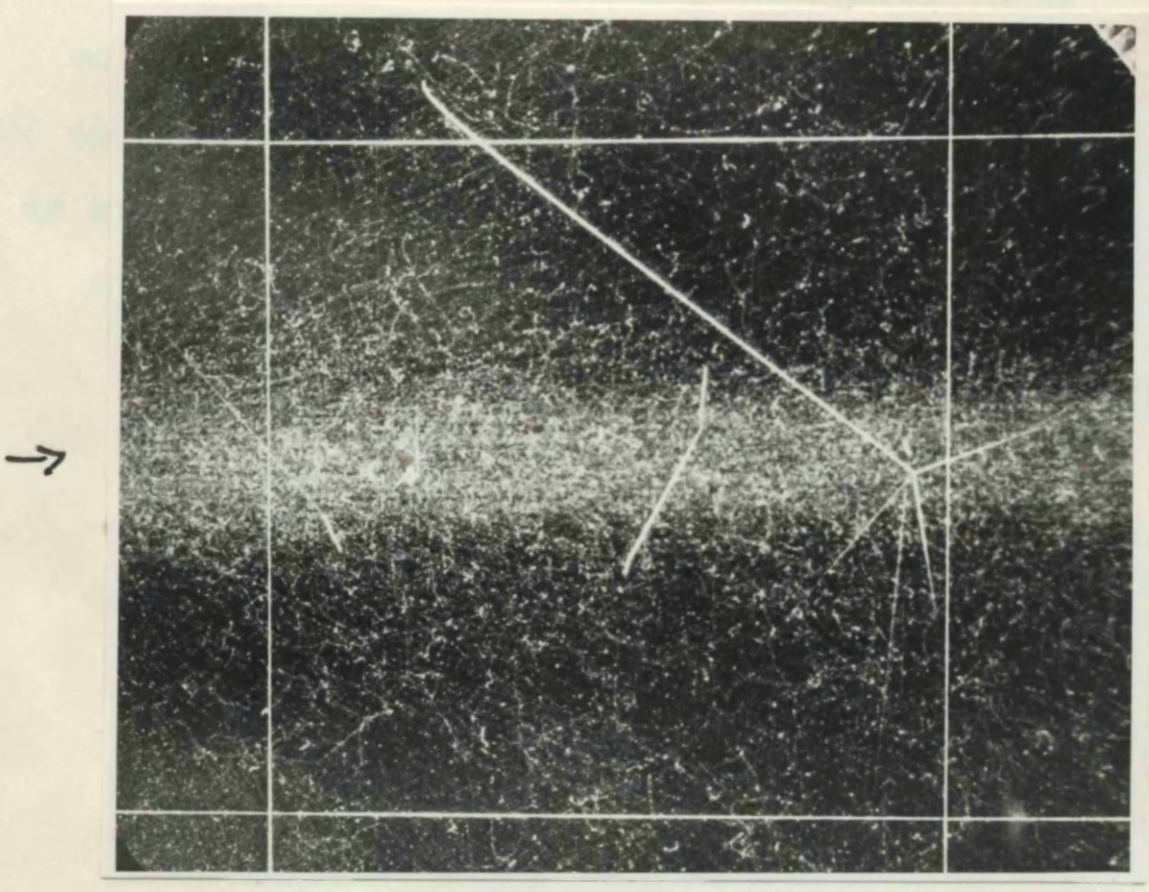

f86b.

Typical expansion chamber photograph to show disintegrations produced by the 200 MeV γ beam.

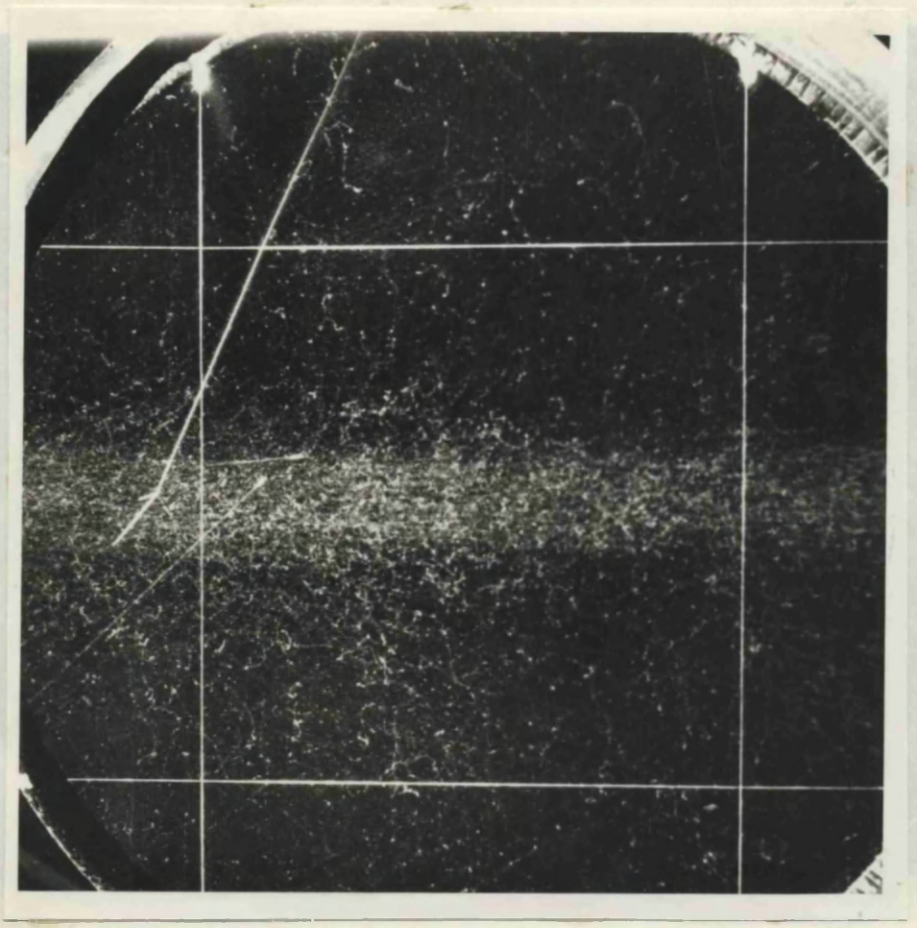

CHAPTER V: NITROGEN PHOTODISINTEGRATION: DISCUSSION.

A.

The $N^{14}(\gamma,p)C^{13}$ Reaction

In studying the histograms associated with the (γ,p) reaction, two factors must be taken into account -

(1) It was found impossible to separate protons from deuterons so that all (γ,d) reactions are also included in the histograms.

(2) It was not possible to measure the excitation energy of the resulting nuclei.

Measured (γ,d) cross sections are in general much lower than those for (γ,p) or (γ,n). Deuterons are more tightly bound than protons and consequently, where there is competition for emission, proton emission should be more strongly favoured. In addition, Radicatti[69] has shown that, for self-mirrored nuclei, electric dipole absorption involves a change in isotopic spin of $\pm$ 1. The initial state has $T = 0$ and so the excited state has $T = 1$. Such a state cannot decay by deuteron emission (for which

T = 0) to a T = 0 state. Hence this type of emission is prohibited until the excitation energy is sufficiently large to enable the residual state to be T = 1.[70] The (γ,α) reaction is suppressed in exactly the same way, and, in fact, few (γ,α) reactions were observed.

Several authors[71] have observed $N^{14}(\gamma,d)3\alpha$ but such a reaction would be classified as a star in our system.

Thus in the rest of the discussion it is assumed that the (γ,d) reaction is less probable than (γ,p), and that the histograms will therefore expose features of the (γ,p) process.

As a result of being unable to measure the excitation energy of residual nuclei, the shape of the histogram (fig. 14a.) below 20 MeV is deceiving. Events in which the resulting nucleus was excited would be displaced to lower energies on the histogram by an amount equal to the excitation energy. Thus only at higher energies where the excitation energy is small in comparison with the incident quantum energy will the histogram give a true indication

of the variation of the (γ,p) cross section.

The form of the cross section curve at higher energies can be obtained only after correcting the measured distribution for the spectrum shape of the incident bremsstrahlung. This is uncertain in the region 0 to 50 MeV. However, assuming that the γ ray spectrum varies as $\frac{1}{E}$, it can be seen that the (γ,p) cross section at 50 MeV has fallen to about $\frac{1}{10}$ of its peak value.

The resolution of the experiment is not sufficiently high for individual energy levels to be exposed, but the form of the distribution is in keeping with the known excited states of C^{13}. If the (γ,p) giant resonance is assumed to have a peak at $\sim$ 23 MeV, then the position of the peak on the histogram between 19 and 20 MeV may be interpreted as resulting from transitions to the first, second and third excited states of C^{13} at 3.08, 3.68 and 3.89 MeV. Also, the peak at 15 MeV may be associated with transitions to the 6.87 and 8.9 MeV levels, and the 11 MeV peak may contain transitions to the levels above 10.8 MeV.

Direct Emission versus Compound Nucleus Formation.

The theoretical attempts to obtain the form of the energy distribution of protons emitted in the photodisintegration of the heavier elements by a bremsstrahlung of γ radiation, were outlined in Chapter I, and the importance of including two contributions was revealed - one due to the statistical decay of a compound nucleus and the other due to a direct process. For the direct process both the Courant and Wilkinson shell models were discussed. Wilkinson has given a straightforward estimate of the order of magnitude of the relative importance of the direct and compound nucleus processes.[50]

Before considering the shape of the energy distribution of protons resulting from the nitrogen photodisintegration, it is of interest to consider the relative importance of the direct process as estimated by Wilkinson. The ratio of the probabilities for direct emission and compound nucleus formation are given by

$$C = \frac{2kP\,\frac{\hbar^2}{mR}}{2W.}$$

where P is the penetrability of the Coulomb and centrifugal barriers,

k is the incident nucleon wave number,

W is the imaginary part of the cloudy ball potential.

For N^{14}, C has the value 1.03P for 8 MeV protons where W is taken to be 8 MeV, and $R = 1.3\ A^{\frac{1}{3}} \times 10^{-13}$ cm. Using a W.K.B. method, Rhodes[72] obtained $P = 0.8$ and 0.4 for values of $\ell = 0$ and $\ell = 2$ respectively.

In addition to the processes for emission just discussed, there is the additional mechanism resulting from a γ interaction with a sub-group of the target nucleus. In particular, such a process might result from the neutron in a quasi-deuteron disintegration being reabsorbed into the nucleus so that only the high energy proton might be emitted. However, the probability of this process happening has been found to be very small and may be ignored here.

Energy Distribution of Protons.

The validity of applying statistical methods

to obtain an energy spectrum of protons evaporating from an excited N^{14} nucleus is indeed questionable. Weisskopf and Ewing[36] cautioned against applying their method to nuclei with A $<$ 50. However, since statistical arguments have been applied with apparent success to light nuclei, a distribution of proton energies was calculated for N^{14} excited by 200 MeV bremsstrahlung. The distribution used by Dawson[42] was utilised:

$$I(\varepsilon)\,d\varepsilon = \varepsilon\,\sigma_p(\varepsilon)\,e^{-\frac{\varepsilon}{T}}\,d\varepsilon \int_{B_{p+c}}^{E_{max}} N(E, E_{max})\,\sigma_{\gamma n}(E)\,dE$$

This has been obtained from the general form presented in Chapter I, by accepting Livesey's[37] level density formula $\omega(E) = C\,e^{\frac{E}{T}}$ where T is a constant nuclear temperature given by $T = (\frac{100}{A})^{\frac{1}{2}}$. This assumption is claimed to be valid only if the excitation energy is less than 10 MeV. In our experiment this is not necessarily fulfilled, but the error involved is likely to be small compared with the error introduced by applying statistical methods.

In the actual calculation $\sigma_{\gamma n}(E)$ was taken from

the results of Johns and Horsley et al[73], $N_\gamma(E)$ was assumed to vary as $\frac{1}{E}$, and the cross section for reabsorption of a proton of energy ε into the nucleus was calculated from the Blatt and Weisskopf[74] theory which reproduces the continuum of σ_p without any resonances.

The distribution obtained by this calculation was accepted to be only very approximate, but the calculated curve peaked at an energy much smaller than that found experimentally, and did not give the observed high energy tail. To obtain the peak of the theoretical distribution at the energy of the observed peak, the value of T required was absurdly high, and, even then, the high energy tail was much too small.

Toms and Stephens[39], and Dawson[42] have given very approximate forms for the energy distribution of directly emitted protons. Osokina and Ratner[75] have applied Courant's calculation of cross section for direct emission, to a shell model of the nucleus. The basic assumption is that the proton is emitted directly with energy $E_\gamma - E_B$ where E_γ is the

initial quantum energy and E_B is the binding energy of that particular proton. Transitions of $\ell \rightarrow \ell + 1$ and $\ell \rightarrow \ell - 1$ are both taken into account in the distribution:-

$$N(\epsilon_p) = \text{const.} \sum_i n_i \sigma(\epsilon_p + B_{p_i}) N_\gamma(\epsilon_p + B_{p_i}, E_{max}) \left[g_{\ell_i - 1} T_{\ell_i - 1}(\epsilon_p) + g_{\ell_i + 1} T_{\ell_i + 1}(\epsilon_p) \right].$$

where n_i = number of protons in the i^{th} level, ℓ_i is the angular momentum of protons in the i^{th} level, and B_{p_i} is the binding energy of these protons.

$N_\gamma (E_p + B_{p_i}, E_{max})$ is the number of quanta of energy $\epsilon_p + B_{p_i}$ in the incident γ spectrum having energy $(\epsilon_p + B_{p_i})$.

$\sigma (\epsilon_p + B_{p_i})$ is the cross section for the direct photoeffect per nucleon as computed by Courant.

$T_{\ell_i \pm 1}$ = the penetrability through the barrier, and

$g_{\ell_i \pm 1} = [2(\ell_i \pm 1) + 1]$ is a statistical factor.

Such a distribution was calculated for N^{14}. $T_{\ell_i \pm 1}$ was calculated from formula given by Blatt and Weisskopf[74] and the tables computed by Bloch[76]. The Courant cross section was calculated from the

original formula assuming a well depth of 50 MeV and radius $R = 1.3A^{\frac{1}{3}} \times 10^{-13}$ cm. The proton configuration in nitrogen is $(1s_{\frac{1}{2}})^2 (1p_{\frac{3}{2}})^4 (1p_{\frac{1}{2}})^1$. The calculation was carried out for the $p_{\frac{3}{2}}$ level assuming $N_\gamma(E)$ to vary as $\frac{1}{E}$. B_p for the $p_{\frac{3}{2}}$ level was taken as 10.5 MeV which is the sum of the binding energy of the last filled proton level ($p_{\frac{1}{2}}$) and the splitting in MeV of the $p_{\frac{3}{2}}$ and $p_{\frac{1}{2}}$ levels computed from $(2\ell+1)\beta$. ($\beta \sim 3$ MeV for N^{14}). [45 refs.]

However, the full spectrum should contain contributions from the $1p_{\frac{1}{2}}$ and $1s_{\frac{1}{2}}$ levels. The contribution from the $1p_{\frac{1}{2}}$ level has the same form as that computed for $1p_{\frac{3}{2}}$. On the assumption that $1s_{\frac{1}{2}} \rightarrow 1p_{\frac{3}{2}}$ transitions yield protons of $\sim$ 22 MeV B_{p_0} is $\sim$ 30 MeV. This would lead to only a relatively small contribution from the $s_{\frac{1}{2}}$ level, and so it may be concluded that the form of the distribution of all directly emitted protons is essentially that given by the distribution for the $p_{\frac{3}{2}}$ level.

Theoretical Angular Distributions./

Theoretical Angular Distributions.

(1) Compound Nucleus Disintegration.

On the assumption that a compound nucleus with well defined spin is formed, it is possible to calculate angular distributions resulting from any multipole absorption if the spin and parity of the initial and final states be known.

The selection rules which determine the spin and parity of the compound nucleus state are given in the following table.[77]

	Δ J.	Parity
Electric Dipole	0, 1	Change
Electric Quadrupole	0, 1, 2	No change
Magnetic Dipole	0, 1	No change

e.g. Dipole absorption of a γ quantum into a 1- initial state, J_i, gives three possible compound nucleus states J_c = 0-, 1-, 2-.

The possible values of the angular momentum, l of a nucleon emitted from a compound nucleus state in going to a known final state are determined by:-

Parity of initial state = $(-1)^l$ (intrinsic parity of nucleon) × (parity of final state)

The compound nucleus states in the above example could therefore decay to a final state of the residual nucleus of $\frac{1}{2}$- by proton emission according to:-

0- state may emit protons with $\ell = 0$

1- " " " " " $\ell = 0, 2$

2- " " " " " $\ell = 2$

Hence angular distributions of protons of known ℓ in transition between states of known spin and parity may be calculated from

$$\sigma(\theta) = \sum_k (-1)^{S-I} Z(\ell_j \ell_j, sk) Z_1(L_j L_j, Ik) P_k \cos\theta$$

where j is the compound nucleus state, L is the multipolarity of the incoming γ ray, S is the channel spin of the outgoing particle ($S = J_{final} \pm \frac{1}{2}$) and I is the initial nuclear state.

$Z(\ell_j \ell_j, sk)$ & $Z_1(L_j L_j, Ik)$ are Racah coefficients which are tabulated.[78]

Thus angular distributions corresponding to

f97a.

Electric Dipole Absorption

	J_i	J_f	J_c	ℓ_p	S	$\sigma(\theta)$
Transitions	$1+$	$\frac{1}{2}-$	$0-$	0	0	isotropic
to	"	"	$1-$	0	1	"
Ground	"	"	$1-$	2	1	$7+3\cos^2\theta$
State	"	"	$2-$	2	0	$2+3\sin^2\theta$
	"	"	$2-$	2	1	$2+\sin^2\theta$
Transitions	$1+$	$\frac{1}{2}+$	$0-$	1	1	isotropic
to	"	"	$1-$	1	0	$1+\cos^2\theta$
First	"	"	$1-$	1	1	$2+\sin^2\theta$
Excited	"	"	$2-$	1	1	$1+0.81\sin^2\theta$
State	"	"	$2-$	3	1	$1+\sin^2\theta$

Magnetic Dipole Absorption

	J_i	J_f	J_c	ℓ_p	S	$\sigma\theta$.
Transitions	$1+$	$\frac{1}{2}-$	$0+$	1	1	isotropic
to	"	"	$1+$	1	0	$1+\cos^2\theta$
Ground	"	"	$1+$	1	1	$2+\sin^2\theta$
State	"	"	$2+$	1	1	$1+0.81\sin^2\theta$
	"	"	$2+$	3	1	$1+\sin^2\theta$
Transitions	$1+$	$\frac{1}{2}+$	$0+$	0	0	isotropic
to	"	"	$1+$	0	1	"
First	"	"	$1+$	2	1	$7+3\cos^2\theta$
Excited	"	"	$2+$	2	0	$2+3\sin^2\theta$
State	"	"	$2+$	2	1	$2+\sin^2\theta$

f 97 b.

Electric Quadrupole Absorption

	J_i	J_f	J_c	ℓ_p	S	$\sigma(\theta)$
Transitions	1+	$\frac{1}{2}$-	1+	1	1	$2 + \sin^2\theta$
to	"	"	1+	1	0	$1 + \cos^2\theta$
Ground	"	"	2+	1	1	$7 + 3\cos^2\theta$
State	"	"	2+	3	1	$3 \times \sin^2\theta + 5\cos^4\theta$
	"	"	3+	3	0	$9 + 42\cos^2\theta - 35\cos^4\theta$
	"	"	3+	3	1	$9 + 12\cos^2\theta - 5\cos^4\theta$
Transitions	1+	$\frac{1}{2}$+	1+	0	1	isotropic
to	"	"	1+	2	1	$7 + 3\cos^2\theta$
First	"	"	2+	2	0	$1 - 3\cos^2\theta + 4\cos^4\theta$
Excited	"	"	2+	2	1	$1 + 2.14\cos^2\theta - 5.35\cos^4\theta$
State	"	"	3+	2	1	$1 + 2.88\cos^2\theta - 2.04\cos^4\theta$
	"	"	3+	4	1	$1 + 2.43\cos^2\theta - 1.83\cos^4\theta$

electric dipole, electric quadrupole and magnetic dipole excitation of the ground state of N^{14} to leave C^{13} in its ground state or first excited state were calculated and are tabulated.

(2) Direct Interaction.

Angular distributions resulting from the direct interaction proposed by Courant have the following form.

$\ell \to \ell+1$. $\quad I(\theta) = \ell(\ell+1) + \frac{1}{2}(\ell+1)(\ell+2)\sin^2\theta$.

$\ell \to \ell-1$. $\quad I(\theta) = \ell(\ell+1) + \frac{1}{2}\ell(\ell-1)\sin^2\theta$.

For N^{14} with the configuration for neutrons and protons - $(1s_{\frac{1}{2}})^2 (1p_{\frac{3}{2}})^4 (1p_{\frac{1}{2}})$ - the possible angular distributions are

$p \to d$. $\quad I(\theta) = 2 + 3\sin^2\theta$.

$p \to s$. $\quad I(\theta) =$ isotropic (e.g. $1p_{\frac{3}{2}} \to 2s_{\frac{1}{2}}$)

$s \to p$. $\quad I(\theta) = \sin^2\theta$.

On the basis of the Wilkinson model the form of the angular distributions is

$$I(\theta) = 1 + \frac{1}{2}\left(1 + \frac{3}{\ell}\right)\sin^2\theta.$$

Thus for p nucleons $I(\theta) = 2 + 3 \sin^2\theta$.

and for s nucleons $I(\theta) \sim \sin^2\theta$

Conclusions from Measured Angular Distributions.

The conclusion deduced from figs.16a,b is that, for protons of energy less than 10 MeV, the angular distribution is essentially isotropic. For higher proton energies the distribution has the form $a + b \sin^2\theta$ and, at the highest energies obtained, the distribution tends towards pure $\sin^2\theta$.

In interpreting these results it is useful to bear in mind how a compound nucleus disintegration is capable of accounting for the lower energy protons, but how, at higher energies, protons resulting from a direct process become more important. Thus the lower energy proton angular distribution is considered in terms of a compound nucleus disintegration, and the highest energy group in terms of a direct interaction.

Since the lower energy protons are all from reactions in the giant resonance energy region we may consider them as resulting from electric dipole

absorption. Magnetic dipole and electric quadrupole absorption are considered to be comparatively smaller. (See Devons).[77] From the table for electric dipole absorption it can be seen that transitions to the ground state of C^{13} can result from only s and d wave emission. Since the d protons experience a high centrifugal barrier, the s emission will dominate and this gives an isotropic distribution. In transitions to the first excited state of C^{13} however there are four possible angular distributions, only one of which is isotropic - that resulting from a compound nucleus state of 0-. Thus it may be claimed that the observed isotropic distribution at low energies has been determined mainly by transitions from a compound nucleus state to the ground state of C^{13}, or to the first excited state of C^{13}, in cases where the compound nucleus state was 0-. A direct interaction process is incapable of giving a pure isotropic distribution.

The $\sin^2\theta$ distribution characteristic of the high proton energy group cannot be explained by a compound nucleus argument.

On the basis of a direct interaction model it is only possible to have a pure $\sin^2\theta$ distribution if the emitted protons have come initially from an s shell. If a proton be ejected directly from the $1S_{\frac{1}{2}}$ state of N^{14}, the resulting C^{13} nucleus has the proton configuration $(1S_{\frac{1}{2}})'\,(1P_{\frac{3}{2}})^4\,(1P_{\frac{1}{2}})'$ and this has $+\omega$ parity. The parity of the ground state of C^{13} has $-\omega$ parity. Hence it must be concluded that such direct interaction leaves the C^{13} in an excited state.

Protons emitted from a p state of N^{14} leave the residual nucleus with $+\omega$ parity, and hence the ground state of C^{13} is accessible by this process. The excitation of p state protons to s and d states leads to s and d wave emission, and interference between these might be capable of giving a predominantly $\sin^2\theta$ distribution.

Previous angular distributions for protons from N^{14} have been measured by Johannson[79] and Spicer[80] at low energies just above threshold, and by Livesey who used a peak bremsstrahlung of 35 and 70 MeV. The most energetic group of protons observed by

Livesey[81] (>8.5 MeV) showed an angular anisotropy with a large b/a ratio (from $a + b \sin^2\theta$) in agreement with our measurements.

B.

The $N^{14}(\gamma,n)N^{13}$ Reaction.

In addition to pure (γ,n) events this class contains also $(\gamma,2n)$ and possibly (γ,π^0) reactions. The cross section for this last reaction is very much smaller than that for (γ,n), and, consequently, the contribution from this reaction may be neglected. The threshold for the $(\gamma,2n)$ reaction occurs above the giant resonance region at 30.9 MeV as compared with the (γ,n) threshold at 10.5 MeV. This fact in itself implies that the $(\gamma,2n)$ events will be far fewer than (γ,n), but, in addition, Panofsky and Reagan[82] have measured a low cross section for this reaction. Consequently, it is assumed that the form of the measured distributions for this class have been determined essentially by the (γ,n) reaction.

(γ,n) Recoil Distribution.

The recoil distribution for the (γ,n) reaction differs from that for the (γ,p) in showing a much

f102.

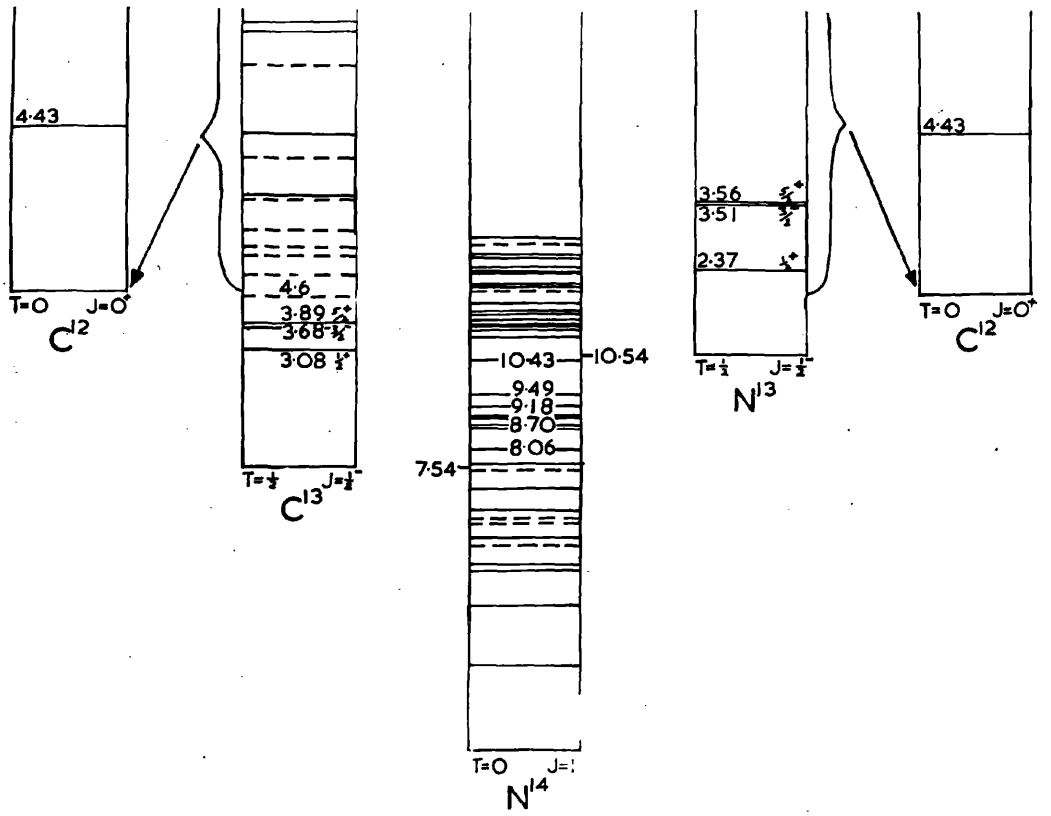

Fig. 26.

Energy level diagrams.

* Since in $N^{14}(\gamma p)C^{13}$, transitions other than to the ground state of C^{13} occur the distribution is broadened. In the (γn) case only transitions to the ground state are possible. Thus the resonance width for the γp cross section is not necessarily greater than that for (γn).

higher peak, at about 0.8 MeV, together with a much narrower half-width. The half-width in the (γ,n) case is only 0.8 MeV whereas it is 1.2 MeV for the proton recoil distribution.* However, above about 1.5 MeV the high energy tail is very similar in the two cases

These features may be explained very well in terms of the energy level diagram for the residual N^{13} (fig.26). The first excited state of N^{13} is already above the threshold for the $N^{13} \rightarrow C^{12} + p$ reaction, and, consequently, any transition to this level would result immediately in the further emission of a proton. Thus (γ,n) reactions must result in the residual N^{13} being left in its ground state. This immediately explains the absence of other subsidiary peaks in the recoil distribution and in the narrower width, the width of the proton spectrum being due to the clustering together of a number of peaks.

The total numbers of (γ,n) and (γ,p) reactions were about the same, a point which is in agreement with the principle of charge independence. The height of the (γ,n) distribution was consequently

higher, to make up for the narrower width of the distribution.

Form of the (γ,n) Cross Section Curve.

Since all (γ,n) transitions must be to the ground state of N^{13} it is possible to deduce from the recoil distribution the shape of the (γ,n) cross section curve.

Since the origin of the event is uncertain - either end of the recoil might be taken in many cases - it is not possible to calculate E_n in the way that E_p was deduced. However, on the average a recoil of energy E_r results from a photon of energy $Q+14E_r$ where Q = 10.54 MeV is the threshold of the $N^{14}(\gamma,n)$ reaction. Using this equation and assuming the photon spectrum to vary as $\frac{1}{E}$, the form of the (γ,n) cross section was deduced. This gives the peak of the resonance at E_{max} = 14 × 0.8 + 10.5 = 22 MeV.

At 50 MeV the cross section has ~~fe~~fallen off to about $\frac{1}{8}$ of the peak value.

The surprisingly broad width of the (γ,n) giant resonance may be explained in terms of the

Wilkinson model. Wilkinson has pointed out that the dipole transitions for valence nucleons are many, and are spread in energy over many MeV. In N^{14} the transitions due to the valence nucleons will constitute a large part of the giant resonance since there are few other transitions possible, and, consequently, the larger width of the resonance is understandable.*

Estimation of Direct Emission.

The Wilkinson C ratio, giving the number of nucleons emitted directly to the number absorbed into a compound nucleus, is considerably higher for neutrons than for protons since there is no Coulomb barrier. The centrifugal barrier is small for neutrons with $\ell = 0, 1$ as emitted from the N^{14} nucleus. For 8 MeV neutrons $C \sim 1$ (see proton case) and above 8 MeV this value will increase.

An 8 MeV neutron has a recoil of $\sim$ 0.6 MeV. Hence if the total recoil histogram be divided in terms of the C ratio to give a distribution which might be associated with the direct process, then this direct contribution exhibits a resonance in the same position as that of the total. This point is

* A similar argument could be applied to the γp reaction.

in support of the Wilkinson theory: the Courant theory does not require that the directly emitted nucleons should show a resonance behaviour.

Angular Distributions of Recoils.

From the results on fig$.19. it can be seen that the degree of anisotropy increases with the energy grouping of the recoils. To a first approximation, the neutron may be considered as being emitted in the opposite direction to that of the recoil, and hence the plot between 0° and 90° for the recoils is equivalent to a similar plot for the neutrons.

The results are in keeping with the fact that, as given by Wilkinson's C factor, the proportion of directly emitted protons increases with increasing energy, if an isotropic distribution be associated with the compound nucleus emission and a form $a + b \sin^2\theta$ with the direct emission.

Angular distributions were calculated, for neutrons resulting from a compound nucleus disintegration, in which the compound nucleus had a well defined state. The treatment is identical to that

for the $(\gamma\ p)$ reaction except that only the ground state of the N^{13} need be considered. The following table shows the possible angular distributions:

J	J	J	ℓ_p	S	$\sigma(\theta)$
1	$\frac{1}{2}$-	0-	0	0	isotropic
"	"	1-	0	1	"
"	"	1-	2	1	$7 + 3\cos^2\theta$
"	"	2-	2	0	$2 + 3\sin^2\theta$
"	"	2-	2	1	$2 + \sin^2\theta$

Thus only s and d wave emission is possible and the d-wave will be suppressed by the centrifugal barrier. Compound nucleus disintegration therefore gives an essentially isotropic distribution.

In this reaction it is not possible to associate the large anisotropy of the higher energy events with the emission of s-state neutrons, because this would leave the residual nucleus in a positive parity state. The ground state of N^{13}, which is the only accessible state for a (γ,n) reaction, has negative parity. Hence direct emission from the s shell should not be possible.

Direct emission from the p states would conserve parity, and the interference of the s and d wave neutrons resulting from the $\ell - 1$ and $\ell + 1$ transitions would give an $a + b \sin^2\theta$ distribution. However, it is doubtful whether the anisotropy resulting from this could be as large as was measured.

C.

The $N^{14}(\gamma,pn)C^{12}$ Reaction.

The information presented in figs. 21-25 are significant in that although (γ,pn) events have been detected by photographic emulsion and cloud chamber techniques, there has not been any previous attempt to analyse this reaction in the region 15 - 50 MeV in terms of energy and angular distributions.

Recoil Energy Histogram.

This distribution shows certain interesting features: (a) the peak of the distribution occurs at a much lower energy than in the recoil distributions obtained from (γ,p) and (γ,n) reactions, and (b) the "tail" of the distribution is similar to that obtained for (γ,p) and (γ,n).

In most of the (γ,pn) events recorded, it was

not possible to calculate the energy of the quantum which initiated a reaction, and, consequently, it is not possible to compute the form of the (γ,pn) cross section curve as in the cases of (γ,p) and (γ,n). Only in the relatively few cases where the proton stopped within the chamber was it possible to calculate E_γ, the energy of the incident quantum. 26 of these events were considered and for all of these E_γ lay between 13 and 28 MeV, within the region of the giant resonance. It seems highly probable, therefore, that the majority of (γ,pn) events recorded have resulted from the absorption of γ rays in the energy region 15 to 35 MeV. It is certainly noteworthy that only two events were recorded with a recoil energy of greater than 6 MeV.

The fact that the peak in the recoil energy distribution occurs at such a low energy may not be so surprising, but may result solely from the geometry of the three body disintegration. On the assumption that the predominant disintegration is typical of the giant resonance behaviour observed for (γ,p) and (γ,n) and assuming that the directions

of the protons and neutrons bear no correlation, it is possible to give a qualitative description of this process. This is best illustrated by an example.

e.g. Consider a (γ,p) reaction resulting from a 20 MeV quantum. The (γ,p) threshold is 7.5 MeV. Hence the resultant energy of the recoil will be approximately $\frac{20-7.5}{14} \approx 0.9$ MeV.

Compare this with the recoil resulting from a (γ,pn) interaction in which both proton and neutron are emitted in the same direction. The (γ,pn) threshold is 12.5 MeV. Thus the resultant recoil energy will be approximately $\frac{20-12.5}{7} \approx 1.1$ MeV.

However, the probability of both proton and neutron being emitted into the same angle is small. In general, if the particles are emitted into random directions with respect to each other the probability of the angle between their directions being α is proportional to $\sin\alpha$ (solid angle factor), and hence there is a large probability of the resultant recoil energy being only $\sim$ half of the above value.

The effect of this geometrical consideration on the recoil distribution would therefore be to displace the maximum to a lower energy.

The occurrence of a high energy tail similar to the case of the (γ,p) and (γ,n) recoil distributions is suggestive of a direct process as in the other cases. This is considered again in the next section.

Angular Distributions.

The strong forward peaking of the proton angular distribution with respect to the direction of the incident γ beam (fig. 24a) might also be interpreted as evidence of a direct interaction. If such an interaction consists of the proton/or neutron being directly emitted and knocking on a neutron/or proton, and it is assumed that the effect of this subsequent impulse will have only a small effect on the recoil angle, then it might be expected that the recoil angular distribution would show a peak at 90° as in the case of the (γ,p) and (γ,n) interactions. However the recoil distribution does not give conclusive evidence on this point.

The angle between the recoil and proton has been recorded as a distribution in fig. 23 . Different mechanism for the (γ,pn) disintegration have been proposed and each of these can be associated with a certain form of this type of angular distribution. Qualitative arguments are used to describe these processes and to deduce the form of the angular distributions resulting:

(1) Quasi deuteron interaction.

In this case the quasi deuteron has initially some motion relative to the centre of mass of the whole nucleus. When the γ quantum interacts with the quasi deuteron the neutron and proton are both ejected and the rest of the nucleus then recoils with momentum equal to that which it had with respect to the centre of mass immediately before the interaction. Nuclear motion is isotropic and consequently the distribution formed by the angle between each proton and recoil should also be isotropic. Thus the measured distribution, not having been corrected for solid angle, should have the form $\sin\frac{\theta}{2}$

(2) Knock-on process./

(2) Knock-on process.

For neutron-proton interactions in which the incident particle has less than 10 MeV kinetic energy with respect to the other nucleons, the scattering in the centre of mass system is isotropic. In the laboratory system where the target nucleus is initially at rest the scattering is always into the forward direction and the angle between the neutron and proton directions is 90°. This means that a plot of χ, the angle between the proton and the recoil, for such an interaction, would be zero between 0 and $\frac{\pi}{2}$, and would have a constant value between $\frac{\pi}{2}$ and π. However, in reality the target nucleon is not stationary and the net result is that, provided the internal momentum of the target nucleon is not much greater than the direct nucleon momentum, the distribution of χ as measured (without correcting for solid angle) rises slowly from 0 at 0° to a maximum value at π. This form has been determined from semi-quantitative considerations: a full computation would be difficult and would involve the momentum distribution of the

emitted nucleons and the internal momentum of nucleons in a nucleus.

(3) Compound nucleus disintegration.

Assuming no correlation between the direction of emission of the neutron and proton, and neglecting the incident γ ray momentum, it can be shown qualitatively that the resulting ψ distribution as measured should increase from small values below $\frac{\pi}{2}$ to a maximum value between $\frac{\pi}{2}$ and π and then fall again to 0 at π. A full treatment would require the inclusion of the momentum distributions of both the emitted nucleons and of the nucleons in the initial nucleus.

The measured distribution agrees with that predicted by compound nucleus disintegration. Lalovic and Reid[85] have shown quasi deuteron disintegrations to have a small cross section, so that only a few events from our total might have resulted from such an interaction.

D.

Conclusions.

This experiment has revealed the relative importance of the (γ,p), (γ,n) and (γpn) reactions

between their thresholds and 50 MeV. The (γ,p) and (γ,n) cross section curves have been shown to fall off to $\frac{1}{10}$ and $\frac{1}{8}$, respectively, of their peak values when the excitation energy is 50 MeV. The angular and energy distributions obtained for each reaction have been considered in terms of the various theories of photodisintegration, and most of the information was explicable in terms of the Wilkinson model. However, the anisotropy obtained in the (γ,p) and (γ,n) angular distributions at high energies was very much higher than could be explained by straightforward application of theory.

APPENDIX I.

The Operation of Low Pressure Diffusion Chambers.

Diffusion cloud chambers operating at very high pressures have given much valuable information on the charged particle interactions.[84] Such a chamber, operated at low pressures, presents certain advantages which might be valuable for photodisintegration experiments in which a synchrotron or betatron is used. Since the diffusion chamber is continuously sensitive it is possible to cycle such a system much faster so that the accelerating machine is more efficiently used. In addition, the mechanical advantage of having no moving parts is one of the virtues of this type of chamber, and, as has been demonstrated by the high pressure chamber designs, it is comparatively easy to incorporate a magnetic field, within the structure, to enable momentum determinations to be made from the resulting curvature of tracks.

A low pressure diffusion chamber had previously been used in the laboratory to investigate electron scattering, but considerable difficulty was experienced

in maintaining good track quality. The aim of the experiments described here was to determine the conditions which would give a maximum sensitive depth, consistent with good track quality and stability of operation over long periods of time.

Principle of Operation.

The principle of the diffusion chamber is that the "working" vapour (usually methyl alcohol) diffuses from a hot to a cold surface. In practice the top of the chamber contains an alcohol source, which may be a felt pad saturated with alcohol or a trough filled with the liquid, and this top plate is heated to a temperature a little above room temperature. The base of the chamber is cooled to $\simeq -40^{\circ}C$ by pumping methyl alcohol under it and through a heat exchanger containing methyl alcohol and dry ice at $-70^{\circ}C$. As the vapour diffuses down to colder regions it becomes supersaturated and, eventually, it is cooled to a temperature at which the supersaturation is equal to the critical supersaturation for drop growth on ions. Below the level of this temperature, the chamber is sensitive. Generally

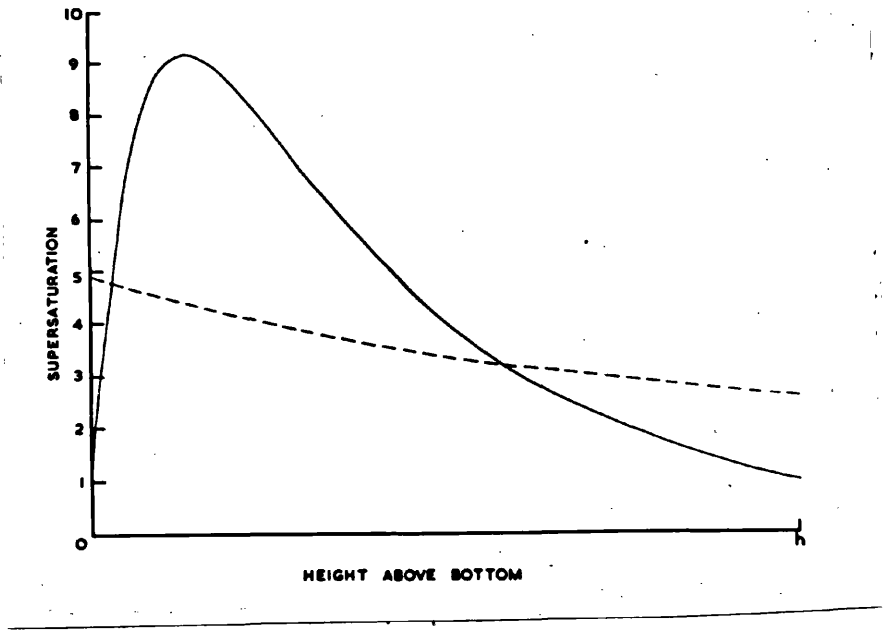

Fig. 27.

Diagram to show the variation of supersaturation with depth in a diffusion chamber. The dotted curve shows the critical supersaturation for drop growth on ions.

the sensitive layer occupies only the bottom 4 ~ 5 cms. of the chamber volume.

Theories of Diffusion Chamber Operation.

Several authors[85-88] have produced theories of diffusion chamber behaviour. Langsdorf[85] gave the first treatment in which he started with an energy flux equation and applied the diffusion equations of Kuusinen[89] for variable temperature to obtain the supersaturation as a function of height within the chamber. Fig.27 gives the calculated supersaturation as a function of height with the dotted curve showing the supersaturation required to produce condensation on ions. The region within the intersections of these curves corresponds to the sensitive depth.

Langsdorf neglected both wall effects and the effects of drop growth. Succi and Tagliaferri[86] have included in their energy equation a term to account for the latent heat release, due to drop formation, and have corrected the Langsdorf distribution. However, in the Langsdorf energy equation, the terms for flux of energy due to thermal conduction and vapour diffusion have been given opposite signs,

whereas, since the energy flux is in the same direction for the two cases, they should have had the same sign. Consequently, even the corrections due to Succi and Tagliaferri are erroneous.

Shutt[87] has given a treatment which includes condensation, drop growth and the fall of the liquid drops. He has deduced the temperature distribution required to produce supersaturation in a definite sensitive depth. This is significant in the case of the high pressure chambers where it was necessary to enforce temperature distributions by including heating elements in the chamber walls. Shutt has also shown that the temperature gradients above, and within, the sensitive depth are constant; with ~~the~~ a break occurring at the top of the sensitive depth.

Conclusions affecting the general behaviour of diffusion chambers resulting from these studies indicate that the sensitive depth will be decreased by:-

(i) decreasing the vapour flow - e.g. by lowering the top temperature,

(ii) increasing the base temperature,

(iii) having an increase in the number of drops formed /cm^3 as, for example, by having a radioactive source nearby.

These facts (together with Shutt's temperature gradient predictions) have all been confirmed experimentally.

Stability condition.

The only condition that must be satisfied for stability is that the density of the gas vapour mixture must decrease with height above the base. When this condition is satisfied there is no convective motion of the gas which would otherwise distort the tracks.

Choice of vapour.

The choice of vapour is governed by the following criteria:-

(a) It must have a large range of vapour pressure with temperature over a temperature range that can easily be achieved.

(b) It must be chemically suitable.

(c) It is best for the vapour to have a low latent

heat so that the process of condensation may not upset the required temperature distribution.

(c) The boiling point and freezing point should be outside the temperature limits of normal chamber operation.

Methyl alcohol, methyl alcohol + water mixtures, ethyl alcohol, and ethyl alcohol + water mixtures were all tested effectively in a diffusion chamber. Methyl alcohol gave the best sensitive depth of ~ 5 cms, although a good sensitive depth was obtained even with as much as 50% water in the alcohol-water mixtures.

Experiments to Determine Optimum Operating Conditions

(1) Temperature measurements.

Since methyl alcohol was chosen as being the most suitable vapour and the choice of gas is usually determined by the nature of the physical problem being investigated, there are only three variables which can be adjusted to obtain optimum sensitivity - gas pressure, top temperature and base temperature. Thus the experimental chamber was operated with different base and top temperatures and the sensitive

f 121.

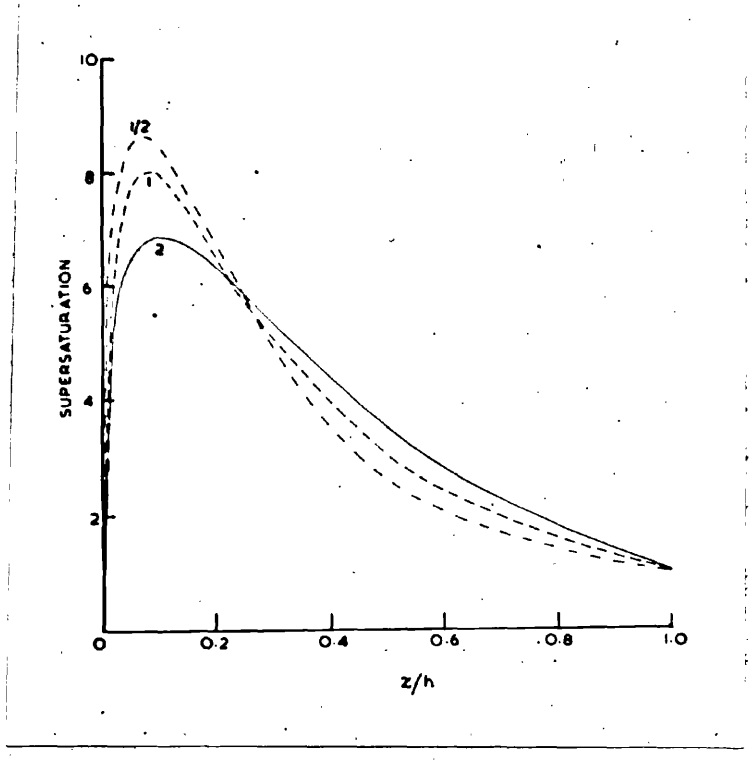

Fig. 28.

Diagram to show the variation of supersaturation with depth in the chamber for different gas pressures within the chamber.

depth was continuously checked. Bursts of X-rays were used to bring down clouds in the chamber, and its speed of recovery was noted. With air in the chamber, a base temperature of -50°C, and a top temperature of + 40°C., a sensitive depth of more than 4 cms. was maintained over several hour periods.

(2) Pressure Measurements.

The stability condition implies that there is a lower limit to the gas pressure to allow sensitivity to be obtained in a diffusion chamber. At the other extreme of high pressures the increased ionic load is detrimental to good operation, since the increased number of drops forming reduces the supersaturation. There must therefore be an optimum pressure between the two.

Langsdorf has computed curves for the supersaturation for gas pressures of $\frac{1}{2}$, 1 and 2 atmospheres. ~~From~~ The intersection of these curves with the critical supersaturation curve gives the top of the sensitive depth for each case. (See fig.28). Thus as the pressure increases, the sensitive depth increases. However, since the supersaturation

decreases with this increase of pressure, the resultant track quality may be poorer. If the curve for critical supersaturation intersects the curves of supersaturation for different pressures near the region at which they themselves intersect, then little change in sensitive depth will be observed.

The theory is in itself insufficient to predict the optimum gas pressure for fixed operating conditions, and, consequently, trial "runs" were recorded in which the pressure of gas was varied between the limits of safety associated with the chamber. Argon gas was used. Thermistors fixed to the top plate and base were used to measure temperature, and a thermocouple supported by two pillars, recorded temperatures in the centre of the chamber and 3 cms. from the base. The results are tabulated ~~opposite~~ on f123. Throughout this pressure range of 25 cms. Hg to 160 cms. Hg. there was no noticeable change in sensitive depth and the track quality remained constant.

Note that while the top and bottom temperatures

Pressure in cms. Hg.	Top temp.	Base temp.	Thermocouple temp.
34.6	55°C	-39°C	-9°C
48.6	"	"	-9.5
61.9	54	"	-9.7
76.6	55	"	-10.2
88.5	"	"	-10.8
102.6	"	"	-10.6
117.5	53	"	-10.6
135.8	54.5	-40°C	-11.2
155.5	55	"	-11.2
136.2	"	"	-11.0
117.5	54	-39.5°C	-10.8
102.6	"	"	-10.6
88.1	55	-39	-10.2
77.4	55.5	-40	-9.5
61.3	55	-41	-9.4
47.6	55	-41	-9.5
26.9	57	-40.5	-8.7

were kept constant the temperature recorded by the thermocouple $2\frac{1}{2}$ cms. from the base dropped by fully 2°C. Since critical supersaturation will occur at a fixed temperature, this drop in temperature might also imply a small increase in sensitive depth, as expected, since the temperature for critical supersaturation would now occur at a higher level in the chamber.

(3) Trials Using Different Gases.

Air, argon, and xenon were all used to fill the diffusion chamber to $\frac{1}{2}$ atmosphere pressure. With top temperature of 56°C and base temperature of $\sim$ -50°C., consistent good behaviour was obtained in each case although, for xenon, the sensitive depth was slightly lower than in the other cases and the track quality was not quite so good.

Conclusion.

The optimum conditions of operation of the circular diffusion chamber were now well established and stable behaviour could be obtained over several hour periods. It was at this stage that the chamber was applied to the argon photodisintegration

experiment described in Chapter II. The comparatively small sensitive depth of the diffusion chamber makes it unsuitable for measuring fragment energies, since the fragments have a large probability of leaving the sensitive volume. However, in the argon experiment only angular distributions and the total number of events were required, and, in this case, the faster cycling time of the diffusion chamber commended it in preference to the conventional expansion chamber.

APPENDIX II

Design of Diffusion Chamber for Operation in a Magnetic Field.

The candidate was responsible for the design and construction of a diffusion chamber which was built to slide between the pole pieces of an existing iron cored D.C. magnet.

The construction was assembled on a hydraulic table so that it could be adjusted in height to the level of the magnet pole pieces and then slid off into position in the magnet. A large wooden base supported the chamber and this whole base was designed to slide onto the bottom pole piece.

The refrigerant was pumped through copper tubes which lay on the bottom of the chamber, the entrance pipes being at the walls, and the exit pipes at the centre of the chamber. Methyl alcohol covered the tubes which, in actual operation, could be cooled to -55°C. Nigrosine black dye was poured into the alcohol to provide a good background for photography. The top heating inclosure contained electrical heaters suspended on pillars from the roof of the enclosure,

f 126.

and the air in the chamber was kept circulating by two motor driven fans, one at each end. This was found necessary to provide uniform heating of the top plate. Non uniformity of temperature on the top plate was often associated with "rain" in the chamber which condensed above the sensitive region and removed the supersaturation to make localised areas of the chamber insensitive.

Long heating elements were clamped against the walls, not to enforce a temperature gradient, but merely to prevent condensation from forming on the inner walls.

The alcohol sources consisted of two troughs attached to the top plate and running the length of the chamber. They were located one at each side.

With a top enclosure temperature of $\sim$ +45°C, and a base temperature of $\sim$ -45°C, a sensitive depth of about two inches was obtained and was maintained for several hour periods.

Additional Note.

Range energy curves for N^{13} and C^{12} were deduced from the C^{13} results by applying

$$R_M(E) = \frac{M}{M_0}\left(\frac{Z_0'}{Z'}\right)^2 R_{M_0}\left(\frac{M_0}{M}E\right).$$

in conjunction with the results due to Lillie for B^{11}.

The effective charge ratio $\frac{Z_0'}{Z'}$ was calculated for B^{11} and C^{13} as a function of the C^{13} energy. These values of $\frac{Z_0'}{Z'}$ were then used in comparing C^{13} with N^{13} and C^{12} to obtain curves for N^{13} and C^{12}. The resulting curves are shown in fig. 10.

Ranges measured experimentally were converted to a range in air at S.T.P. by :-

$$\text{Range in air} = \text{Range in chamber} \times \frac{\text{pressure in chamber}}{\text{atmos. pressure}} \times \frac{14}{14.4}$$

where 14 is the number of electrons associated with nitrogen and 14.4 is the average number associated with air. Thus the energy of recoils was obtained directly from the computed curves.

REFERENCES

1. CHADWICK and GOLDHABER, Nat. 134, 237, 1934.

2. SZILARD and CHALMERS, Nat. 134, 494, 1934.

3. BOTHE and GENTNER, Naturwiss, 25, 90, 126, 191, 284, 1937.

4. HUBER, LIENHARD, SCHERRER and WAFFLER, Helv, Phys. Acta., 17, 1944. p.139.

5. BALDWIN and KLAIBER, Phys. Rev. 70, 289, 1946.

6. " " " " 73, 1156, 1948.

7. WEINSTOCK and HALPERN, Phys. Rev. 94, 1651, 1954.

8. MONTALBETTI, KATZ and GOLDEMBERG, Phys. Rev., 91, 659, 1953.

9. HALPERN and MANN, Phys. Rev. 82, 733, 1951.

10. NATHANS and HALPERN, Phys. Rev. 92, 207, 1953. See 8.

11. LEVINGER, Phys. Rev. 84, 43, 1951.

    DEDRICK, Phys. Rev. 100, 58, 1955.

12. ODIAN, STEIN, WATTENBERG, FELD and WEINSTEIN, Phys. Rev. 102, 837, 1956.

    FELD, DOBBOLE, ODIAN, SCHERB and WATTENBERG, Phys. Rev. 94, 1000, 1954.

    LEVINTHAL and SILVERMAN, Phys. Rev. 82, 822, 1951.

    KECK, Phys. Rev. 85, 410, 1952.

13. See Handbuch der Physik XLII (1957), 315-330.

14. NATHANS and HALPERN, Phys. Rev, 92, 207, 1953.

14. (Contd.)

HALPERN, MANN and NATHANS, Rev. Sci, Inst. 23, 678, 1952.

JONES and TERWILLIGER, Phys. Rev. 91, 699, 1953.

KATZ, HASLAM, CAMERON and MONTALBETTI, Phys. Rev. 95, 464, 1954.

Also Ref. 8.

15. JOHNS, KATZ, DOUGLAS and HASLAM, Phys. Rev. 80, 1062, 1950.

16. KATZ and CAMERON, Can. J. Phys. 29, 518, 1951.

17. KATZ, HASLAM, GOLDEMBERG and TAYLOR, Can. J. Phys. 32, 580, 1954.

18. KATZ, HASLAM, HORSLEY, CAMERON and MONTALBETTI, Phys. Rev. 95, 464, 1954.

GOLDEMBERG and KATZ, Phys. Rev. 95, 471, 1954.

19. " " " " " " "

PENFOLD and SPICER, " " 100, 1377, 1955.

20. TITTERTON, Prog. Nuc. Phys. Vol. 4, 1, 1955.

21. WRIGHT, MORRISON, REID and ATKINSON, Proc. Phys. Soc. LXIX, 77, 1956.

22. GAERTNER and YEATER, Phys. Rev. 83, 146, 1951.

23. GUDDEN and EICHLER, Naturwiss., 44, 508, 1957.

24. KOMAR and IAVOR, J.E.T.P., 4, 432, 1957.

KOMAR and IAVOR, J.E.T.P., 5, 508, 1957.

25. WILKINSON and CARVER, Phys. Rev. 83, 466L, 1951.

26. OPHEL and WRIGHT, Proc. Phys. Soc. Vol. 71, 389, 1958.

OPHEL, Aust. Natl. Univ. p. 185, 1958.

27. FERRERO, HANSON, MALVANO and TRIBUNO, Nuo. Cim., 4, 418, 1956.

28. WHITEHEAD, McMURRAY, AITKEN, MIDDLEMASS and COLLIE, Phys. Rev. 110, 941, 1958.

29. LEVINGER and BETHE, Phys. Rev. 78, 115, 1950.

30. GELL-MANN, GOLDBERGER and THIRRING, Phys. Rev. 95, 1612, 1954.

31. BISHOP and WILSON, Hand der Phys. XII, p.338, 1957.

32. GOLDHABER and TELLER, Phys. Rev. 74, 1046, 1948.

33. STEINWEDEL and JENSEN, Z. Naturf. 5a, 343, 1950.

34. DANOS and STEINWEDEL, " " 6a, 217, 1951.

35. WOLFENSTEIN, Phys. Rev. 78, 322A, 1950.

36. WEISSKOPF and EWING, Phys. Rev. 57, 472, 1940.

37. LIVESEY, Can. J. Phys, 33, 391, 1955.

38. DIVEN and ALMY, Phys. Rev. 80, 407, 1950.

39. TOMS and STEPHENS, Phys. Rev. 82, 709, 1951.

40. CURTIS, HORNBOSTEL, LEE and SALANT, Phys. Rev. 77, 290, 1950.

41. BYERLY and STEPHENS, Phys. Rev. 83, 54, 1951.

42. DAWSON, Can. J. Phys. 34, 1480, 1956.

43. LIVESEY, Can. J. Phys. 34, 1022, 1956.
35, 978, 1957.

44. HIRZEL and WAFFLER, Helv. Phys. Acta., 20, 374, 1947.

45. JENSEN, Naturwiss, 35, 190, 1948.

46. MARQUEZ, Phys. Rev. 81, 897, 1951.

47. COURANT, Phys. Rev. 82, 703, 1951.

48. POSS, Phys. Rev. 79, 539, 1950.

49. EICHLER and WEIDENMULLER, Private communication, 1958.

50. WILKINSON, Proc. Glasgow Conference, 1954. Physica, 22, 1039, 1956.

51. LANE and RADICATTI, Proc. Phys. Soc. A.67, 167, 1954.

52. TOMS and STEPHENS, Phys. Rev. 92, 362, 1953.

53. PETREE, WEISS and FULLER, Bul. Am. Phys. Soc. 2, 16, 1957.

54. OKAMOTO, Phys. Rev.(1958.) 110, 143.

55. DANOS, Bul. Am. Phys. Soc. 1, 135, 1956.

56. WILKINSON, Phil. Mag, 3, 567, 1958.

57. BRINK, Nucl. Phys. 4, 215, 1957.

58. MANN, STEPHENS and WILKINSON, Phys. Rev. 97, 1184, 1955.

LEIKIN, OSOKINA and RATNER, Supp. Nuv. Cim. Ser. 10 3, 1956.
Nuv. Cim. 6, 387, 1957.

59. FERRERO, HANSON, MALVANO and TRIBUNO, Physica, 22, 1148, 1956.

59. (Contd.)

OSOKINA and RATNER, J.E.T.P. 5, 1, 1957.

60. McPHERSON, PEDERSON and KATZ, Can. J. Phys. 32, 593, 1954.

61. SPICER, Phys. Rev. 100, 791, 1955.

62. PENNING, MALTRUD, HOPKINS and SCHMIDT, Phys. Rev. 104, 740, 1956.

63. ~~KATZ~~, See ref. 8.

64. MATTAUCH, Nuclear Physics Tables.

65. EICHLER and GUDDEN, Naturwiss, 19, 508, 1957.

66. BLACKETT, Proc. Phys. Soc. A.107, 349, 1925.

BLACKETT and LEES, Proc. Phys. Soc. A.134, 658, 1931-32.

67. LILLIE, Phys. Rev. 87, 716, 1952.

68. BETHE, Rev. Mod. Phys. 22, 213, 1950.

69. RADICATTI, Phys. Rev. 87, 521, 1952.

70. BURCHAM, Prog. Nucl. Phys. 4, ~~204~~. 202, 1955.

71. MILLAR and CAMERON, Can. J. Phys. 31, 723, 1953.

GOWARD and WILKINS, Proc. Phys. Soc. A.65, 671, 1952.

DAWSON and BINGHAM, Can. J. Phys. 31, 167, 1953.

72. RHODES, Univ. of Pennsylvania, NR - 022 - 019, No. 3, 1958.

73. JOHNS, HORSLEY, HASLAM and QUINTON, Phys. Rev. 84, 856, 1951.

74. BLATT and WEISSKOPF, "Theoretical Nuclear Physics", p.352.

75. OSOKINA and RATNER, J.E.T.P. Vol. 5, No. 1, 1957.

76. BLUCH, HULL, BROYLES, BOURICIUS, FREEMAN and BREIT, Rev. Mod. Phys. 23, 147, 1951.

77. DEVONS, "Excited States of Nuclei", p.92 et ser.

78. SHARP, KENNEDY, SEARS and HOYLE, A.E.C.L. 97.

79. JOHANSSON, Physica, 22A 1144A, 1956.

80. SPICER, Aust. J. Phys. 6, 391, 1953.

81. LIVESEY, Can. J. Phys. 35, 987, 1957.

82. PANOFSKY and REAGAN, Phys. Rev. 87, 543, 1952.

83. LALOVIC and REID, Lab. notes - to be published.

84. BATSON, COOPER and RIDDIFORD, J. Sci. Inst. 33, 302, 1956.

ALSTON, CREWE, EVANS, GREEN and WILMOT, Proc. Phys. Soc. 67, 657, 1954.

FOWLER, FOWLER, SHUTT, THORNDIKE and WHITMORE, Phys. Rev. 91, 135, 1953.

FOWLER, SHUTT, THORNDIKE and WHITMORE, Phys. Rev. 93, 861, 1954.
95, 1026, 1954.

85. LANGSDORF, Rev. Sci. Inst. ~~33~~ 10, ~~302~~ 91, ~~1956~~ 1939.

86. SUCCI and TAGLIAFERRI, Nuv. Cim. 9, 1092, 1952.

87. SHUTT, Rev. Sci. Inst. 22, 730, 1951.

88. BEVAN, J. Sci. Inst. 31, 45, 1954.

FOWLER, SHUTT, THORNDIKE and WHITMORE, Rev. Sci. Inst. 25, 996, 1954.

ARGAN, ANGELO and GIGLI, Nuv. Cim. 1, 761, 1955.

ARGAN, GIGLI and ANGELO, " " Ser. X Vol. 3, 1337, 1956.

89. KUUSINEN, Ann. der Phys. 14, 445, 1935.